

POLITECNICO DI TORINO

Dipartimento di Ingegneria Meccanica e Aerospaziale
Collegio di Ingegneria Biomedica

Corso di Laurea Magistrale in Ingegneria Biomedica

Tesi di Laurea Magistrale

Three-dimensional Printing of a multi-material model of the Knee Joint



Relatori:

Prof. Yasin Y Dhaher

Prof. Cristina Bignardi

Tesi di Laurea Magistrale di:

Oliver Grimaldo Ruiz

Matricola 238989

2019

Abstract

Three-dimensional printing (3D) is an additive manufacturing technology based on material deposition layer by layer for 3D object construction. Every year, 3D Printing offers more alternatives and solutions in the healthcare field. Nowadays, applications such as 3D Printing labs in hospitals, low-cost patient-specific prosthetics, customized medical implants and manufacture of anatomical models with high dimensional accuracy are the most immediate emerging trends. Indeed, 3D Printing application is the convergence of multiple factors, including improvements in medical software, 3D printers evolution and new printing materials. In particular, anatomical models manufacturing is becoming increasingly popular and accessible due to its application in medical training and pre-operative planning. Anatomical models manufacturing is based on several data acquisition techniques such as computed tomography (CT), optical coherence tomography (OCT), magnetic resonance imaging (MRI) or 3D solid modeling through computer-aided-design (CAD) and anatomical structures 3D scanning.

The Shirley Ryan AbilityLab research hospital has a full-color multi-material 3D printer Stratasys J750™. It uses Photopolymer jetting (Polyjet™ technology) for manufacture of highly realistic and functional 3D models in a wide range of colors and materials with variable durometers.

Materials and methods: Polygonal mesh files (*.hm) corresponding to a finite elements (FE) model of the right knee joint reported by Dhaher et al. 2014 were the basis of this study. The 3D model included femur, tibia, patella, fibula, ligaments, articular cartilage, menisci, retinacula, patella and quadriceps tendons (PT-QT). Three anatomical models were projected and printed achieving the following objectives.

- (1) 3D model improvement of the right knee joint emulating the hierarchical structure of the collagen fibers matrix of the tendons and ligaments.
- (2) Anterior cruciate ligament reconstruction (ACL-R) model manufacturing using a bone-patellar-tendon-bone (BPTB) auto-graft and pre-operative planning to improve surgery outcomes, incorporating key surgical elements, such as orientation-architecture of the femoral and tibial tunnels and auto-graft dimensions reported by Dhaher et al. 2014. The surgical planning considers single bundle (SB) reconstruction and includes a customized surgical guide (SG) based on PT anatomy (it used in the graft harvest). The SG requirements followed the indications reported by Wang et al. 2017 with the aim to avoid graft tunnel length mismatch.
- (3) Total knee replacement (TKR) model manufacturing considering a cruciate sacrificing (CS) implant with customized design of symmetric tibial bearing, adjustment and assembly of standard prosthetic components in the improved 3D model emulating a TKR procedure. The selection process and printing materials matching with anatomical structures was based on stiffness and elastic modulus analysis of different Agilus30 printing material combinations. Mechanical uniaxial tensile tests were conducted in Northwestern University Kaiser Lab using an Instron S3300, Canton, MA Uniaxial Testing Instrument following ASTM test designation D412-C. The combinations No 1-4 were the most similar to real materials with elastic modulus of 1.8-0.7 and Pearson coefficients of the linear region of 0.980-0.991 respectively.

Keywords: Three-dimensional Printing, Knee joint, planning surgery, anterior cruciate ligament reconstruction, total knee replacement.

Acknowledgments

Firstly, I would like to express my sincere gratitude to my supervisor *Professor Yasin Dhaher* for his continuous support of my investigation, for his patience, motivation, and immense knowledge. His guidance helped me in all the time of research of this thesis. Besides my supervisor, I would like to thank my co-supervisor *Professor Cristina Bignardi* for her support and guidance during the development of my thesis project. My sincere thanks goes to *Engineers Kunal Shah, and Samuel Sung*, who provided me an opportunity to join their team, and who gave me access to the laboratories and research facilities. Without their precious support, it would not be possible to conduct this research.

I would also like to thank my mother *Architect Ana Lucia Ruiz* and my family for all the love and support that they have given me. Thanks for always encouraging me to believe in myself and always do the best.

Finally, this work would not have been possible without financial support from *Shirley Ryan AbilityLab* and *Northwestern University*.

List of Abbreviations

2D	Two-Dimensional
3D	Three-Dimensional
ABS	Acrylonitrile Butadiene Styrene
ACL	Anterior Cruciate Ligament
ACL-R	Anterior Cruciate Ligament reconstruction
AVG-E	Average Elastic Modulus
AVG-PL	Average Proportional Limit
AVG-YS	Average Yield Strength
AM	Anteromedial
AMT	Additive Manufacturing Technology
AL	Anterolateral
BPTB	Bone Patellar Tendon Bone Auto-Graft
CAD	Computer Aided Design
CAE	Computer-Aided Engineering
CKC	Closed Kinetics Chain
CS	Cruciate Sacrificing
CT	Computed Tomography
DICOM	Digital Imaging and Communications in Medicine
DOF	Degrees of Freedom
FDM	Fused Deposition Modeling
FEA	Finite Element Analysis
FMAa	Anatomic-Mechanic Femoral Angle
FDLMa	Mechanical Lateral Distal Femoral Angle
FDLaa	Anatomic Lateral Distal Femoral Angle
GRS	Global Reference System

KA	Knee Arthroplasty
LCL	Lateral Collateral Ligament
LPR	Lateral Patella Retinaculum
MCL	Medial Collateral Ligament
MPR	Medial Patella Retinaculum
MRI	Magnetic Resonance Imaging
NFC	Number of Fibers Calculated
NFD	Number of Fibers Designed
OA	Osteoarthritis
OCT	Coherence Tomography
OKC	Open Kinetics Chain
OTT	Over the Top
PCL	Posterior Cruciate Ligament
PF	Patella Femoral Joint
PKA	Partial Knee Arthroplasty
PT	Patella Tendon
QT	Quadriceps Muscle Tendon
RC	Rotation Center
SA	Cross-Sectional Area of the Structure
SAF	Cross-Sectional Area of the Fiber
SB	Single Bundle
STD-E	Standard deviation Elastic Modulus
STD-PL	Standard Deviation Proportional Limit
STD-YS	Standard Deviation Yield Strength
STL	Standard Triangle Language
TF	Tibia Femoral Joint
TKA	Total Knee Arthroplasty

TKR Total Knee Replacement

TT Transtibial Technique

Table of contents

1. Theoretical framework.....	13
1.1. Anatomical references of the Knee Joint	13
1.2. Knee Joint general aspects	14
1.3. Bone component.....	14
1.4. Soft tissues.....	16
1.5. Muscular complex	18
1.6. Knee Joint: Tibiofemoral joint and Patellofemoral joint.....	20
1.7. Definitions	21
1.8. Knee Joint Biomechanics	22
1.9. Tendons and ligaments: Structure and mechanical behavior	25
1.10. Injuries of the Knee Joint.....	27
1.11. Anterior Cruciate Ligament Reconstruction: Anatomic placement-fixation.....	30
1.12. Anterior Cruciate Ligament Reconstruction: Anatomic femoral and tibial tunnel placement.....	33
1.13. Anterior Cruciate Ligament Reconstruction: Surgical technique.....	36
1.14. Knee joint Osteoarthritis.....	38
1.15. Total knee replacement.....	39
1.16. 3D printing: FDM and PolyJet technologies	39
1.17. Past and present of 3D printing in healthcare filed.....	41
2. Research Theme	45
3. Methodology	45
4. Chapters	47
4.1 Chapter 1: Manufacture of the improved 3D knee joint model	47
4.1.1 Introduction.....	47
4.1.2 Problem specifications.....	49
4.1.3 Materials and methods.....	50
4.1.4 Results.....	58
4.1.5 Discussion.....	60
4.2 Chapter 2: ACL-R biomodel manufacture and Pre-operative surgical planning to improve surgery outcomes.....	61
4.2.1 Introduction.....	61

4.2.2	Problem specifications.....	63
4.2.3	Materials and methods.....	64
4.2.4	Results.....	66
4.2.5	Discussion.....	67
4.3	Chapter 3: TKR biomodel manufacture, custom design and adjustment of prosthetic components in the improved 3D knee joint model.....	69
4.3.1	Introduction.....	69
4.3.2	Problem specifications.....	70
4.3.3	Material and methods.....	71
4.3.4	Results.....	73
4.3.5	Discussion.....	74
5.	Conclusion.....	75
6.	Biography.....	75

List of figures

- Figure 1. Anatomical references of the knee joint.** Three-Dimensional (3D) representation of the anatomy of the lower limbs in anatomical position. Lateral-Medial standard terms of the right knee joint, representation of midline. Proximal-distal standard terms of the right lower limb. Anterior-Posterior view of the right knee joint. Lateral view cross-section, superficial-deep standard terms of the right knee joint Hoehn et al.2007..... 13
- Figure 2. Knee joint.** Three-Dimensional (3D) representation of the anatomy of the knee joint. (A) Anterior view of the knee joint with the musculature removed to visualize the bones and major ligaments. (B) Posterior view of the knee joint with the musculature removed to visualize the bones and major ligaments. (C) Postero-lateral view of the knee joint showing the bone, muscle and soft tissues Hoehn et al.2007..... 18
- Figure 3. Knee joint.** Three-Dimensional (3D) representation of the anatomy of the right knee joint (muscular complex). (A) Anterior view of the right knee joint with the superficial musculature. (B) Anterior view of the right knee joint with the deep musculature (C) Posterior view of the right knee joint superficial musculature. (D) Posterior view of the right knee joint deep musculature Hoehn et al.2007..... 20
- Figure 4.** (A) Tendon strain-stress curve with characteristic regions. (B) Sequential images of the tendon rupture, (i) at initial loading, (ii) defibrillating immediately after the maximum stress and (iii) rupturing to the point where the ruptured ends were bridged by only a single strand of collagen fiber. The displacement rate corresponds of 10 mm/min (intended for modeling normal physiological loading a displacement rate of 500 mm/min is intended for modelling extreme loading) Goh et al. 2014. 26
- Figure 5.** (A) The oval-shaped tibial insertion of the anterior cruciate ligament (ACL) in the transverse plane. The distance from the PCL notch to the posterior fibers of the ACL of 5.7 mm. The length of 18.5 mm, and the width of 10.3 mm. The closest point from the medial aspect of the insertion to the medial tibial articular cartilage of 1.9 mm. The center of the footprint of 15 mm anterior to the PCL notch. (B) The tibial footprint of the anterior cruciate ligament lies between the spines of the intercondylar eminence and does not extend posterior to the medial spine. (C) The oval-shaped femoral insertion of the ACL viewed in the sagittal plane. The footprint rotated to 28.8° to the shaft of the femur the footprint length 18.4 mm, and the width 9.5 mm. (D) Depiction of the femoral intercondylar notch with the knee flexed 90 °. The femoral ACL footprint lies on the lateral wall of the notch and spans a region on a clock face from 10:14 to 11:23. This location of the footprint is based on 3 to 9 o'clock axis placed on the posterior femoral condyles. Changing the knee flexion angle or the stipulated 3 to 9 o'clock transverse axis will change the appearance of the footprint Steiner et al 2008. 33
- Figure 6.** Point A is proximal and high in the notch and typically demonstrates an isometry pattern that mimics normal anterior cruciate ligament. Point B is distal (anterior as viewed arthroscopically) and generally demonstrates unacceptable elongation in flexion. Point C is lateral and posterior in the notch and generally demonstrates excessive strain in extension. Femoral site behavior will vary slightly depending on the accuracy of the previously selected tibial location.

(From Acufex, Smith and Nephew Endoscopy, Andover, MA, with permission.) Daniel et al. 2003. 35

Figure 7. Schematic illustration of the study methodology. The workflow illustrates the different file formats used throughout the investigation. Prosthetic components were integrated and print materials selection were chosen in the based on the results of the mechanical characterization...47

Figure 8. Hierarchical structure of ligaments. The basic structural element is the collagen molecule Frank et al. 2004. 48

Figure 9. Standard strain-stress curves of tendon and ligament. Experimental data reported by David et al. 1978 was represented with WebPlotDigitizer V4.1 and MATLAB R2018a. Two regions of interest of the curve: (1) The toe region and (2) The linear region, yield limit points are illustrated. 49

Figure 10. Workflow PISK: Practice Interactive Surgical Knee. (A) *.SLDPRT file of knee joint. (B) Printout of entire knee model made using 3D printer. (C) Sample of Femur mold to produce a part of the knee joint. 50

Figure 11. Comparative between FDM and PolyJet™ technologies Stratasys J750™ High-End PolyJet uses photopolymers, which are capable of simulating properties ranging from rubber-like to transparent even high toughness and heat resistance. Digital materials expand the possibilities by blending two or more base resins to create thousands of material combinations. Achieve full color capabilities, translucencies, Shore A values and other properties for maximum product realism Stratasys Ltd 2016. 51

Figure 12. Front view of the Stratasys J750 printer, features and commercial materials Stratasys Ltd 2016. 52

Figure 13. PolyJet™ photopolymers, materials and outstanding features Stratasys Ltd 2016. 52

Figure 14. (A) Illustration of fibers tracing through the MCL, contour and sketches are shown (B) set of 60 individual collagen fibrils manually created to MCL (C) Posterior view of the knee joint with all created fibers (D) Anterior view of the knee joint, cross-section MCL, the diameter of the fiber is reported. 53

Figure 15. Fiber optic sensor positioned inside LCL. Fiber and multi-sensing platform are shown. 55

Figure 16. Illustration of the initial model of ACL-R without fibers: (A) Anterior view of the knee joint with BPTB graft,(B) Posterior view of the knee joint with BPTB graft inside, (C) Lateral view of the knee joint in flexion, rupture of the LPL. 57

Figure 17. Schematic illustration of the application of the standard D412-C: (A) Dimensions bone specimen, (B) Render bone specimen in SolidWorks software, (C) Printed bone samples with different combinations, (D) Bone specimen attached to a materials testing system Instron S3300, Canton, MA uniaxial testing instrument, to apply tensile load. 58

Figure 18. Average Stress–Strain curves for anatomical structures and hardness combinations. 59

Figure 19. Average linear tendencies for anatomical structures. Hardness combinations, equations and correlation coefficients were reported. 60

Figure 20. Search trends in the last fifteen years related to 3D printing and 3D printed. Ordinate axis represents search interest relative to the highest point on the graph. A value of 100 is the peak popularity for the term. A value of 50 means that the term is half as popular. A score of 0 means there was not enough data for this term. Abscissa axis represents the period of time in which the search was made.63

Figure 21. Schematic illustration central part of patellar tendon removed for ACL-R in the improved biomodel of the right knee joint: (A) Lateral view BPTB auto-graft. Anterior view SG positioned on the knee joint. (B) Isometric view knee joint - SG.64

Figure 22. Schematic illustration of the pre-operative measurements of the virtual surgical planning. (A) Preliminary measures (mm) and landmarks of BPTB auto-graft, (B) Simulation of the cut-planes in the graft resection (harvest), (C) Positioned SG and graft resection according to the pre-operative guidelines.65

Figure 23. Schematic illustration of the tunnel directions and locations.66

Figure 24. Illustration of 3D printed biomodels of the knee joint. Posterior-Anterior-Lateral-Isometric views ACL-R (last version) and ACL-R. They show the same details as the 3D digital models, the fibers are evident in the grafts and other anatomical structures. The surgical guide was adapted perfectly to the anatomy of the knee joint. Lateral views show conservation of the ligaments without rupture when the knee joint is flexed.....67

Figure 25. Comparison between the initial FE model and the improved ACL-R model68

Figure 26. Traditional approach harvest BPTB autograft and use of the SG......68

Figure 27. Prosthetic components designed for the TKR: (A) Isometric view (B) Posterior view (C) Lateral view.....70

Figure 28. Schematic illustration of the pre-operative measurements and anatomical angles of the surgical planning: (A) Mechanical and anatomical axes, and anatomical angles, $FMAa = 6.09^\circ$ - $FDLa = 79.62^\circ$ - $FDLMa = 86.72^\circ$, (B) Anatomical measurements and simulation of the cut planes in the bone components, (C) subtraction of the prosthetic components of the bone component.72

Figure 29. Schematic illustration of the design and adaptation of the prosthetic components designed based on the anatomy of the bone components. Patellar and tibial bearings were designed based on the real articular component.....72

Figure 30. Schematic illustration of the developed TKR biomodels (A) Posterior view knee joint with prosthetic components, femoral and tibial component are aligned perpendicular to the mechanical axis. (B) Lateral view of the knee joint with prosthetic components, the alignment corresponded to 90° with respect to the mechanical axis. (C) Transverse view of the knee joint with the femoral component, anatomic axes-alignment surgical epicondylar axis and mechanical axis corresponded to 90° . (D) Isometric view assembly of all the components of the TKR.....73

Figure 31. Schematic Illustration of assemblies and list of anatomical structures of the printed models of the knee joint with the selected materials.74

Figure 32. Illustration of TKR biomodel. Posterior-Anterior-Lateral-Isometric views show some details as the fibers and prosthetic components.74

List of tables

Table 1. The Muscular complex of the knee joint.	19
Table 2. Graft choices Daniel et al. 2003.	29
Table 3. 3D File formats used in the study. Extensions, file names and software applications.	46
Table 4. Dimensions, cross-sectional area SA) volume (Vol), number of fibers calculated (NFC) and number of fibers designed (NFD) of tendons and ligaments of the knee joint model.	54
Table 5. Range of the elastic modulus (tension) and Durometers of the shore hardness scale reported for the anatomical structures and Stratasys j750™ materials: Engineering plastics: Digital ABS Green (RGD5160-DM-RGD5161-DM-RGD515-RGD535), Ivory (RGD5130-DM-RGD5131-DM-RGD515-RGD531) and High Temperature (RGD525). Transparent standard plastics: (RGD720), Veroclear (RGD810). Rigid opaque: VeroPurewhite (RGD837), Verogray (RGD850), Veroblackplus (RGD875), Verowhiteplus (RGD835), Veroyellow (RGD836), Verocyan (RGD841), Veromagenta (RGD851) and Veroblue (RGD840). Simulated polypropylene: Duruswhite (RGD430), Rigur and (RGD450). Rubber-like: Tango black plus (FLX980), Tango plus (FLX930) Tango black (FLX973), Tango gray (FLX950), Agilus30 (FLX935), Agilus30 black (FLX985) Stratasys Ltd 2016.	56
Table 6. Fibers-specimen hardness combinations (Agilus30) for the tensile test.	57
Table 7. Tensile test data. The average and standard deviations of the strain-stress curve properties of the different combinations of the print materials.	59
Table 8. Match of the anatomical structures with the selected combinations for the printing of the model.	60

1. Theoretical framework

1.1. Anatomical references of the Knee Joint

The names and positions of the knee joint structures are described using terminology and anatomical references. In the human skeleton most of the joints have duplicates, therefore, it is common to describe the anatomical structures using as reference an imaginary line located in the middle of the body. The directional terms used to indicate the relative positions of the anatomical structures of the knee joint are:

- The terms *medial* and *lateral* that describe a position that is closer or further of the middle line of the body.
- The terms *anterior* and *posterior* that describe a position that is the front and the back of the body.
- The terms *superior* and *inferior* that describe a position that is above or below from another part of the body.
- The terms *proximal* and *distal* that describe a position that is closer or further from the trunk of the body.
- The terms *superficial* and *deep* that describe a position that are closer or further from the surface of the body.

Anatomical structures described following these directional terms will include in their names the suffix to which reference was made *Betts et al. 2014*.

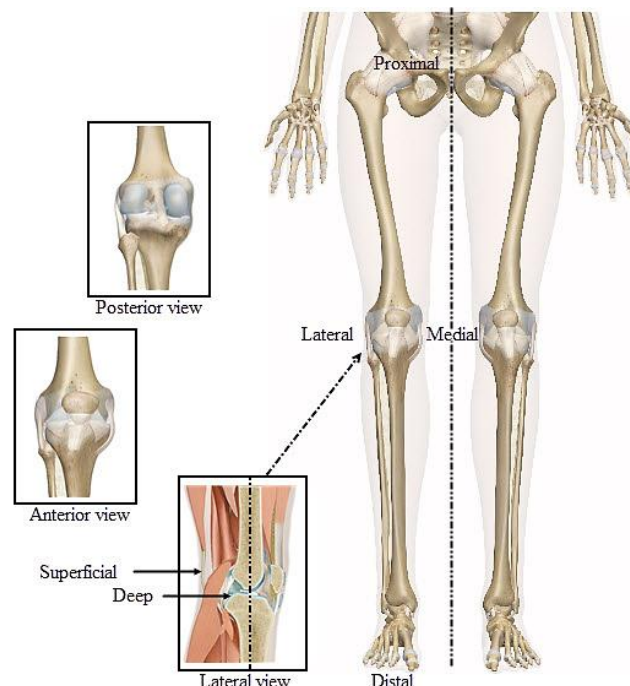


Figure 1. Anatomical references of the knee joint. Three-Dimensional (3D) representation of the anatomy of the lower limbs in anatomical position. Lateral-Medial standard terms of the right knee

joint, representation of midline. Proximal-distal standard terms of the right lower limb. Anterior-Posterior view of the right knee joint. Lateral view cross-section, superficial-deep standard terms of the right knee joint *Hoehn et al.2007*.

1.2. Knee Joint general aspects

The knee is the intermediate joint of the lower limb, it is the largest, most complex and important joint of the human skeleton. The number of anatomic and functional asymmetries that characterize this joint is remarkable. Probably the most studied, because it is the most exposed and least protected against mechanical and degenerative injuries. The structures that make up the knee joint are divided in several categories, these includes; bone, muscular and soft tissues component. The parts work together to maintain normal function.

The knee joint serves as a join between the thigh and the leg, the femur and tibia make up the main body of the joint, while the patella acts as a pulley gliding through special groove formed by the two femoral condyles. It serves as an insertion of the quadriceps muscle tendon (QT) and patella tendon (PT) whose function is to transmit the force generated when the quadriceps muscle is contracted *Burgener et al 2002*.

The knee joint is surrounded by the articular capsule that forms a closed space in which the joint components converge. The inner shell of the articular capsule is the synovial membrane, it produces the synovial fluid that lubricates the joint, reducing the friction between the surfaces in contact and avoid the wear of the joint components. In addition, it performs nutrition and defense functions. The presence of the articular cartilage that covers the entire articulating surface of each bone, acts like a Teflon coating allowing the articulating bones to move smoothly against each other *Hoehn et al. 2007*.

Outside of their articulating surfaces, the bone component is connected by ligaments, which are strong bands of fibrous connective tissue. These strengthen and support the knee joint by anchoring the bones together and preventing their separation. The ligaments allow for normal movements at a joint, but limit the range of these motions, thus preventing excessive or abnormal joint movements *Betts et al. 2014*.

1.3. Bone component

The bone component is designed to accept, transfer, and dissipate the high loads between and among the femur, tibia, fibula, and patella. It is formed by the femur distal part, tibia proximal part and patella anterior part, the fibula really do not enter in the knee joint *Láctico et al. 2006*.

The femur is classified as the longest and strongest bone in the entire human body. Its function is to support most of the body's weight during kinematic activities *Abdallah et al. 2007*. The femur extends from the hip to the knee. It has an oblique inward direction, since the distance between the hips is greater than between the knees *Láctico et al. 2006*.

The femur distal part has two round knobs; medial and lateral femoral condyles, separated by an intermediate gap called intercondylar space. The femoral condyles diverge slightly, distally and posteriorly, with the lateral femoral condyle being wider in the anterior view than in the posterior view, while the medial femoral condyle maintains a constant width. In the sagittal plane, the radius of the femoral condyles curvature decreases toward the back. The decreasing radius allows the sliding and rolling motion in the flexing knee while ensuring the collateral ligaments are sufficiently lax to allow the rotation associated with the curvature of the medial femoral condyle about a vertical axis. The contact areas of the femur, the middle region of the femoral condyles and in the anterior region of the distal part of the femur, known as the femoral trochlea are covered by a layer of thick cartilage called the femoral cartilage *Kahle et al. 2004*.

The anterior and posterior cruciate ligaments (ACL-PCL) are respectively attached into the antero-lateral and postero-medial surface of the femoral condyles, while the collateral ligaments are attached into the lateral and medial distal region of the femur. The lateral collateral ligament (LCL) is not attached into the tibia, it extends from the lateral region to the head of the fibula *Kahle et al. 2004*.

On the other side is located the tibia, it is articulated with the femur. Its function is to support the weight and transmit it to the ankle joint. It is oriented vertically in the company of the fibula, the tibia proximal part provides a resting surface for the femur distal part. It has two cavities, medial and lateral tibial plateau, between them, there are two prominences, internal and external tibial spines. The ACL crosses the intercondylar space obliquely from its femoral insertion to be attached into the internal tibial spine. The PCL crosses with the ACL in the anterior-posterior direction from its femoral insertion descending obliquely to a posterior point of the tibial surface where it is attached *Arcas et al. 2004*.

The medial collateral ligament (MCL) extends from the medial part of the femoral condyle to be attached in the proximal medial part of the tibia. In the anterior part of the tibia, there is another prominence. The anterior tuberosity that serves as an insertion of the patellar tendon *Arcas et al. 2004*.

In the tibial surface the layer of protective cartilage is not constant, it increases in the center of the tibial plateau and it thins out in the periphery, the menisci fibro-cartilages semilunar, medial and lateral, have attachments; anterior and posterior horns, that prevent their displacement and keep them in its peripheral position. The horns, of both menisci have their own insertions in the tibial intercondylar region *Láctico et al. 2006*.

The patella or kneecap as commonly called is the largest sesamoid bone in the body, it has as a function the knee extension and protects the knee joint from compression forces. It has a form flattened and rounded, extends down from the base to its vertex *Betts et al. 2014*. The posterior surface has two faces; medial and lateral, which are articulated with the medial and lateral condyles respectively, the middle region articulates with the femoral trochlea during flexo-extension movements. On the other side, the anterior surface is inserted into the anterior wall of the articular

capsule. The posterior surface is covered through a layer of protective cartilage; patellar cartilage, it is smaller dimension than that of the femur, It varies considerably during movements, cushioning the pressure *Kahle et al. 2004*.

1.4. Soft tissues

The soft tissues of the knee joint provide protection, stability, lubrication and nutrition during the articular kinematics. They represent the weak point of the knee joint, due to the forces and tensions to which the joint is subjected. These are articular capsule and Synovial membrane, Bursae, Retinaculum, Tendons, Cartilages, Menisci and Ligaments.

Articular capsule is a fibrous wrap that extends from the femur distal part to the tibia proximal part, surrounding the entire joint and providing stability and protection. It leaves a fluid-filled space, joint cavity where articulating surfaces of the bones contact each other. Inside the articular capsule is located the synovial membrane, that covers the whole capsule in its joint cavity. The cells of this membrane secrete synovial fluid that provide adequate lubrication to the articulating components. The synovial membrane is attached on the margin of the cartilage both in the femur and in the tibia, to the horns of the meniscus and the ligaments *Gosling et al. 2016*.

The Bursae are localized continuous to the joint capsule, are structures of connective tissue filled with synovial fluid. Their function is protective, serving as a cushion to absorb the friction and separating the adjacent structures. Bursae that are found in the articulation of the knee are Sub-cutaneous pre-patellar bursa, located between the skin and the anterior surface of the patella. Superficial sub-cutaneous infrapatellar bursa located between the PT and the skin. Deep infrapatellar bursa, located between the PT and the tibia. Finally, medial and lateral sub-tendinous bursa arranged between the gastrocnemius and the articular capsule *Betts et al. 2014*.

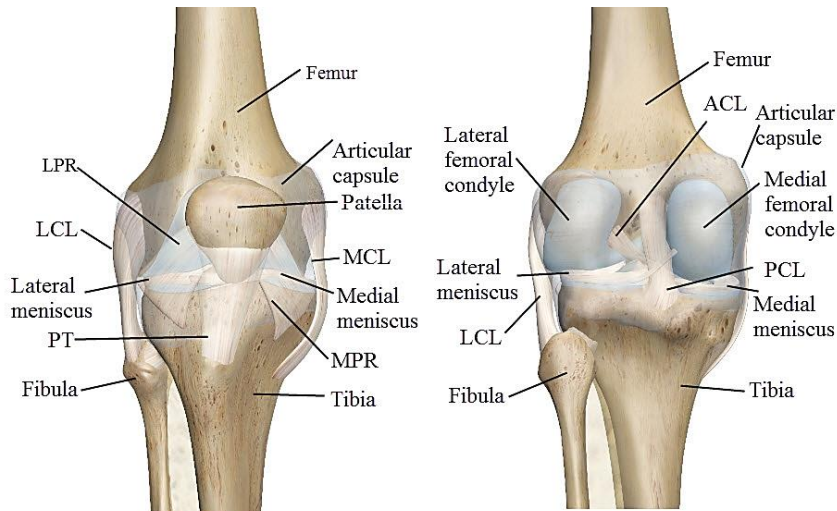
The retinaculum are connective structures that join the patella to the femur, the menisci and the tibia. There are two, medial patella retinaculum (MPR) and lateral patella retinaculum (LPR). The LPR is stronger and thicker than MPR, it is made up of condensations of tissue, which merge with the femoral quadriceps to form a single tendon. It is composed of the various fascial layers, in general, two; superficial and deep layers oriented longitudinally. The MPR is thinner than the LPR one and it does not intervene directly on the position of the patella in relation to the femur. It crosses the knee joint on the medial side of the patella. It also fuses with the femoral quadriceps. Most fibers of the medial patellar retinaculum originate in the femoral region of the vastus medialis muscle *Merican et al. 2008*.

The PT is a ligament that connects the patella with the tibia, is a flat and wide band, very strong, it is in the anterior region of the knee joint, just like the retinaculum, distal to the patella and anterior to the tibia. It is attached in the vertex of the patella, and its fibers continue until inserted into the tibial tuberosity. The QT allows the quadriceps femoris muscles to converge on the base of the patella, both work together to extend the leg. It extends over the patella, and it becomes the PT *Kahle et al. 2004*.

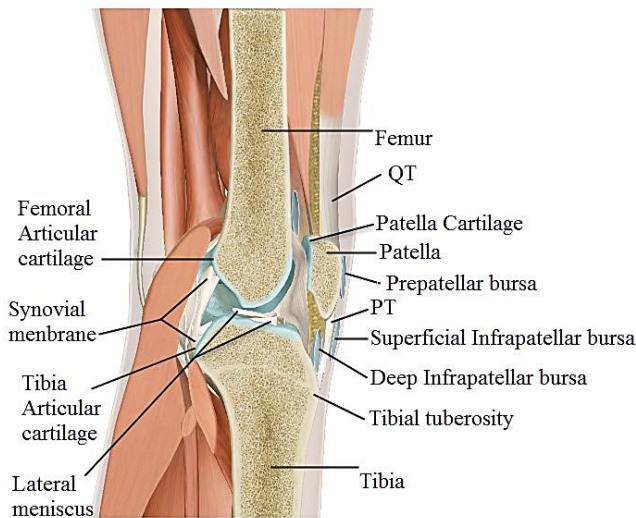
Articular cartilage is highly specialized, its principal function is to provide a smooth, lubricated surface for articulation and to facilitate the transmission of loads with a low frictional coefficient Sophia Fox *et al.* 2009. All the joint sliding surfaces are covered by protective cartilages in the areas of contact. There is, therefore, a cartilaginous covering for both femoral condyles, tibial plateau and patellar contact surface. The layer of cartilage is thicker at points of higher friction. In the femur it is in the femoral condyles and in the throat of the femoral trochlea. The articular cartilage lubrication efficiency is an order of magnitude superior to the best bearing surfaces known to modern engineering. Such efficiencies are achieved despite the lack of blood supply and a tissue thickness. However, its great weakness is the limited repair capacity Merican *et al.* 2008.

The medial and lateral menisci are two asymmetric structures of fibrous cartilage with a semilunar shape that interpose between the femoral condyles and the tibial plateau. The meniscus has two functions. Transfer the load and stabilize the knee during flexion, extension and during circular movements. The menisci move during the backward flexion and the forward extension of the knee to balance the change of the articular surfaces. The medial meniscus moves by up to six millimeters forward and backward during flexion and extension, and it deforms in the process. The lateral meniscus moves even more. It slides up to twelve millimeters forward and back each time when we flex or extend the knee. It also deforms during each flexion and extension movement Vrancken *et al.* 2013. They present greater thickness in the peripheral zone than in the central region. Each meniscus is attached to the tibia through the horns. The lateral meniscus is much closed almost as a ring, while the medial is wider and open. There are common and proper unions for each of them, which allow the stability of these during the movements of the knee joint. The medial meniscus presents greater restrictions at the capsular and ligament level than the lateral meniscus Panesso *et al.* 2009. The common unions are the coronary ligaments, continuations of the joint capsule, which join the periphery of the meniscus to the tibial plateau and transverse ligament in the anterior part. Additionally, the medial meniscus has union in the anterior horn with the ACL and in the posterior horn with the PCL, and is attached to the MCL, while the lateral meniscus only joins in the posterior part to the PCL. The peripheral edges of the menisci are vascularized, but in general, they are considered avascular. The menisci can obtain nutrients through the compressive forces that occur during the kinematics of the knee in motion Smith *et al.* 2002.

The Ligaments are strong bands of connective tissue that provide stability and support, limiting abnormal movements. They work together with menisci and bursae to protect the integrity of the joint. Outside of the articular capsule, the knee joint has two collateral ligaments, located at the medial and lateral region. The LCL or Fibular collateral ligament is in the lateral side and extends from the femur to head of the fibula and it has an oblique orientation down and back. It does not have unions with lateral meniscus. The MCL or tibial collateral ligament is in the medial side and extends from the femur to proximal medial part of the tibia. It is firmly attached on its deep side to the articular capsule and to the medial meniscus. Inside of the articular capsule, the knee joint has two cruciate ligaments, ACL and PCL, these fix femur and tibia, preventing the displacement of both bones on the center pivot beyond the limit of permission Betts *et al.* 2014.



(A) Anterior view of the right Knee joint (B) Posterior view of the right Knee joint



(C) Sagittal section through the right Knee joint

Figure 2. Knee joint. Three-Dimensional (3D) representation of the anatomy of the knee joint. (A) Anterior view of the knee joint with the musculature removed to visualize the bones and major ligaments. (B) Posterior view of the knee joint with the musculature removed to visualize the bones and major ligaments. (C) Postero-lateral view of the knee joint showing the bone, muscle and soft tissues *Hoehn et al.2007*.

1.5. Muscular complex

The muscular complex responsible for the movement of the knee joint is composed by the anterior, medial and posterior compartment of the thigh. The extensors muscles belong to the anterior compartment and the flexors to the posterior compartment. Two exceptions, Gracilis, a flexor, which belongs to the medial compartment and Sartorius, a flexor, which belongs in the anterior compartment *Hoehn et al. 2007*.

Table 1. The Muscular complex of the knee joint.

Description of the muscles belonging to the anterior, medial and posterior compartment of the thigh according to the function, type and action *Drake et al. 2009*.

Agonist muscle	Antagonism muscle	Muscle type	Action
Articularis genus	-	Extensor	It Pulls the supra-patellar bursa superiorly during extension of the knee and prevents impingement of the synovial membrane between the patella and the femur.
Quadriceps femoris; Rectus femoris and three Vastus	Hamstring	Extensor	Extension of the knee; flexion of the hip, stabilizing the patella and the knee joint during gait.
Rectus femoris	Hamstring	Extensor	Extension of the knee; flexion of the hip.
Vastus lateralis	Hamstring	Extensor	Extends and stabilizes knee
Vastus intermedius	Hamstring	Extensor	Extension of the knee.
Vastus medialis	Hamstring	Extensor	Extension of the knee also contributes to correct tracking of the patella.
Biceps femoris; long and short	Quadriceps femoris	Flexor	Flexion of knee, laterally rotates leg at knee (when knee is flexed), extends hip joint (long head only)
Semitendinosus	Quadriceps femoris	Flexor	It Flexes knee, extends hip joint, medially rotates leg at knee.
Semimembranosus	Quadriceps femoris	Flexor	It Flexes knee, extends hip joint, medially rotates leg at knee.
Gastrocnemius	Tibialis anterior muscle	Flexor	Minor flexion of knee and plantarflexion.
Popliteus	-	Flexor	Medial rotation and flexion of knee.
Gracilis	-	Flexor	Is a synergist muscle involved weakly in the flexion and medial rotation of knee; adduction of hip, flexion of hip.

Sartorius

-

Flexor

Is a synergist muscle involved weakly in the flexion and medial rotation of knee;

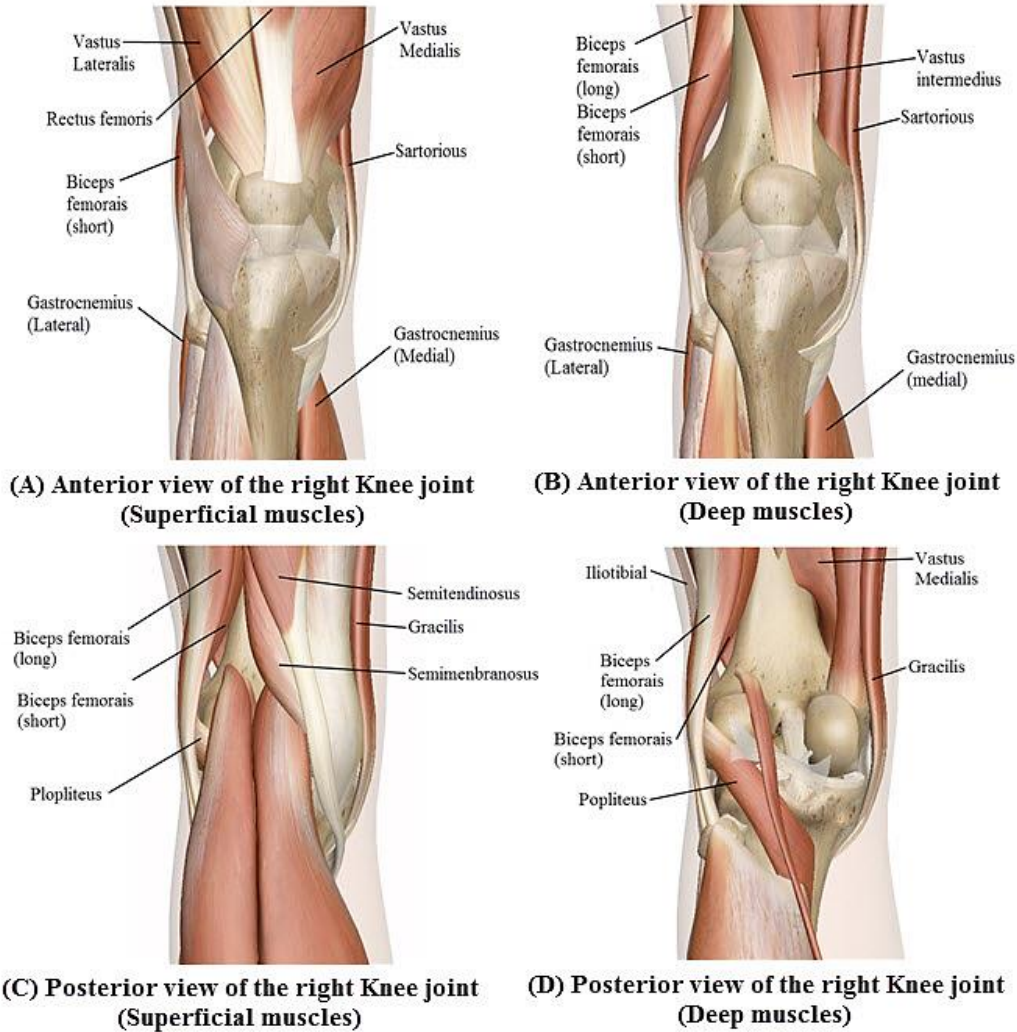


Figure 3. Knee joint. Three-Dimensional (3D) representation of the anatomy of the right knee joint (muscular complex). (A) Anterior view of the right knee joint with the superficial musculature. (B) Anterior view of the right knee joint with the deep musculature (C) Posterior view of the right knee joint superficial musculature. (D) Posterior view of the right knee joint deep musculature *Hoehn et al.2007.*

1.6. Knee Joint: Tibiofemoral joint and Patellofemoral joint

The knee joint can be divided in two functional compartments according to the *McConaill* classification, which consists of two different joints. One between the femur and tibia, Tibiofemoral

joint (TF), and one between the femur and patella. Patellofemoral joint (PF). 2004. The TF is the most important, because puts the surfaces of the femoral condyles in contact with the tibial plates allowing movements of flexion and extension *Kahle et al.* It is classified as joint is of *modified hinge*, a type of *synovial joint*; due to the presence of the articular capsule that contains the synovial membrane and synovial fluid, *composed*; because within the same articular capsule converge the bone components of the leg and thigh. *Ovoid*, because it presents convex femoral condyles and concave tibial plateau. *Complex*, because of it presents the menisci and *biaxial*, in reference to its two degrees of freedom. The PF is formed by the patella and the femoral trochlea. It is classified as *synovial joint, composed, biaxial, in the chair*; due to the shape of the femoral trochlea; concave in medial-lateral direction and convex in superior-inferior sense. On the other side, the patella is convex in medial-lateral direction and concave in superior-inferior sense, connecting perfectly *Kaltenborn et al. 2006.*

1.7. Definitions

Mechanics: It studies and analyzes movement, repose of bodies, and their evolution or change of position over time. Two areas of study; the static and the dynamic. The static responsible for the study of bodies at rest or balance as the result of the forces acting on them; that is, it studies magnitude and strength. Dynamics studies bodies in movement. It includes the kinematics and kinetics *Panesso et al. 2009.*

Biomechanics: It is the study of the mechanical phenomena present in biological systems at any level, from complete organisms to organs, cells and cellular structures. Biomechanics is mainly interested in movement, balance, physics, resistance and the injury mechanisms that can occur in the human body because of the diverse conditions to which it can be subjected. This area of knowledge is supported by various sciences, using the knowledge of engineering, anatomy, physiology and other disciplines *Hatze et al. 1974.*

Kinetics: It is concerned with the relationship between motion and its causes, specifically, forces and torques *Britannica et al. 1965.*

Kinematics: It describes the motion of points, bodies (objects), and systems of bodies (groups of objects) without considering the mass of each or the forces that caused the motion. The description of motion includes position, velocity, and acceleration *Whittaker et al 1988.* Two fields of interest:

Osteokinematics: It is concerned with the description of bone movement when a bone swings through a range of motion around the axis in a joint, such as with flexion, extension, abduction, adduction, and rotation. It does not consider articular surfaces; the possible movements of the bones in the space are:

- **Spin:** The bone rotates around an axis of motion, which is perpendicular to the plane of the articular surface.

- **Balance:** Any movement that is not a spin or that occurs outside the axis of motion perpendicular to the plane of the articular surface.
- **Displacement:** It occurs when one surface moves on another stationary surface.

Arthrokinematics: It studies the intrinsic movement that occurs in the joint without considering the bone segment in each one of its planes, or the joints and the cause that produces it, i.e. the relationship between two joint planes when the movement occurs. The possible movements generated are:

- **Spin:** Movement of an articular surface at the same point on another articular surface around its mechanical axis.
- **Roll:** It occurs in non-congruent joints, i.e. on surfaces with different radius of curvature. It consists of new points on one surface taking new points on another. It occurs on an articular surface in the same plane of sliding but with different axes of movement. The bearing direction of an articular surface always coincides with the movement of the bone, regardless of moving the concave or convex joint surface.
- **Sliding:** It occurs in congruent surfaces, curves or flat. It consists of a point on an articular surface taking new points on another articular surface. Generally, this movement is combined with bearing. The direction of sliding is opposite to the movement of the distal end of the bone where it is produced.
- **Rock:** It is the movement that occurs on the joint surface and it occurs at the end of the rotation with different axes or with an axis, which changes the planes.
- **Rotation:** can be *combined*; rolling but it does not correspond to a free movement and it occurs in the same articulation. *Congruent*; it is performed in adjacent joints and facilitates functional patterns. *Non-congruent*, it occurs in a direction opposite to the adjacent joints, resulting in non-functional patterns of movement *Whittaker et al 1988*.

1.8. Knee Joint Biomechanics

The knee joint acts as a pivot between the two longest bones in the human body whilst the strongest muscles in the body (the quadriceps muscles) act across it. The TF joint has a wide range of motion, reaching up to 160 of flexion (rotation in the sagittal plane), with coupled rotations in the other two planes; this leads to incongruency between articulating surfaces across part of the range of motion. Similarly, the PF joint has a complex, three-dimensional range of motion across TF joint flexion in order to allow minimal quadriceps contraction to extend the knee.

This complex mechanism of knee joint motion means that the geometry itself is not adequate to maintain stability, requiring input from passive soft tissues and muscle tensions. It also means that large forces acting on small articulating areas generate high articular stresses, commonly called joint contact pressure. The complexity of knee joint behavior is a result of the individual behavior of and interaction between three biomechanical demands:

- Static stability e geometry and anatomy of the joint surfaces.

- Active stability e muscle contraction.
- Passive stability e ligaments, menisci and retinacula *Masouros et al. 2010*.

Knee Joint Kinematics

The knee joint to move in six degrees of freedom (three translational motions: anteroposterior, medio-lateral, proximo-distal, three rotational motions: flexion-extension, internal-external, abduction-adduction). The main movements are flexion and extension and in smaller amplitude the internal and external rotation, the last ones take place in the TB. Because of the joint non-congruence and the variation of the elasticity of the ligaments, the knee performs anterior or posterior sliding movements of the tibia or the femur according to the type of kinematic chain, accompanied by a slight abduction and adduction, which seek to balance the forces in varus or valgus. The movements of abduction and adduction are not considered in the osteokinematics of the knee joint *Levangie et al. 2000*.

Knee Joint Osteokinematics

The flexo-extension movement of the knee joint is one of the two degrees of freedom that the articulation has. It is performed in a sagittal plane, with a horizontal axis that passes through the femoral condyles. This axis presents a slight obliquity, but lower in the medial side of the knee joint. This causes that the tibia is directed laterally in the movement of extension and medially in the movement of maximum flexion. The instantaneous rotation center (RC) is a hinge point or axis that only exists in a short space of time. This is where the rolling movement is performed, not sliding movement. When two surfaces are in motion, at any moment there is one that does not move and acts as a RC. In the case of the TF joint, it is located in the femoral condyles and performs semi-circles in the posterior and superior direction. *Fanelli et al. 1996*.

The knee complex has muscles that can generate variations in the range of motion. A standard motion range for knee flexion varies between 130-140 degrees. However, if the hip is in a hyperextension position, the range may decrease to 120 degrees. In the maximum hip flexion, the motion range can increase to 160 degrees. When a closed kinetic chain (CKC)- (foot is fixed in space) is performed, the restriction of movement in other articulations may limit the movements of the knee extension, that is, if there is a restriction on plantar flexion will perform to a restriction in the knee flexion *Levangie et al. 2000*.

The second degree of freedom of movement of the TF joint is constituted by the axial rotation movement, which is generated as a mechanism of automatic rotation. This occurs in the narrow position of the articulation, that is, where the greatest tension of the articular tissues exists. The active rotation of the tibia is different from the automatic rotation, caused by the muscular force and transmitted to the passive components, due to the differences of movements that occur between medial and lateral compartments. The automatic rotation is added by the tension of the cruciate ligaments. The axial rotation occurs around the longitudinal axis when the tibial tubercle is closed. The medial and lateral rotation are movements of the tibia and they are a consequence of joint incongruence and ligamentous laxity. Its range of rotation depends on the degree of flexion-

extension in which the joint is located. Thus, when the knee is in full extension, axial rotation is not possible since the joint surfaces are at their maximum congruence and the soft tissues are tense. From 60 to 70 degrees, rotations can already be produced, at 90 degrees of flexion, the capsule and ligaments are lax and allow external rotation of the tibia, approximately 40 degrees and internal 30 degrees. As with the extension movement, with maximum flexion rotations are limited *Levangie et al. 2000*.

Knee Joint Arthrokinematics:

In the TF articulation, it is necessary to remember the volumetric differences between femoral condyles and tibial plates, since this will determine the movements of the bone surfaces. It is a CKC, in which the articular surface of the femoral condyles moves with respect to the tibial plates. During the flexion, a posterior movement occurs simultaneously with an anterior glide of the femoral condyles that prevents the posterior bearing of the femur, outside the tibial condyle. From 0 to 25 degrees, a posterior bearing occurs, which is accompanied by a previous glide to create a tibia turn. It is considered that there is a pure bearing at the beginning and end of the flexion. The previous sliding is facilitated by the forces, secondary to the movement of the articulating surface, are generated in the menisci. In the extension movement, when the femur moves with respect to the tibia. A bearing of the femoral condyles occurs on the tibia, placing the condyle in the neutral position. Then, there is a posterior sliding of the femoral condyles and finally a turn. There is a difference in the size of the femoral condyles at the end of the flexion and extension movements, there is a mechanism called 'screw home' or automatic rotation of the knee. This occurs in an open kinetic chain (OKC) and CKC *Scott et al.1992*.

In the OKC, the tibia rotates laterally when the femur remains fixed for the last 30 degrees of extension. In the flexion, a medial rotation of the tibia occurs in the femur. This mechanism is due to the existence of an area of greater charge in the medial condyle than in the lateral one. When the entire articular surface of the external condyle has been overcome, the femur rotates around the spine of the tibia until the knee is engaged in extension. The mechanics of PF joint is different to TF joint. The PF joint has various functions such as increase the lever arm of the quadriceps, provide functional stability under load, allow the force of the quadriceps to be transmitted among others. In PF joint, osteokinematics is not mentioned, since its function is to contribute to flexion-extension movements of the TF joint. PF joint describes the movements of medial and lateral inclination, medial and lateral rotation and medial and lateral translation *Levangie et al. 2000*.

During complete extension, the patella is located on the upper surface of the femur and is called patellar extension. In complete flexion, the patella is in the intercondylar groove and it moves to the distal end of the femur. The inclinations of the patella contribute to its adaptation to the irregularities in the intercondylar groove. The medial inclination occurs between 0-30 degrees of flexion and the lateral inclination occurs between 20-10 degrees of knee flexion. In addition, the patella rotates around an antero-posterior axis, which is called according to the rotation movement of the lower pole, either medial or lateral. The movement of medial translation occurs in complete extension with medial rotation of the tibia and laterally with complete knee flexion. It is possible

to note that not all the articular surface of the patella is in contact with the femur during knee flexion-extension movement. During the movement of extension towards flexion of the same, the lower face of the patella comes into contact from 20 degrees, the media face at 45 degrees, the upper face at 90 degrees and the lateral faces at 135 degrees *Scott et al. 1992*.

1.9. Tendons and ligaments: Structure and mechanical behavior

Tendons and ligaments enable musculoskeletal forces to be transmitted and redirected across skeletal joints within the body. In doing so, they also facilitate provide a wide range of joint motion and considerable weight and energy savings associated with locomotor movement. Because of their high tensile strength $\sim 100\text{-}140$ MPa and stiffness $\sim 1.0\text{-}1.5$ GPa, tendons transmit muscle forces over long lengths with minimal “in-series stretch”. Nevertheless, tendon compliance is important for storing and releasing elastic energy to reduce locomotor costs, as well as for allowing muscles to contract economically at lower velocities and strains, and for minimizing the risk of damage to musculoskeletal structures. Given that the maximum tensile stress produced by skeletal muscles is $\sim 200\text{-}400$ kPa, a tendon about only $\sim 1/1000$ the physiological cross-sectional area of a muscle can, therefore, safely transmit the muscle’s force without failing. To the extent that tendons suffer damage through repeated loading activity and require repair, or must be sufficiently stiff, rather than being of adequate strength, their thickness and safety factor will tend to be higher. By transmitting tensile stresses, as flexible structures tendons and ligaments also easily bend and change shape to accommodate changes in joint position and skeletal orientation *Biewener et al. 2008*.

Highly paralleled collagen fibrous units characterize tendons and ligaments. Accordingly, it can be argued that these tissues are analogous to engineering fiber composites where fibers are laid down in parallel for directional reinforcement. Although tendons and ligaments are structurally very similar, the highly paralleled collagen fibers feature is found in both tissues differences in the anatomical locations of tendons (attaching muscle to bone) and ligaments (attaching bone to bone) mean that they serve different functions in the musculoskeletal system. Thus, the tendon transmits load generated by the muscle (during contraction) to the bone to enable joint movement. Ligaments provide mechanical stability (being shorter than tendons) by constraining and guiding joint motion through tensile and torsional loading action *Goh et al. 2014*.

The collagen type I is the predominant protein of these structures, making up approximately 90% of the dry weight, type III collagen is also present but has been found to be more involved in healing and remodeling processes *Hsieh et al. 2000*. All collagen type I based tissues exhibit non-linear elastic properties, reflected by stress-strain curves this means that tendons and ligaments exhibit greater compliance at low stresses than at intermediate to higher stresses, enhancing their energy absorption capacity at low stress levels. A greater compliance at the onset of loading, combined with slight viscous damping, therefore, represent key properties of tendons and ligaments that reduce their susceptibility to damage, as well as the susceptibility of their skeletal attachments and the skeleton more generally. This is clearly important given that these structures must function over

a large number of loading cycles during an individual's lifetime *Biewener et al.* The composition of tendons and ligaments plus the hierarchical organization of those components are, therefore, crucial to the ability of the tissues to perform their structural roles *Shrive et al. 2003*.

Tendons and ligaments are composed of collagen fibrils, which appear parallel under high magnification. These fibrils form fibers that run parallel to the long axis of the ligament. A large number of collagen fibers merge together to make sub-fascicular unit. A thin band of connective tissue called the endotenon surrounds the sub-fasciculus. In humans, the amount of endotenon is great, which makes the ligament appear to be made of bundles and less uniform. Three to 20 sub-fasciculi are bound together to form the collagen fasciculus. Other connective tissue called epitenon surrounds the fasciculus and is denser than the endotenon. Surrounding the entire ligament is the paratenon, which blends with the epitenon. The synovium then covers the ligament, making it extrasynovial *Danylchuk et al. 1978*.

A sketch of a typical stress–strain relationship is illustrated in Figure 4 (A) for a tendon, with sequential images to depict how it is recruited into tension and how it eventually ruptures. The basic features associated with the following regions: (1) Toe to heel, (2) Linear (elastic deformation), (3) Yielding, transition (peak stress), and (4) Plastic deformation and (5) Failure, is also found in ligaments.

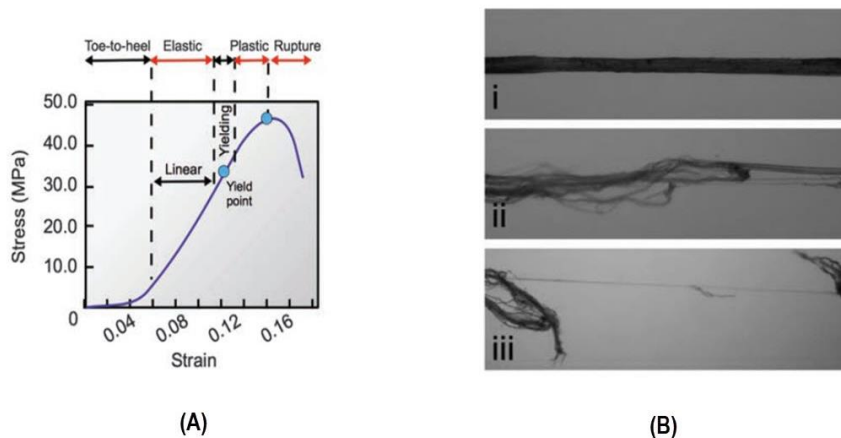


Figure 4. (A) Tendon strain-stress curve with characteristic regions. (B) Sequential images of the tendon rupture, (i) at initial loading, (ii) defibrillating immediately after the maximum stress and (iii) rupturing to the point where the ruptured ends were bridged by only a single strand of collagen fiber. The displacement rate corresponds of 10 mm/min (intended for modeling normal physiological loading a displacement rate of 500 mm/min is intended for modelling extreme loading) *Goh et al. 2014*.

The mechanical response of soft connective tissues to an external load depends of displacement rate. The profiles are not quite the same, at high displacement rates, the mechanisms regulating

fibril rupture predominate. High displacement rates are associated with high stiffness and high strength; low displacement rates are associated with low stiffness, and low strength. The reason for these differences is that the mechanical response is time-dependent and the overall mechanical response is a combination of both the elastic response and the viscoelastic responses.

In particular, the viscoelastic behavior can be investigated by creep tests and stress relaxation tests. It is well-known that the mechanical response associated with the creep process involves increases in strain with time when the tissue is subjected to a constant load. When the structures are kept at a constant stretch for a continuous time, the load required to maintain elongation decreases and reaches a steady state after a certain time. This phenomenon is called the stress-relaxation behavior. When collagen I based structures are exposed to a constant load over a period of time, these lengthen until a steady state is obtained, which is called creep. These properties are facilitated by a complex interaction of cross-links, collagen fibers, and cellular components *Scheffler et al. 2012*.

In fact, knee soft connective tissues are shown to be exceptionally well suited to their roles, with an efficient mechanism to resist creep and fatigue. However, during repetitive activity, ligaments are subjected to tensile repeated load, and in elastic systems, repetitive loading can lead to failure through fatigue. For that reason, the consequences of ligament injury or reconstruction become comprehensible in the light of normal growth, architecture, and mechanics. Attempts at ligament reconstruction inevitably have difficulty in recreating the original structure *Shrive et al.2003*.

1.10. Injuries of the Knee Joint

Ligamentous injuries of the knee joint are among the most common ligament injuries reported by clinicians *Fetto et al. 1980*. The ACL and MCL are major ligaments contributing to the stability and normal functioning of the knee joint. Indeed, Injuries of various degrees occur to these ligaments during exercise, sports, and nonspecific trauma *Balkfors et al. 1982*.

Injuries to these ligaments can be clinically classified in three degrees. A first-degree, it involves a tear of a minimum number of fibers or less than one third of the ligament. There is minimal hemorrhage and swelling, localized tenderness, and no clinical instability or laxity. Second-degree, it involves a tear of more ligamentous fibers, two thirds of the ligament, with a greater loss of function, localized tenderness, and an effusion, but there is no laxity or noticeable instability. Third-degree injuries have greater disruption (greater than two thirds of the ligament), more tenderness, and demonstrable laxity of the knee joint. Finally, outside the classification is the total rupture of the ligament. Research have demonstrated that the ACL has a poor repair response to injury, whereas, the MCL heals readily without even the need for surgical repair in most cases *Anderson et al. 1992*.

The main difference between cruciate and collateral ligaments is the blood supply. For example, the MCL has a rich blood supply, which it derives from the inferior medial artery geniculate and from its osseous attachments. On the other hand, the blood supply to the ACL is possible thanks to a paraligamentous network of vessels courses through the synovial membrane. These vessels enter

the ligament transversely and anastomose freely with endoligamentous vessels. The core of the midportion of the cruciate ligament is less well vascularized than the proximal and distal cores. Other differences between ligaments are mechanical forces, number of bundles of microfilaments and local environment. *ALM et al. 1974.*

The cruciate ligaments (ACL and PCL, respectively) resides in a unique environment. Both ligaments are intracapsular, and both are enveloped by a synovial membrane, effectively making them extra synovial. The synovial membrane has only a few cells thick and separates the ligaments from the synovial fluid that bathes the other intracapsular knee joint structures. During ACL injury, the synovial membrane is usually torn, exposing the frayed ligament ends to the synovial fluid and to a host of potentially destructive enzymes released by the breakdown of hemarthrosis fluid in the injured joint. This local environment has been referred to as the "hostile" environment of the synovial joint space *ALM et al. 1974.*

Studies conducted by Burrige and Chrzanowska found that the number of bundles of microfilaments (representing stress fibers) in the ACL is greater than in the MCL. The fiber bundles were separated by narrow spaces and the crimp pattern for the ACL collagen fiber bundles were more compact. The results supported the conclusion that due to number of bundles of microfilaments, crimp pattern, cellular-biological characteristics and cellular alignment, the intrinsic properties of collateral and cruciate ligaments had diverse mechanical behavior *Ehrlich et al. 1977.*

Most ligament knee injuries result from high energy trauma and may have nerve and vascular injuries accompanying them. Nowadays, patient clinic history and physical examination remains the core of the clinician's diagnostic expertise. However, the diagnostic imaging provide an accurate assessment of internal derangements of the knee. Routine and advanced imaging techniques can define the extent of ligamentous injuries of the knee, and give important information regarding additional knee injuries in the setting of ligamentous injury. Typically, conventional radiography is the initial step in diagnostic evaluation of the injured knee. The routine radiographic examination of the knee consists of multiple projections. In evaluating acute knee injuries, the antero-posterior and lateral views are routinely obtained. Complete assessment with conventional radiography may require supplemental projections, including tunnel, merchant, oblique, and cross-table lateral views. Routine radiographs, by themselves, do not allow direct visualization of injured ligaments or tendons. Soft tissue abnormalities that may accompany tendinous or ligamentous injury of the knee include swelling, joint effusion, and change in contour or configuration of an injured tendon or ligament. A bloody effusion, often associated with intra-articular ligament damage, is detected as a soft tissue density in the supra-patellar pouch on the lateral projection *Cockshott et al.1985.*

Advanced imaging techniques, and in particular MRI, has become a common, accurate, and cost-effective method for diagnosis of ligamentous knee injuries. In the United States (US), MRI has all but replaced arthrography, conventional tomography, and CT in the assessment of internal knee derangements. CT plays a role in the further assessment of suspected or diagnosed fractures of the

knee on routine radiographs, although are less helpful in the diagnosis of ligamentous or tendinous injuries without associated fractures. The excellent tissue characterization, high resolution, lack of ionizing radiation, and multiplanar capabilities of MRI have led to its rapid acceptance in the workup of patients with suspected ligamentous injury. Indeed, MRI is playing an increasingly large role in the diagnosis of many musculoskeletal abnormalities *Groof et al.2003*.

As mentioned, the ligaments injuries are the most frequent in the knee joint. Especially The ACL tear, the structure is one of the most commonly injured in US. It is estimated that 1 in 3,000 Americans sustains an ACL disruption every year, with approximately 95,000 new injuries each year, and approximately 50,000 reconstructions performed each year. Consequently, a great deal of effort has been directed at reconstructing this structure. The overall success of ACL-R is a function of multiple factors, including, the presence of concomitant injuries, mechanical properties of the graft, graft placement and tensioning, the method of graft fixation, the biologic response and remodeling of the graft tissue, and postoperative rehabilitation of the knee among others. When choosing a graft, the surgeon must consider the initial mechanical properties of the graft, the morbidity of graft harvesting, the remodeling and incorporation of the graft, and ultimate stiffness and strength over time. The biochemical, histologic, neural, and vascular changes that take place in the ACL graft ultimately determine the graft’s viability and consequently its ability to act as a functional replacement for the native ACL *Daniel et al. 2003*.

Common graft sources for ACL reconstruction include Achilles tendon allograft, quadriceps tendon, (BPTB), and hamstring autografts or allografts. Table 2 illustrates general categories of grafts. Reconstruction procedures with auto-graft tissue, either medial hamstring or bone patellar tendon-bone (BPTP) grafts, has become the treatment of choice for disabling instability due to ACL deficiency. Other options such as prosthetic replacement have been universally abandoned *Richard et al. 1989*.

Table 2. Graft choices *Daniel et al. 2003*.

Autografts

Patellar tendon

Hamstring tendon

Semitendinosus

Gracilis

Multiple looped

Central quadriceps

Achilles tendon

Fascia lata/iliotibial band

Meniscus

Reharvested patellar tendon

Allografts

Patellar tendon
Hamstring (semitendinosus/gracilis)
Fascia lata/iliotibial band

Achilles tendon
Anterior cruciate ligament
Tibialis anterior
Peroneal tendon

Synthetic grafts

Gore-Tex
Dacron
Carbon filaments
Polyester

Engineered grafts

Fabricated collagen bundles
Demineralized bone matrix

Choosing the best type of graft for reconstruction of the ACL remains controversial. Whatever the choice may ultimately be, it must possess some important characteristics such as ease of implantation, durability over time, functional similarity to native ACL, low risk for complications, and economic feasibility. A key component of graft durability and function is the appreciation that the ACL is a complex viscoelastic organ. It not only displays inherent strength, but also serves as a proprioceptive device *Daniel et al. 2003*.

1.11. Anterior Cruciate Ligament Reconstruction: Anatomic placement-fixation.

Surgical reconstruction in chronic ligament injuries is indicated for functional instability. Knees may have early post-traumatic arthrosis, so, it is important to define all the structural injuries. These may include ligaments, meniscus, articular surface, and TF malalignment pathology. Surgical treatment may include ligamentous reconstruction, osteotomy, articular cartilage resurfacing, and meniscus surgery (resection, repair, transplantation). For this reason, it is necessary to control key factors within the reconstructive procedure. Tunnel placement is probably the most important factor in successful ACL surgery. Errors in both femoral and tibial tunnel placement have been blamed for limited postoperative knee range of motion, recurrent effusions, pain, graft elongation, and graft failure. Tunnel placement not only affects the mechanical properties of the graft but also affects the ligamentization process of graft healing *Amiel et al 1986*.

Girgis reported the ACL tibial footprint fans out anteriorly as it inserts into a wide depressed area in front of and lateral to the medial intercondylar tubercle. It sends a well-marked slip into the

anterior horn of the lateral meniscus. The ACL tibial footprint fans out anteriorly as it inserts into a wide depressed area in front of and lateral to the medial intercondylar tubercle. It sends a well-marked slip into the anterior horn of the lateral meniscus. He noted that the tibial attachment was wider and stronger than the femoral attachment and he reported the average footprint length of the ACL was 15 mm. However, recent studies have reported tibial insertion lengths of 15 to 18.5 mm and widths of 10 to 13 mm (figure). Morgan measured the distance from the anterior border of the PCL to the center of the ACL tibial insertion as 7 mm or 10 mm when the intercondylar spines were removed. This would place the posterior border of the ACL virtually adjacent to the posterior margin of the tibial plateau. More recently, *Colombet* and *Heminget* have referenced ACL tibial footprint measurements to the fovea on the tibial plateau containing the PCL (Figure). This indentation on the posterior tibial plateau has been described as the posterior fovea, retroeminence ridge, or PCL notch. Colombet measured the distance from this notch to the posterior boundary of the ACL as 10 mm, while Heming recorded this same measurement as approximately 6 mm (Figure 5(A)). Colombet placed the center of the tibial insertion 19 mm anterior to the PCL notch, while Heming placed the center 15mm anterior to the PCL notch. The implication of these studies is that ACL reconstructions seeking a tunnel in the center of the tibial insertion should direct a guide pin approximately 10 mm further anterior than suggested by Morgan. Grafts tend to lie in the posterolateral region of a tibial tunnel; therefore, tunnels should be placed anterior and medial to the desired location of the graft *Steiner et al 2008*.

Radiographically, the center of the tibial insertion in the sagittal plane has been described relative to a line parallel to the tibial plateau and passing through the most anterior and posterior points on the plateau. *Amis* and *Jakob* reported the center of the ACL tibial insertion as 43% along this line from its anterior border. Other reported measurements have been in close agreement. Image-guided surgical guidance systems use radiographic anterior-posterior and medial-lateral measurements in their algorithms to identify the location of the tibial tunnel. A practical land-mark for the medial to lateral insertion of the ACL is the space between the spines of the intercondylar eminence (Figure 5 (B)). The ACL does not attach directly to these spines, but its insertion is framed on its medial and lateral aspects by these spines *Steiner et al 2008*.

The ACL is attached to the femur and tibia not as a singular cord but as a collection of individual fibers of different lengths that are not parallel. This has led to a simplistic grouping of fibers as two distinct bands, anteromedial and posterolateral bands. These bands as distinct bundles do not exist *Clark et al. 1990*.

Girgis established firm anatomic measurements for the femoral insertion of the ACL, and other studies have further characterized the anatomy. They measured the length of the femoral insertion as 23 mm with the posterior border 4 mm from the articular cartilage. *Odensten* and *Gillquist* measured a femoral insertion 18 mm long and 11mm wide. *Mochizuki* measured a 15 mm length and a 5 mm width, but fibrous tissue was removed to measure the mid-substance only. *Colombet* measured a length of 18 mm, a width of 10 mm, and a 2.5 mm separation from the articular cartilage. *Heming* measured a femoral length of 18.4 mm, a width of 9.5 mm, and a distance to the

posterior articular cartilage of 4 mm (Figure 5 (C)). Consolidating these studies and emphasizing the more recent data, the ACL femoral insertion has an approximate average length of 18 mm, width of 10 mm, and a separation of up to 4 mm from the articular cartilage. The long axis of the femoral insertion is rotated in the sagittal plane relative to the axis of the femur, reflecting the insertion's congruity to the posterior border of the femoral condyle. Girgis measured this rotation as 25°, Odensten and Gillquist 26°, and *Heming* 29° (Figure 5 (C)). A generalization would be a rotation of the footprint or “flexion” of 25° to 30° relative to the femur in the sagittal plane *Steiner et al 2008*.

The femoral insertion can also be arbitrarily partitioned into insertion sites for the anteromedial and the posterolateral bands. This delineation of the ACL into two bands is based on the ligament's gross appearance; best visualized when the knee is flexed 90°. The two bands take their names from their tibial insertions, but they can be traced to continuous origins on the femur. Both *Mochizuki* and *Colombet* described a transverse partition of the femoral insertion to delineate the attachments of the slightly larger proximal anteromedial band and the slightly smaller distal posterolateral band. While length, width, and posterior condylar offset measurements are important, the proximal-distal and medial-lateral ACL locations are most challenging to identify during surgery. The arthroscopic image of the femoral insertion changes with flexion of the knee.

The anteromedial band is at the top of the notch, regardless of knee flexion angle, but the posterolateral band appears to rotate anteriorly and laterally with knee flexion. Adding to the complexity is the variable inclination of the intercondylar roof. Front, to back visualization of the notch is best when the roof is parallel to the tibial plateau, and on average, this is when the knee is flexed 65°, but there is considerable variability. Further complexity is provided by inconsistency in the shape of the arch of the intercondylar notch. In some knees, it can be very challenging to identify and place an anatomically correct femoral tunnel. To identify the proximal-distal position of a femoral tunnel or ACL insertion, there has been a general convention of characterizing the femoral position as referenced to the face of a clock. Although this method can be useful, it requires two stipulations to be precise. One, the flexion angle of the knee must be specified, and second, the transverse reference axis for the clock face must be established (Figure 5 (D)). Unfortunately, most clock face descriptions of the femoral ACL insertion have not made either of these stipulations. Only data from *Mochizuki* and *Heming* have stipulated knee flexion and an anatomic axis for a clock. Both reports specified knee flexion of 90° and a clock face referenced to the posterior femoral condyles. Viewed in this fashion, both reports placed the center of the femoral origin halfway between the apex of the notch and the edge of the articular cartilage at the base of the notch. When the knee is flexed 90° and the 3 to 9 o'clock axis is the lateral wall–articular cartilage junction, the proximal margin of the ACL will be at approximately 11 o'clock, and its distal ACL margin will be at approximately 10 o'clock *Steiner et al 2008*.

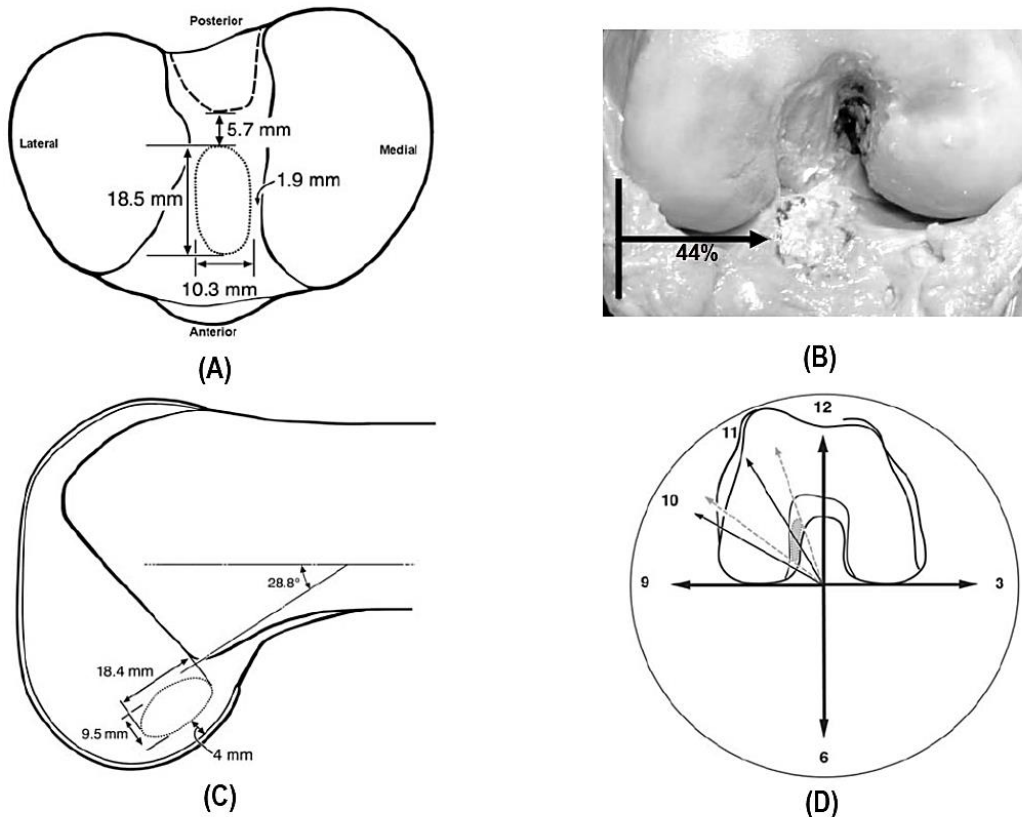


Figure 5. (A) The oval-shaped tibial insertion of the anterior cruciate ligament (ACL) in the transverse plane. The distance from the PCL notch to the posterior fibers of the ACL of 5.7 mm. The length of 18.5 mm, and the width of 10.3 mm. The closest point from the medial aspect of the insertion to the medial tibial articular cartilage of 1.9 mm. The center of the footprint of 15 mm anterior to the PCL notch. (B) The tibial footprint of the anterior cruciate ligament lies between the spines of the intercondylar eminence and does not extend posterior to the medial spine. (C) The oval-shaped femoral insertion of the ACL viewed in the sagittal plane. The footprint rotated to 28.8° to the shaft of the femur the footprint length 18.4 mm, and the width 9.5 mm. (D) Depiction of the femoral intercondylar notch with the knee flexed 90° . The femoral ACL footprint lies on the lateral wall of the notch and spans a region on a clock face from 10:14 to 11:23. This location of the footprint is based on 3 to 9 o'clock axis placed on the posterior femoral condyles. Changing the knee flexion angle or the stipulated 3 to 9 o'clock transverse axis will change the appearance of the footprint *Steiner et al 2008*.

1.12. Anterior Cruciate Ligament Reconstruction: Anatomic femoral and tibial tunnel placement

In a widely referenced study conducted by *Hefzy*, it was demonstrated that altering the femoral attachment of the ACL had a much larger effect than altering the tibial attachment, which helped

encourage further evaluation of femoral tunnel placement. In the past, the most common femoral tunnel error was to place the femoral tunnel too far anteriorly resulting in a graft lax in extension, tight in flexion. This resulted in a knee with limited flexion or if flexion was regained, a nonfunctional graft. Partially as a result of this anterior placement problem, the over-the-top (OTT) position was recommended, which resulted in a graft tight in extension but lax in flexion. The OTT position results in laxity from extension to flexion and, therefore, causes the graft to tighten excessively in knee extension *Acker et al 1989*.

Currently, there are three commonly used ways to find the center of the femoral tunnel, which allows placement of a Beath pin or K wire. This location may be selected using direct visualization (freehand), a guide that keys off anatomic landmarks, or a device that measures isometry. All methods require finding the true OTT position, the most posterior aspect of the intercondylar notch. Once a notchplasty (surgical procedure to enlarge the intercondylar notch and space available for an ACL graft during knee reconstruction) has been performed, this is relatively easy. A shaver is used to remove the proximal portion of the remaining ACL and or fibrous tissue posteriorly. Care is taken not to take a significant amount of bone posteriorly off the femur, because this can change isometry. Clear visualization of the posterior notch is mandatory. There are often small vessels there that require electrocautery. Once clear visualization of the posterior notch has occurred, then a nerve hook can palpate the OTT position superiorly. The nerve hook tip will completely fall behind the notch in contrast to “resident's ridge.” Freehand techniques and the use of an OTT-referenced guide are similar: both pick a specific distance anterior to the OTT position as the entry point for the guidewire. If femoral interference screw fixation is desired, the tunnel site should have 1 to 2 mm of posterior cortex remaining to protect vascular structures and provide adequate bone for fixation. If the surgeon has a 10 mm block of BPTB graft, a 10 mm femoral tunnel is selected. A 7 mm offset femoral guide is used; this leaves 2 mm of posterior cortex. Many user-friendly femoral guides use an OTT referenced system. The “shoe” of the guide slips around the back of the notch with care taken to maintain contact with the posterior cortex with the anterior portion of the shoe *Daniel et al. 2003*.

Hefzy noted a larger isometric (2mm) zone proximally, so most authors are recommending an entry point high in the notch, at the 11 or 1 o'clock position. Because this position puts the K wire and, therefore, the reamer close to the PCL, care needs to be taken to not damage the PCL. These guides require use of a more inferior medial portal; however, some guides can be used through the tibial tunnel. *Cooper* evaluated femoral tunnel placement variables in a cadaveric study. A central tibial tunnel was used. The authors evaluated placing the femoral tunnel at the 12 o'clock (straight up) position or a rotated position at the 10:30 or 1:30 o'clock position. The other variable in the study was in the amount of posterior wall offset using a 5.5 or 7 mm offset guide. A 10 mm femoral tunnel was then reamed. Thus, for the 5.5 mm offset guide, 0.5 mm of posterior wall remained, and for the 7-mm offset guide, 2 mm of posterior wall remained. Therefore, four pin positions were tested with a custom isometer. Excursions of the resulting PT reconstructions were then tested. Isometry was tested and plotted at 15° increments from 0° to 120° of knee flexion. The straight up, 12 o'clock position using the 7 mm offset guide was the most isometric *Daniel et al. 2003*.

Freehand techniques are similar to that described earlier, however, the surgeon measures the distance with a graduated nerve hook or estimates the distance anterior to the OTT position. The third commonly used method to find the femoral tunnel involves the use of an isometer. *Graf* introduced the use of a spring-scale isometer that measures displacement between two points. A small screw or tack is placed at the center of the femoral origin of the ACL after drilling the tibial tunnel. The knee is taken through a range of motion from full extension to the maximum available flexion (usually about 110°) based on patient positioning. An acceptable position is one that allows 1 to 3 mm of elongation (tightening) in the final 20° of extension and 0 to 1 mm of tightening in flexion past 90°. This pattern most closely mimics the native ACL *Beck et al. 1992*.

Based on the known biomechanics of ACL, the tack position can be changed. A commonly used isometer (Acufex, Smith and Nephew Endoscopy, Andover, MA) is described in Figure 6. For example, if the tack is moved directly anteriorly, the effect is lengthening of the distance between the tack and the isometer (as the knee is flexed from full extension), which means the graft will tighten in flexion. Some experienced knee surgeons routinely use isometers. *Paulos and Rosenberg* stated that in their experience, at least 25% of the femoral sites initially selected were changed by the use of an isometer. However, other knee surgeons report no benefit in the routine use of isometers. *Barrett* compared two groups in which BPTB graft reconstructions were performed with the only variable being the use of an isometer. No benefit was found with the use of an isometer. *Morgan* compared the current isometers, which have the measuring device at the level of the distal tibial tunnel, to an experimental device measuring isometers proximally at the level of the ACL insertion on the tibia. Significant differences were found between the two methods. The authors report that current isometers do not accurately measure the intra-articular length changes. *Johnson* report that care must be taken in interpreting isometry data and that clinical judgment and attention to anatomic position of the tunnel is needed *Daniel et al. 2003*.

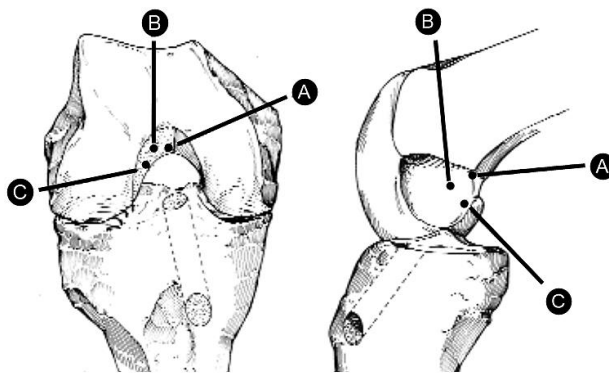


Figure 6. Point A is proximal and high in the notch and typically demonstrates an isometry pattern that mimics normal anterior cruciate ligament. Point B is distal (anterior as viewed arthroscopically) and generally demonstrates unacceptable elongation in flexion. Point C is lateral and posterior in the notch and generally demonstrates excessive strain in extension. Femoral site behavior will vary slightly depending on the accuracy of the previously selected tibial location. (From Acufex, Smith and Nephew Endoscopy, Andover, MA, with permission.) *Daniel et al. 2003*.

In reference to the tibial tunnel, over the past decade, femoral graft placement has been emphasized as a source of non-isometric placement. *Hefzy* also noted earlier, evaluated tibial and femoral attachment sites and noted the greatest effects on isometry by changing the femoral positions. However, minor changes were noted on the tibial side as well. Moving the tibial insertion point in the antero-posterior plane altered specific geometric variables, altering the location of the most isometric (2 mm zone) femoral zone. Medial lateral changes had a much smaller effect. Although the tibial side has a smaller effect on isometry, controversy exists regarding placement of the tibial tunnel. *Jackson* and *Gasser* described four consistent anatomic landmarks to select the central point of the tunnel: (a) the anterior horn of the lateral meniscus, (b) the medial tibial spine, (c) the PCL, and (d) the ACL stump. They extended an imaginary line from the anterior horn of the lateral meniscus into the stump of the old ACL. This point is consistently located 6 to 7 mm anterior to the anterior border of the PCL, which can be measured with a probe. This tunnel should be in the posterior one half of the ACL footprint. Using their guide system, a 60° tibial angle is selected. By using a calibrated tibial guide system at 55° to 60°, the tibial tunnel will be parallel to the intercondylar roof. They recommended the center of the tunnel medial to lateral be at the base of the midportion of the medial tibial spine. The ideal tibial tunnel angle is one that is parallel to the intercondylar roof with the knee in full extension. *Müller* noted that the ACL and the intercondylar roof must lie on a line that forms a 40° angle with the long axis of the femur. *Good* measured this roof angle to be about 35°. If one assumes a femoral intercondylar roof angle of 35°, the tibial guide needs to be set at 55° to the long axis of the tibia to make the tibial tunnel parallel. Most of the current ACL guides can be adjusted, and usually a tibial tunnel angle of about 55° to 60° is fine than or equal to 2 mm. *Daniel et al. 2003*.

1.13. Anterior Cruciate Ligament Reconstruction: Surgical technique

When performing arthroscopic ACL-R, it is important to make tibial and femoral entrances in the anatomic location. The autograft arthroscopic single bundle (SB) is the “gold standard” technique for ACL-R. Initially, the most popular femoral drilling method was the two-incision technique, where were necessary two tunnels and a lateral femoral incision or with a femoral half-tunnel drilled from the joint, thus avoiding the lateral incision. Nowadays, the single-incision techniques have shown better clinical outcomes. Techniques such as transtibial technique (TT), anteromedial (AM) portal technique, and outside-in technique have been employed for many surgeons. Among them, TT is the method of choice for the femoral/tibial tunnels placements. The TT is the most widely practiced technique, this has an extensive record, showing excellent results.

The TT is familiar to most orthopaedic surgeons. It has that the femoral tunnel position is dictated by the tibia bone tunnel. Several studies have been performed to show that techniques such as AM portal and outside-in methods, where femoral tunnel positioning is independent of the tibial tunnel, can produce an anatomically positioned femoral tunnel more easily than the transtibial technique. However, both techniques have their disadvantages. In the case of the AM portal technique, early rehabilitation tends to be stalled owing to short femoral tunnel length, risk of posterior wall damage,

and relatively weak graft fixation, and thus, in the long-term, it leads to tunnel expansion and failure of ACL-R. Although the outside-in method can produce a longer femoral tunnel, the steep slopes of the graft and tunnel result in complications such as graft damage and tunnel expansion. Furthermore, additional incision of the skin that is required in this process makes it esthetically unpleasing *Lee et al.2017*.

Surgical technique

Description and summary of main steps of the TT of anatomic single-bundle ACL-R.

1. Initial marking of anatomic femoral ACL footprint via transanteromedial portal
2. Making a triangular, funnel-shaped bony trough
3. Free handling of femoral guide pin without offset guide
4. Gradual widening of femoral tunnel by changing the knee angle
5. Stronger fixation of the graft with dual fixation at tibia and femur *Lee et al.2017*.

After detecting ACL rupture by arthroscopy (remove of ACL portions), the graft is harvested (BPTP or semitendinous tendon most common). A microfracture is placed through the AM portal just behind the *bifurcate ridge* to make the center of the anatomic femoral tunnel. This center is deepened and widened to allow space for the guide pin through the tibial tunnel. Since the anatomic femoral tunnel is prepared by the AM portal viewing from the anterolateral (AL) portal, the transtibial guide pin tends to be located more to the anterior and distal position of anatomic center than anticipated. *The triangular*, funnel-shaped bone trough is employed via the AM portal to slip the eccentrically positioned guide pin into the anticipated anatomic center, which is part of modified transtibial technique. An ACL-guide is used to make the tibial tunnel at an angle of 47.5°. The tunnel is positioned in the center of the remnant ACL stump. The guide pin is placed above the *pes anserinus* and in front of the MCL. The tibial tunnel is made to have the same diameter as the graft using an expansion *reamer*. As soon as the reamer penetrates into the cortical bone of the tibial plateau, the expansion is ceased immediately to prevent further damage of residual fibers of the ACL. The guide pin is inserted into the tibial tunnel toward the preformed funnel-shaped bone trough with a free-hand technique. Generally, the guide pin is placed more distally and anteriorly than the anatomic center of the femoral attachment site, as seen by arthroscopy. When the knee joint is moved to an extension position during surgery, the guide pin will engage in a way to slip into its anatomic center from the tip of the bone trough. At this time, the guide pin is bent at the intra-articular aperture of the tibial tunnel. Since the femoral tunnel was made following the bent guide pin, the smallest diameter (6 mm on average) was used to start off the reaming just near the cortex. Then the new straight guide pin is inserted, redirecting in the same orifice. The reamer for a suspensory fixation system is used for the reaming until the far cortex, and the length of the femoral tunnel is measured. Upon femoral tunnel expansion, in order to gain sufficient length and reduce posterior wall damage, the knee joint is moved gradually from the extension to the flexion position. When the reamer passes over the bending portion of the guide pin, the knee should be moved to extension. Once the reamer passes through this region, the knee joint is returned to a flexion position and the reamer is expanded to produce a femoral tunnel that has a similar diameter

to that of the graft. The graft is channeled through the tibial tunnel and then through the femoral tunnel. After the graft passage, femoral fixation is achieved using the suspensory fixative device and the *bio-cross pin*. If the femoral tunnel length is below 30 mm, the Endobutton is used solely in a press-fit approach. Tibial fixation is performed with a *bioabsorbable interference screw* and a cortical bone screw with washer. The diameter of the bioabsorbable screw is made to be the same size as the graft *Lee et al.2017*.

1.14. Knee joint Osteoarthritis

OA was clinically defined as an articular degenerative condition characterized by progressive loss of articular cartilage, marginal bone hypertrophy (osteophytes) and changes in the synovial membrane *Figueroa et al. 2015*. The diagnosis of osteoarthritis (OA) has most often based on radiographic evidence, rather than clinical features *Arnett et al. 1988*. An osteoarthritic (OA) knee patient usually presents to the clinician with varying symptoms including pain, stiffness, instability, and difficulties in activities of daily living. In patients with significant symptoms, the decision of whether to offer a knee arthroplasty (KA) (surgical reconstruction of the knee joint) is dependent on confirmation of bone-on-bone arthritis in the affected knee *Oosthuizen et al.2019*.

The degenerative disease results in cartilage failure at synovial joints and is classified according to its severity. OA is classified as primary or secondary to a diagnosed cause. Primary osteoarthritis (OA) is the most commonly diagnosed form of OA, this is largely due to the "wear and tear" of the joint due to its use. Because of this, it is associated with aging; in fact, age is the most potent risk factor for OA. Theoretically, primary OA is inevitable. People tend to develop this type of OA from the age of 55 or 60. On the other hand, it have the secondary Osteoarthritis (OA) that results from the conditions that induce a change in the cartilage microenvironment. Such conditions include major trauma, common congenital abnormalities, metabolic defects, infections, diseases and disorders that alter the normal structure and function of cartilage. Common risk factors that can lead to secondary osteoarthritis include trauma (particularly ACL and meniscal injury), obesity, and sedentary lifestyle among other conditions *News-Medical 2018*. While knee osteoarthritis is a slowly progressive disorder, it has recently been appreciated a rapid progression of phenomenon in the knee joint. Studies has been demonstrated that individuals with a history of joint trauma (knee injuries) are 3 to 6 times more likely to develop knee osteoarthritis *Driban et al. 2014*.

Typically, OA tends to start in one compartment and with time progresses to be tri-compartmental. In cases with single compartment disease, partial (or uni-compartmental) knee arthroplasty (PKA) could provide significant advantages over total knee arthroplasty (TKA). These include better function, reduced morbidity and mortality, and more natural feel of the replaced knee. Although excellent results following PKA are seen in appropriate patients, there is significant variability in outcomes and globally higher revision rates of PKA are observed when compared to TKA. The reasons for this higher revision rate are multi-factorial and include variation in patient selection, surgical technique, as well as differing thresholds for revision of PKA, compared to TKA *Oosthuizen et al.2019*. Although the decision about the type of procedure depends on the patient

and the orthopedist. TKA has been the procedure that has performed most frequently as a solution to severe damage to the knee joint.

1.15. Total knee replacement

Knee replacement is the commonest surgical procedure performed in older adults and its incidence is increasing rapidly. TKA is the only solution procedure for knee osteoarthritis. In most cases, it has excellent outcomes in functional outcomes and cost-effectiveness. The commonest form of knee replacement is total knee replacement (TKR), where the entire knee joint is excised and replaced *Liddle et al 2013*.

In TKR, the knee joint is accessed through a midline incision and the patella and extensor mechanism are everted to allow access to the joint surfaces. The ACL is excised and the tibial *plateaux* are resected using horizontal saw cut. The distal femoral joint surfaces are resected in their entirety using a transverse cut and anterior and posterior chamfers. Depending on the severity of disease and surgeon preference, the posterior cruciate ligament (PCL) and the patellar joint surface may also be resected. Soft tissue deformity is corrected with sequential ligamentous and capsular releases until the knee is seen to be in equal tension medially and laterally, and in flexion and extension. The tibial joint surface is replaced by a polyethylene bearing, normally attached to a metal base-pate, whilst the distal femur is resurfaced using a metal component. If there is patellofemoral osteoarthritis, the patella may be resurfaced using a polyethylene ‘button’. In most cases, the implants are cemented into place, but in around 5% of cases, the implants are coated to encourage bone ingrowth and fixation without cement. The excision of the menisci and cruciate ligaments necessitates the imposition of a degree of constraint between the tibia and femur, which is normally achieved by dishing of the tibial component with or without a cam-post mechanism to replicate PCL function *Liddle et al 2013*.

1.16. 3D printing: FDM and PolyJet technologies

Fused Deposition Modeling (FDM) and PolyJet are two of the most advanced and effective additive manufacturing (AM) technologies available. They can produce a range of output from precise, finely detailed models to durable production goods. While there is crossover in applications and advantages, these two technology platforms remain distinct and bring different benefits *Stratasys Ltd 2016*.

FDM Process

Thermoplastic filament feeds through a heated head and exits, under high pressure, as a fine thread of semi-molten plastic. In a heated chamber, this extrusion process lays down a continuous bead of plastic to form a layer. This layering process repeats to manufacture thermoplastic parts *Stratasys Ltd 2016*.

PolyJet 3D printing Process

A printing carriage with four or more inkjet heads and ultraviolet (UV) lamps traverses the workspace, depositing tiny droplets of photopolymers, materials that solidify when exposed to UV light. After printing a thin layer of material, the process repeats until a complete 3D object is formed *Stratasys Ltd 2016*.

Compare and contrast

Comparing three categories between FDM and PolyJet will address the common decision-making criteria. Part characteristics cover items that address: quality and material options considering the physical properties available from FDM and PolyJet processes *Stratasys Ltd 2016*.

Operations

Speed: Build speed, while a flawed measure of performance, tends to be a priority for many. There are too many factors to make qualified speed generalizations of any AM technology, including FDM and PolyJet. At times, PolyJet is faster, but this is not always true. All similarities between FDM and PolyJet cease when it comes to support removal and part cleaning. PolyJet gives you a quick, manual step to remove the gel-like support material: spraying with a waterjet. With FDM, you have either a fully automated, but longer, soak in a tank to remove soluble supports or a manual step that removes rigid, breakaway supports with simple hand tools *Stratasys Ltd 2016*.

Part characteristics

About surface, finish PolyJet gives you a near-paint-ready surface right out of the 3D printer. With a little wet-sanding and polishing, it can deliver a smooth, glossy surface that is ready for any process where even minor surface imperfections are glaring, such as electroplating for a mirror-like finish. About FDM the extrusion process can produce visible layer lines on side walls and “tool paths” on top and bottom surfaces. These can be eliminated, but that requires additional post-processing, such as an automated finishing station or some manual finishing *Stratasys Ltd 2016*.

Resolution & feature detail

High resolution and fine feature detail are hallmarks of the PolyJet process. Using 600 x 600 dpi printing in 16- to 32-micron layers, PolyJet can reproduce very small features and fine-grained textures. Therefore, if feature resolution is a prime consideration, PolyJet is your best bet. For dimensional accuracy, the published specifications show that comparable FDM and PolyJet platforms have similar results for parts when they are removed from the systems. However, over time and under a load, FDM materials are more dimensionally stable, which is critical when used for production parts *Stratasys Ltd 2016*.

Materials

For many, the greatest distinction between FDM and PolyJet comes from materials. Combined there are nearly 600 options, ranging from real thermoplastic to thermoplastic-like resin, rigid to flexible, and opaque to transparent. PolyJet offers product realism across a wide band of requirements. With its unique, unmatched Digital Materials (two materials blended at the print

head), there are over 450 options offering a range of hues, transparency, strength, rigidity and flexibility. For example, flexible, rubber-like parts can be printed with *Shore A* hardness ratings of 27 to 95. Another factor that contributes to product realism is multi-material printing. Any part can have up to 46 distinct material properties, so applications like flexible overmolding of rigid structures can be reproduced in one print job. Both FDM and PolyJet offer bio-compatible materials with USP Plastic Class VI to ISO 10993 ratings. They can be used for hearing aids, dental procedures, and surgical guides and fixtures as well as food and pharmaceutical processing *Stratasys Ltd 2016*.

1.17. Past and present of 3D printing in healthcare filed

The creation of patient-specific anatomical models derived from medical imaging data is reported as early as 1981. These first anatomical models, generated by contouring computed tomography (CT) images and milling manufacturing techniques, were low resolution, labor intensive and prohibitively expensive to produce at scale. This work, however, laid the foundation, which would later be established as a valuable application for 3D Printing. By 1986 the first stereolithography printer was commercialized by Chuck Hull, opening the door for anatomical models to be created more rapidly and with a higher accuracy. With 3D Printing in healthcare becoming a viable solution for creating patient-specific models, the barrier of the process was quickly recognized as a data handling and software limitation. Materialise founder *Wilfried Vancraen* 3D printed his first anatomical model in 1990 and in response to the workflow challenges he faced, developed and later commercially released the first version of the *MIMICS (Materialise Interactive Medical Image Control System)* software in 1992. Mimics was an innovation that enabled the stack of cross-sectional CT images to be converted to the series of contours needed to drive the 3D printer, building the patient's anatomy one layer at a time.

Looking to understand and demonstrate the clinical effectiveness of 3D-printed anatomical models, *Materialise* acted as the project manager for the Phidias project in the mid-1990s. This study supported maxillofacial surgeons with 3D-printed replicas of their patient's anatomy in order to understand the influence of the additional tool on the planning of the procedure. In total, 253 surgical procedures were supported with the aid of 3D-printed anatomical models, which provided valuable data on the effectiveness of this new technology. The results of this study showed a positive impact on the surgeon's ability to plan and communicate the procedure with unanimous agreement of the benefit over using imaging alone *Pietila et al. 2018*.

In the years following the Phidias project, the industry began to leverage 3D printing technology to deliver patient-specific products with many of these innovations driven by *Materialise* technology. Hearing aids, dental surgical guides and computer-based preoperative planning were all pioneered in the late 1990s. Custom cranio-maxillofacial and orthopedic devices were brought to the market during the 2000s. By 2010, the software and hardware had matured to a level where it became more feasible to adopt the technology, increasing accessibility and broadening the potential use cases. This is the period where we saw increased adoption of medical applications of

3D Printing being implemented at the point-of-care, or within the footprint of a hospital, primarily for the purposes of anatomical modeling, to improve patient care through better planning and communication, to save costs by reducing operating room times and medical errors, and to more efficiently educate trainees and patients *Pietila et al. 2018*.

Increased accessibility of 3D Printing in the medical field has led to significant growth in the applications of the technology in medicine. This is demonstrated by the growing body of literature featuring clinical work and medical research with 3D Printing. Physicians and hospitals are also driving this growth as they look to leverage medical 3D Printing with greater autonomy by implementing in-house operations, thus reducing the reliance on external medical 3D printing companies. This model enables more rapid turnaround times and broadens the potential use cases where the technology may be applied. 3D Printing within the footprint of the hospital has also shown to increase the collaboration of the provider teams resulting in the ability to work iteratively and capture intellectual property that may be generated through the routine use of the technology *Pietila et al. 2018*.

Further driving the adoption of 3D printing in the healthcare industry in recent years is the convergence of multiple factors, including increased awareness and demand from surgeons, improvements to medical software for preparing imaging data for 3D Printing, new 3D printers and materials, improved industry support and increasing engagement from medical societies and regulators. Prominent societies such as the Radiological Society of North America (RSNA) have shown support for the development of medical 3D Printing by establishing a Special Interest Group in order to develop and educate physicians on best practices, clinical appropriateness criteria, and laying the foundation for eventual reimbursement from medical payers¹. The engineering organization Society of Manufacturing Engineers, who hosts annual 3D manufacturing exhibitions such as RAPID, has also created a dedicated medical working group to address challenges and develop resources for the industry. This group supported the proposal, which led to the recent establishment of DICOM standard for 3D printing file formats, which will result in a standardized method to store data within existing hospital infrastructure *Pietila et al. 2018*.

Ensuring patient safety when applying 3D Printing to patient care is increasingly in focus as the technology grows and shifts to a more mainstream market. From a regulatory perspective, the U.S. Food and Drug Administration (FDA) has supported multiple workshops open to industry, academia and hospitals to collect feedback and facilitate a discussion around safety and effectiveness. This has enabled the additive manufacturing in medical industry to gain clarity on the regulatory environment and led to a published guidance document in regards to using 3D Printing in the manufacturing of medical devices. Given the momentum in the industry, the outlook for point-of-care 3D Printing is positive and the growth trend is expected to continue. So much so that Gartner predicts that by 2021, 25% of surgeons will be practicing on 3D-printed models of a patient prior to surgery. Industry, academia, clinical institutions and governments are all investing resources to ensure safety and effectiveness as the market grows to a broader audience of users. In

order to support growth in the coming years, further clinical and economic evidence will be needed to justify investments and receive reimbursement through payers *Pietila et al. 2018*.

Education and clinical training

Clinical training and education of students and staff is traditionally managed with cadavers, animals or mannequin models used in a simulation environment. These methods can be limiting given the often-high cost, low accessibility and lack of representative pathology especially for rare conditions. Many medical schools and hospitals are beginning to use realistic 3D-printed anatomical models for certain training scenarios, which have been shown to increase learning effectiveness and save costs. Two studies are summarized detailing improvements in education using models over medical imaging and traditional methods.

Patient specific 3D anatomical models were used in a study at Children's National Medical Center that included 70 physicians delivering care to patients in the pediatric cardiac intensive care unit post-congenital heart surgery. The models were used to study the impact of training physicians, nurses and ancillary care providers on proper postoperative care of specific patients. Likert scale questions revealed that the enhancement of understanding and clinical ability averaged 9.0 on the 10 point scale showing benefit over the traditional patient hand-off method. In a similar training study, 3D-printed models were used to train medical students on spinal fractures. 120 medical students at a Chinese university were randomized into three groups and were required to complete a 10-question test on two different spinal fracture cases. One group was given the CT images, the second a 3D computer model and the third group a 3D-printed model. The 3D groups performed much better than the CT group and the 3D-printed model group was able to complete the questions much faster than the other groups. In addition to the superior performance of the trainees, the training with the printed models also showed a higher level of engagement and pleasure from the trainees. In addition to the growing use of 3D Printing in the education and training of clinicians, it has also been shown as an exceptional tool to aid in the informed consent process with patients. 3D-printed models give patients a better understanding of their situation and the proposed treatment plan, presented in personalized way. This has the potential to increase the patient's comfort level with their care providers and makes a positive impact on the patient's experience *Pietila et al. 2018*.

Additional opportunities enabled by 3D Printing

With reimbursements declining and pressures to lower healthcare costs, hospitals have to been looking to uncover opportunities for non-traditional sources of revenue. Outside of applying 3D Printing to patient care and education activities, there are also several non-clinical opportunities for value capture if the technology is leveraged in the proper way. The availability of research grants and the solicitation of philanthropic funds is often a successful model to fund the necessary personnel and tools to support a medical 3D Printing program. Medical 3D Printing has roots in innovation and serves as a means to prototype new ideas. This concept can be leveraged by an in-house 3D Printing resource as a means to generate and monetize intellectual property of physicians. The 3D printing resource may also serve as an opportunity to collaborate with industry through the

support of training and education of physicians on new devices by using 3D-printed anatomical models and providing an opportunity to capitalize on the resource. Lastly, there is certainly value in offering cutting-edge technology to patients as a tool for marketing and public relations for the hospital. The value of Medical 3D Printing is highest in the most complex of cases, which often garner the greatest interest from the lay public. Many hospitals have leveraged the use of 3D Printing as a central theme in featuring patient cases. The use of 3D Printing and impact on patient care may also increase the ranking of a hospital in certain specialties leading to higher patient recruitment and potentially greater access to grants and funding opportunities *Pietila et al. 2018*.

Outlook for 3D Printing in hospitals

Personalized healthcare is being delivered through the use of 3D Printing at an increasing rate. Much of this is through the ability to build accurate anatomical replicas of patients' anatomies for surgical planning, training and education. As this adoption continues to expand, there will be many market needs to support the growing use. Medical software and equipment for the 3D Printing workflow has and will continue to become more user friendly for adoption within the clinic. Integration between medical imaging systems, dedicated software for 3D Printing and the 3D printers themselves is being pursued by several firms via strategic collaboration. *Materialise* has offered integration of the *Mimics inPrint software* within the Siemens platform enabling an efficient workflow with the 3D modeling software embedded in the clinical image viewer. Also on the backend, *Materialise* has enabled integration with specific 3D printers such as *Formlabs* to reduce the effort needed to translate the anatomical model to the virtual build area¹⁴. These collaborations have also led to the first FDA clearance to enable 3D-printed models for diagnostic use when the medical software is used in conjunction with a *Materialise* validated 3D Printer and material *Pietila et al. 2018*.



Figure 7. Strategic integration. Medical images acquisition, Software and 3D printing manufactures.

Although the number of case reports and series continues to grow, more robust and multi-center studies will be needed to better support the clinical and economic evidence of 3D Printing for specific indications. In addition to supporting efforts for reimbursement with payers, it will help to drive and understand appropriateness criteria for 3D Printing when it is clinically useful and when it is not. As regulators and standards bodies take further notice, it will also support the need for

better standards and best practices for implementing 3D Printing at the point-of-care, ensuring patient safety and the most effective use of the technology *Pietila et al. 2018*.

2. Research Theme

The overarching theme of this research is centered on exploring possible solutions for knee joint injuries, integrating pre-operative planning, surgical simulation and performing a custom made devices thanks to specialized medical software and the use of multi-material 3D printing technology. We have limited our focus to achieve the following objectives:

- (1) Improvement of the 3D model of the right knee joint obtained in the previous study. For this, the plan to follow is to mimic the structure of the collagen fiber matrix of the connective tissue, and manage the problems presented in the previous project and conduct the stretching test of the ligaments using *sensuron multiplatform system*.
- (2) ACL-R biomodel manufacture and Pre-operative planning to improve ACL-R surgery outcomes, incorporating key surgical elements, such as orientation-architecture of the femoral/Tibial tunnels (derived of TT technique) and BPTB auto-graft dimensions reported by *Dhafer et al. 2014*. The surgical planning consider single bundle reconstruction. It will include a personalized surgical guide (SG) based on the anatomy of the patella tendon (PT) (it will be used in the graft harvest). The SG requirements will follow the indications reported by *Grawe et al. 2014* with the aim to avoid graft tunnel length mismatch.
- (3) TKR biomodel manufacture and custom design and adjustment of prosthetic components in the improved 3D model of the right knee joint emulating a TKR procedure. It will be performed considering a cruciate sacrificing implant (CS) with symmetric tibial bearing fixed.

3. Methodology

The present study was developed in the *Shirley Ryan Abilitylab research hospital*, which has a *Stratasys J750™* full color multi-material 3D printer. It uses photopolymer injection (*Polyjet™* technology) for the production of highly realistic and functional 3D biomodels in a wide range of materials and colors with variable durometers.

Mechanical uni-axial tensile tests were conducted in *Northwestern University Kaiser Lab* using an Instron S3300, Canton, MA Uniaxial Testing Instrument following ASTM test designation D412-C. The process of selection and matching of the print materials with the real anatomical structures was based on analysis of the mechanical characteristics of the different combinations of the Agilus30 rubber-like materials family.

There were developed the following 3D biomodels:

- (1) Improved 3D model of the right knee joint emulating the hierarchical structure of the collagen fibers matrix.

- (2) ACL-R biomodel manufacture and Pre-operative surgical planning model of anterior cruciate ligament reconstruction (ACL-R) using a bone-patellar-tendon-bone (BPTB) auto-graft adding surgical guide (SG) avoiding graft tunnel length mismatch.
- (3) TKR Biomodel with a cruciate sacrificing implant (CS) with symmetric tibial bearing fixed.

They were based on polygonal mesh files **.hm* corresponding to a 3D model of the right knee joint reported by *Dhafer et al.2014*. It includes the following anatomical components: femur, tibia, patella, fibula, ligaments, articular cartilage, menisci, retinacula, patella and quadriceps tendon (PT-QT).

Table 1. Reports format extensions and the file names (these are usually associated with a software application, which opens, manages and saves these types of files) used in this study. The Overall workflow of the study methodology was schematically illustrated in Figure 1.

Table 3. 3D File formats used in the study. Extensions, file names and software applications.

Extension	File name	Software application
<i>*.hm</i>	Mesh	Altair Hypermesh
<i>*.3dm</i>	Part	Rhinoceros 3D
<i>*.mxd</i>	Project	Materialise 3-matic
<i>*.SLDPRT</i>	Part	SolidWorks
<i>*.SLDASM</i>	Assembly	SolidWorks
<i>*.print</i>	Print project	Stratasys Grabcad
<i>*.STL</i>	Standard geometry	different CAD software

In the previous work, two-dimensional (2D) medical images **.DICOM* (Digital Imaging and Communications in Medicine) were converted to three-dimensional (3D) surface geometries **.STL* (Standard Triangle Language) through manual segmentation of the different anatomical structures of the knee joint via specific software. Currently, there are different applications that perform a successful automatic segmentation. These use specific filters allowing the reconstruction and generation of the 3D objects. Among them, the most recognized are *3D slicer multi-platform* (open source) and *Materialise Mimics Innovation Suite*.

The objective of the previous study was to perform a finite element analysis (FEA), for which polygonal mesh files of the each structure of the 3D model of the knee joint were set and optimized. From these meshes **.STL* files were generated with standard meshes in computer aided engineering (CAE) *Hypermesh Software*, after then, were exported to 3D develop and modeling *Materialise 3-matic Software*. This application allows the design of medical devices such as implants, splints and SG from **.STL* files. In this application the fiber matrix of the connective tissue were designed following the manual method according to shape and dimensions reported in the literature. In the

same way, pre-operative surgical plan models of two of the most common affectations of the knee joint were performed, integrating SG and prosthetic components designed in Rhinoceros 3D V5.0.

The final biomodels were exported in *.STL format to the computer-aided design (CAD) SolidWorks Software, where they were converted to *.SLDPRT format, before being assembled through the same application. The final assembly format *.SLDASM is compatible with the Stratasys Grabcad™ software of the Stratasys J750™ multi-material printer. The process of selection and matching of the print materials with the anatomical structures was based on analysis of the mechanical characteristics of the different combinations of the Agilus30 printing material following ASTM test designation D412-C. Finally, model's orientation and printing time were optimized.

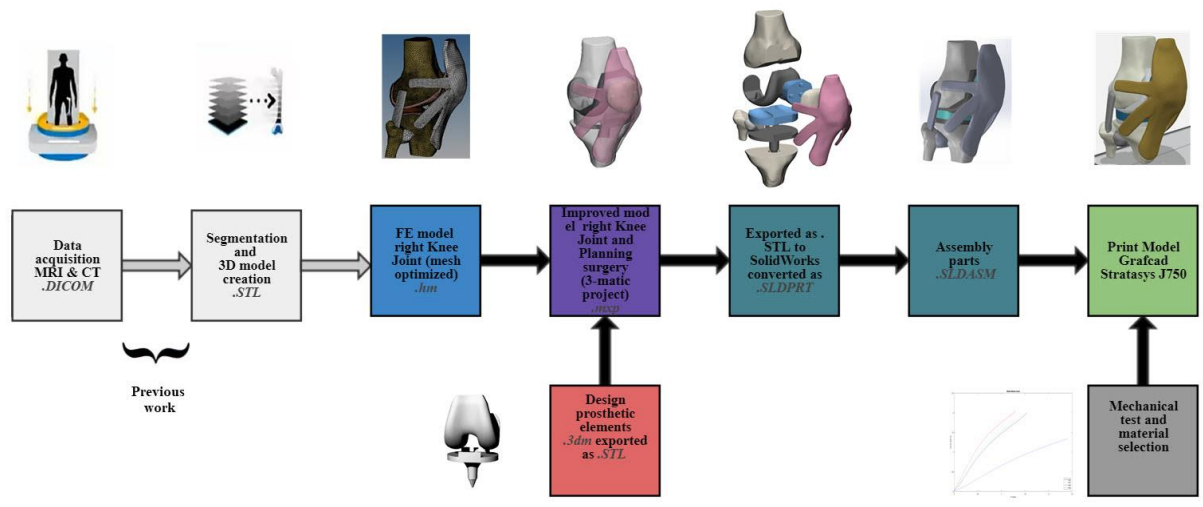


Figure 8. Schematic illustration of the study methodology. The workflow illustrates the different file formats used throughout the investigation. Prosthetic components were integrated and print materials selection were chosen in the based on the results of the mechanical characterization.

4. Chapters

4.1 Chapter 1: Manufacture of the improved 3D knee joint model

4.1.1 Introduction

As mentioned, knee joint fibrous connective tissues play a crucial role, providing strength, transmitting mechanical loads and contributing with the passive support and stability. One of the most demanding tissues in the knee joint are the tendons, these connect the muscles with the bones, this connection allows the tendons to passively modulate the forces during locomotion, generating movement and providing additional stability without active work *Thorpe et al. 2013*. The ligaments

are found internal or external to the joint capsule, bind bone to bone and offer quick and increasing resistance to tensile loading over a narrow range of joint motion. This allows knee joint to move easily within normal limits while causing increased resistance to movement outside this normal range *Frank et al. 1984*.

Tendons and ligaments share many similar features. They are load-bearing structures and have the same hierarchical organization, being their primary building unit the collagen molecule type I *Hsieh et al. 2000*. The matrix of collagen fibrils aligned (approximate diameter \varnothing collagen fibril 1.5 nm) are organized into long cross-striated fibrils that are arranged in bundles to form fibers (approximate diameter \varnothing fiber 50-500 nm). Fibers are further grouped in arrays called fascicles (\varnothing fascicle 50-300 μm) these arrays together form the ligament (\varnothing ligament fiber 0.1-0.5 mm) *Frank et al. 2004*. In the knee joint, the hierarchical structure of connective tissues described determines the mechanical behavior. Therefore, the knowledge of its mechanical properties is essential to elucidate behavior and its function, as well as for selecting appropriate materials used in surgical reconstructive procedures.

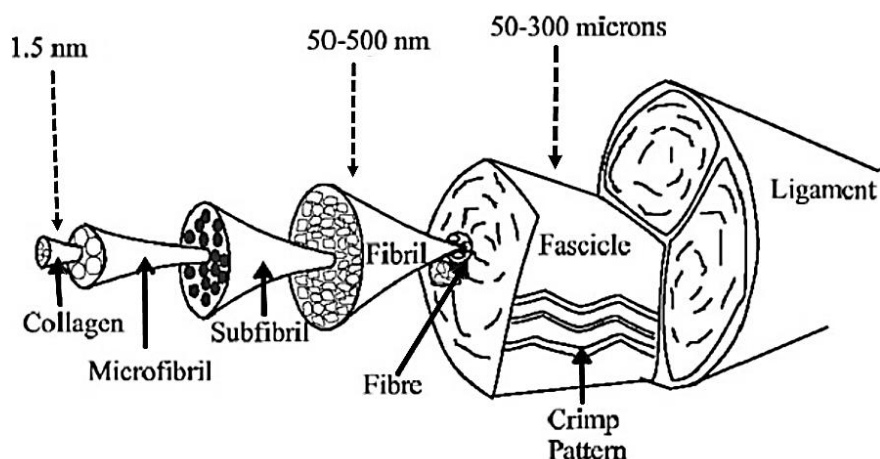


Figure 9. Hierarchical structure of ligaments. The basic structural element is the collagen molecule *Frank et al. 2004*.

Mechanical properties of biological tissues are usually determined through some form of mechanical testing (e.g. tensile tests, compressive tests, bending and torsion tests). In general, several authors report the mechanical characterization of the isolated tendon and ligament in terms of the stress–strain relationship. The material properties are determined from force–elongation data of the tensile test, dividing the recorded force by the original specimen cross-sectional area is possible obtain the stress, in a same way the strain is determined as the change in length of the specimen relative to its initial length, divided by its initial length *Pal et al. 2014*.

In a first approach, the stress–strain behavior is independent of the tissue dimensions and the stress–strain curves are typically described in terms of five regions (previously mentioned). The region No 1 is the "toe region" or "toe to heel". In the connective tissues, a non-linear response is observed in this region, it is due to the straightening of the "crimp" pattern resulting in successive recruitment

of the fibers as they reach their straightened condition. As the strain increases, the "crimp" pattern is lost and further deformation stretches aligned the collagen fibers themselves (The region *No 2, linear or elastic region*). As the strain is further increased, the yield point is reached (in a stress–strain curve the point indicates the limit of elastic behavior and the beginning of plastic behavior) exceeding this limit structural damage occurs (The region *No 3-4, yielding and plastic regions*). The stretching causes progressive fiber disruption and ultimately complete rupture (The region *No5 Failure*) *Diamant et al. 1972*.

The purpose of this study is to highlight the hierarchical structure importance of connective tissues in the mechanical response of the knee joint. In order to mimic their mechanical behavior and measure the stretching of the ligaments. Real data of the stress–strain curve of the tendons and ligaments are reported below in the Figure 10.

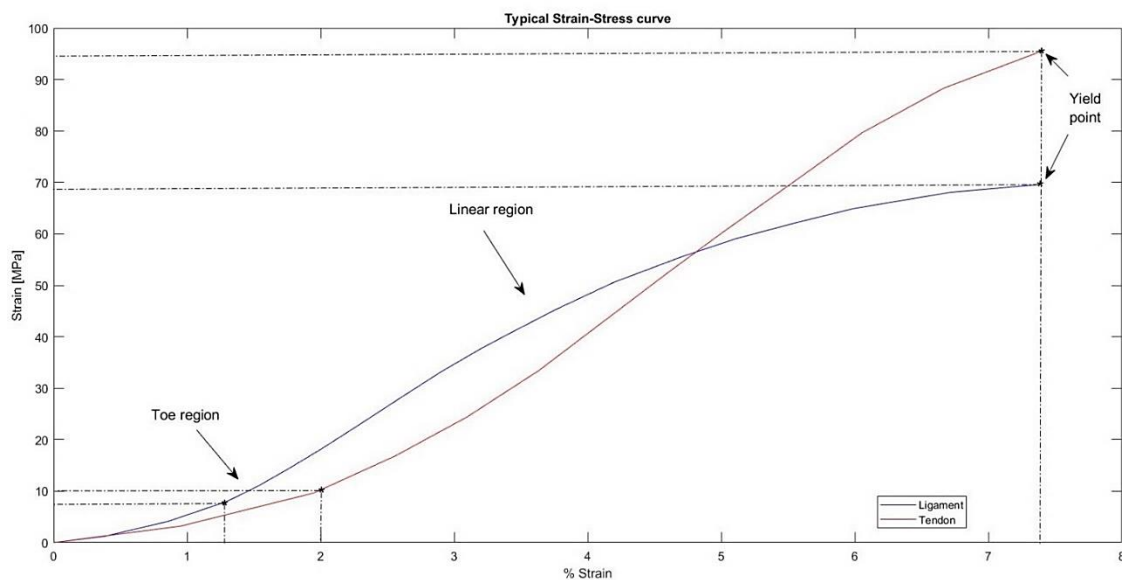


Figure 10. Standard strain-stress curves of tendon and ligament. Experimental data reported by *David et al. 1978* was represented with *WebPlotDigitizer V4.1* and *MATLAB R2018a*. Two regions of interest of the curve: (1) The toe region and (2) The linear region, yield limit points are illustrated.

4.1.2 Problem specifications

A study performed by Northwestern University students aimed to create an instrumented knee model that will provide accurate information about the stretching of the ligaments. The team in charge identified human-like set of synthetic polymers that exhibited similar mechanical properties of biological connective tissues. There were created molds and modeling procedures that captured the anatomic morphologies derived from the existing knee model. A first prototype was created, the next step was to improve the aesthetics of the structure and develop the measurement and acquisition systems to measure the mechanical data of the connective tissues. The initial idea was

to include strain sensors inside the ligament molds. Unfortunately, it was not possible to assemble all the components of the knee. The recorded mechanical information would be the validation of the model proposed for the use in surgical training of orthopedic clinicians. Statistically it has been shown that during reconstructive procedures such as ACL-R other ligaments may suffer excessive stretching which could generate damage in the structures involved. In addition, the model could provide useful data to simulation the biomechanical behavior of the knee through software and replace the limited availability of real cadaveric joints. Figure 9. Illustrates the workflow of the previous approach.

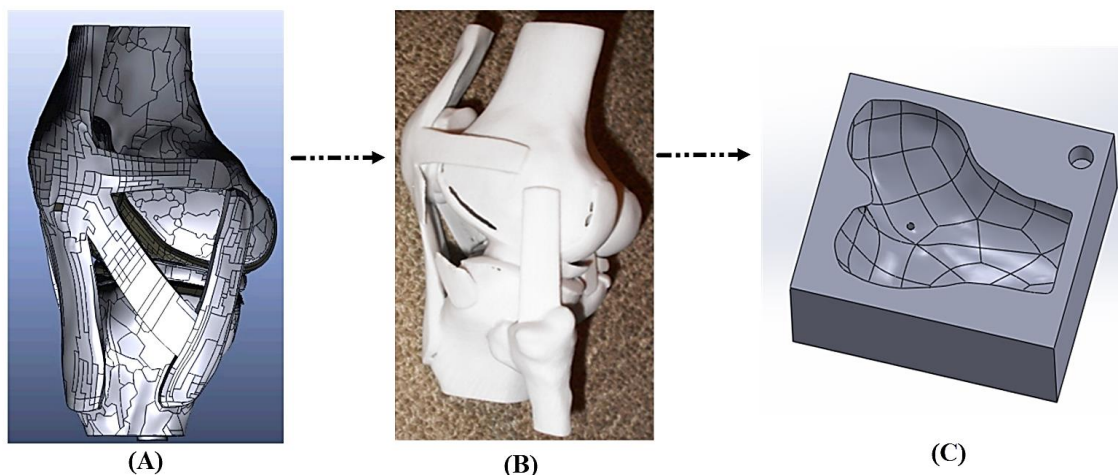


Figure 11. Workflow PISK: Practice Interactive Surgical Knee. (A) *.SLDPRT file of knee joint. (B) Printout of entire knee model made using 3D printer. (C) Sample of Femur mold to produce a part of the knee joint.

4.1.3 Materials and methods

Stratasys J750™ 3D printer

The *Stratasys J750™* 3D Printer is a full-color multi-material system. It has an incomparable performance and high material capacity. The system allows mixing up simultaneously six different materials in specific concentrations to different durometers. In addition, 3D Printer allows choosing between more than 360,000 colors, textures, gradients and transparencies. The *Stratasys J750™* is by far the most accessible and widely used form of 3D multi-material printing. The multi-material printing is based on photopolymer jetting (*PolyJet™ technology*); curable liquid photopolymers capable of producing very thin layers for smooth surfaces, intricate details and vivid colors. The technology works in a similar way to traditional *inkjet printing*, but, instead of jetting ink onto paper, it jets liquid photopolymers onto a build tray where each droplet is cured in a flash of UV light. A microscopic, layer resolution and an accuracy of up to 0.1 mm. The *Stratasys J750™* offers many advantages, such as sharp precision, smooth surfaces, fine details in the production of 3D models, incorporation of a wide range of colors and materials in a single project, optimization of

printing time, printing of materials with variable hardness, easy support material removal among others. There are print materials available with features such as translucency, biocompatibility, resistance to UV rays, high temperature and deflection. The Figure 1. Presents a comparison between traditional fused deposition modeling FDM and PolyJet™ technology.

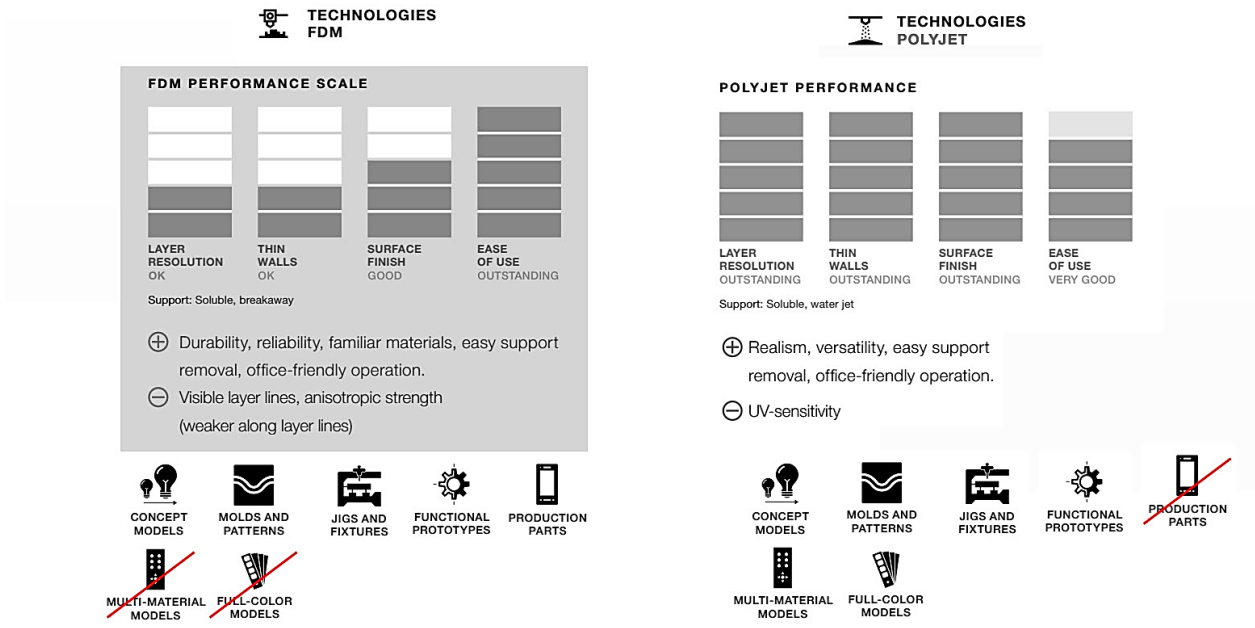


Figure 12. Comparative between FDM and PolyJet™ technologies Stratasys J750™ High-End PolyJet uses photopolymers, which are capable of simulating properties ranging from rubber-like to transparent even high toughness and heat resistance. Digital materials expand the possibilities by blending two or more base resins to create thousands of material combinations. Achieve full color capabilities, translucencies, *Shore A* values and other properties for maximum product realism *Stratasys Ltd 2016*.

The Figures 12-13 show the features of the printer Stratasys j750™ and the printing materials available (flexible, rigid, opaque, transparent), included engineering material acrylonitrile butadiene styrene (ABS) in its digital version(main material of FDM technology). The hardness of PolyJet™ materials can be modified according to the durometer shore hardness scale. The Stratasys j750™ has three print modes (1) High Quality six different materials 14µm layer thickness, (2) High Mix six different materials 27µm layer thickness and (3) High Speed three different materials 27µm layers thickness double speed. The printing process is relatively simple, from the software Stratasys Grabcad™ software materials, color tones, opacity, hardness, scale, orientation and print mode are set. The software accepts single pieces or projects (several pieces) with extensions *.STL *.SLDASM. The last update includes an extension which enables direct printing from SolidWorks Software.

STRATASYSJ750

Maximum Build Size (XYZ)

Stratasys J750: 490 × 390 × 200 mm (19.3 × 15.35 × 7.9 in.)

Layer Thickness

Horizontal build layers down to 14 microns (.00055 in.)

Accuracy

Up to 200 microns for full model size (for rigid materials only, depending on geometry, build parameters and model orientation)

Model Material Options

- Full Vero family of opaque materials including neutral shades and vibrant colors
- Rubber-like: Agilus30, TangoPlus and TangoBlackPlus
- Transparent VeroClear and RGD720
- VeroFlex™ family

Digital Material Options

- Unlimited number of composite materials including:
- Over 500,000 colors
 - Digital ABS Plus and Digital ABS2 Plus™ in ivory and green materials in a variety of Shore A values
 - Translucent color tints



Support Material

- SUP705 (WaterJet removable)
- SUP706 (soluble)

Figure 13. Front view of the Stratasys J750 printer, features and commercial materials *Stratasys Ltd 2016.*

Material	Highlights
 <p>Digital Materials</p>	<ul style="list-style-type: none"> • Wide range of flexibility, from Shore A 27 to Shore A 95 • Rigid materials ranging from simulated standard plastics to the toughness and temperature resistance of Digital ABS Plus • Vibrant colors in rigid or flexible materials, with over 360,000 color options on the Stratasys J750 • Available on PolyJet multi-jetting 3D printers
 <p>Digital ABS Plus</p>	<ul style="list-style-type: none"> • Simulates ABS plastics by combining strength with high temperature resistance • Digital ABS2 Plus offers enhanced dimensional stability for thin-walled parts • Ideal for functional prototypes, snap-fit parts for high or low temperature usage, electrical parts, castings, mobile telephone casings and engine parts and covers
 <p>High Temperature</p>	<ul style="list-style-type: none"> • Exceptional dimensional stability for thermal functional testing • Combine with PolyJet rubber-like materials to produce varying Shore A values, gray shades and high temperature parts with overmolding • Ideal for form, fit and thermal functional testing, high-definition models requiring excellent surface quality, exhibition models that endure strong lighting conditions, taps, pipes and household appliances, hot air and hot water testing
 <p>Transparent</p>	<ul style="list-style-type: none"> • Print clear and tinted parts and prototypes with VeroClear and RGD720 • Combine with color materials for stunning transparent shades • Ideal for form and fit testing of see-through parts, like glass, consumer products, eyewear, light covers and cases, visualization of liquid flow, medical applications, artistic and exhibition modeling
 <p>Rigid Opaque</p>	<ul style="list-style-type: none"> • Brilliant color options for unprecedented design freedom • Combine with rubber-like materials for overmolding, soft touch handles and more • Ideal for fit and form testing, moving and assembled parts, sales, marketing and exhibition models, assembly of electronic components and silicone molding
 <p>Simulated Polypropylene</p>	<ul style="list-style-type: none"> • Simulates the appearance and functionality of polypropylene • Ideal for prototyping containers and packaging, flexible snap-fit applications and living hinges, toys, battery cases, laboratory equipment, loudspeakers and automotive components
 <p>Rubber-like</p>	<ul style="list-style-type: none"> • Offers various levels of elastomer characteristics • Combine with rigid materials for a variety of Shore A values, from Shore A 27 to Shore A 95 • Ideal for rubber surrounds and overmolding, soft-touch coatings and nonslip surfaces, knobs, grips, pulls, handles, gaskets, seals, hoses, footwear, and exhibition and communication models
 <p>Biocompatible</p>	<ul style="list-style-type: none"> • Features high dimensional stability and colorless transparency • Has five medical approvals including cytotoxicity, genotoxicity, delayed type hypersensitivity, irritation and USP plastic class VI • Ideal for applications requiring prolonged skin contact of more than 30 days and short-term mucosal-membrane contact of up to 24 hours

Figure 14. PolyJet™ photopolymers, materials and outstanding features *Stratasys Ltd 2016.*

Design collagen fibers matrix

For the design of the collagen fiber matrix, **.STL* files of the initial model were exported to *Materialise 3-matic Software*. A frequent problem in the management of 3D objects was the relative position of the structures. Overall, these do not coincide with the global reference system (GRS) of the applications. Design applications used integrate translation and orientation tools to perform an adequate positioning of the anatomical components that are part of the 3D biomodel. The first step to design the fibers was set the orientation of the knee joint (with the commands *Translate & Rotate*) in reference to the anatomical planes and global reference system (GRS) of the *Materialise 3-matic Software*.

A diameter of 0.6 mm was selected, based on approximate diameter for the fiber (\emptyset ligament fiber 0.5 mm) reported by *Frank et al. 2004*. A tolerance of 0.1 mm was provided considering the expansion of the material during printing. The next step was calculate the number of fibers (NFC) within each structure. This was determined from the relationship between cross-sectional area of the structure (SA) and cross-sectional area of the fiber (SAF) (cross-sectional area was calculated assuming circularity) (Equation 1).

$$NFC = \frac{SA}{SAF}$$

Manual method was used to generate the contours and paths for each fiber. The fibers were created along the each structure from traced paths using commands *Soft curve* and *Sweet-loft*. The final fiber structure involved the use of the *Reduce, Smooth & Wrap* commands in order to correct surface errors and generate a more refined model for printing (Figure).

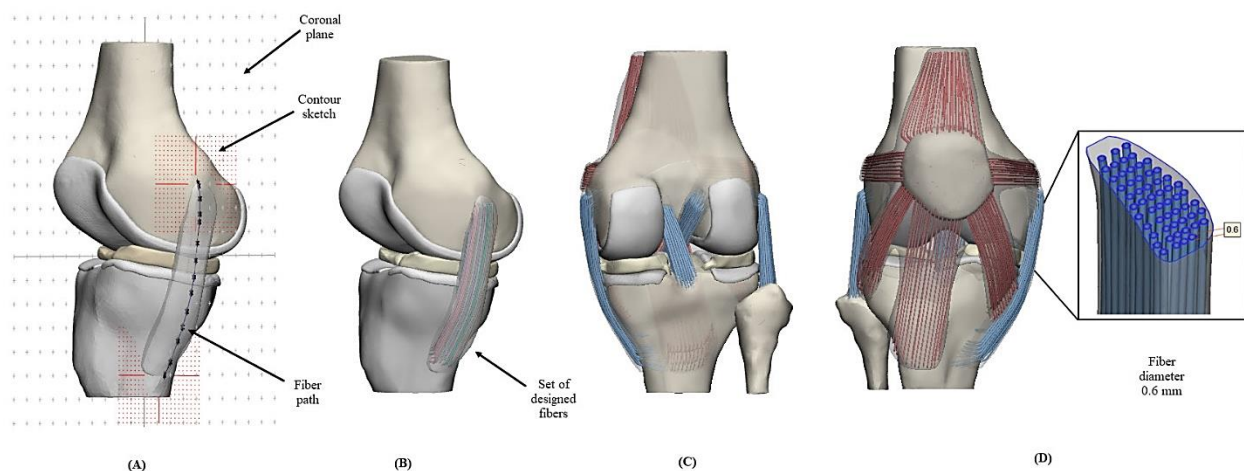


Figure 15. (A) Illustration of fibers tracing through the MCL, contour and sketches are shown (B) set of 60 individual collagen fibrils manually created to MCL (C) Posterior view of the knee joint

with all created fibers (D) Anterior view of the knee joint, cross-section MCL, the diameter of the fiber is reported.

The NFC does not correspond to the actual number of fibers designed (NFD). These differ because the objective was to keep the fibers and trajectories separated (place where the sensor will pass) between them avoiding printing errors. The NFD corresponds approximately to a quarter of the NFC. The dimensions - SA - volume (Vol), number of fibers calculated (NFC) and number of fibers designed (NFD) were reported for: Cruciate ligaments (ACL-PCL), collateral ligaments (MCL-LCL), patellar and quadriceps tendons (PT-QT), medial and lateral patella–femoral ligaments (MPL -LPL) and medial and lateral patellar retinacula (MPR-LPR) Table 4.

Table 4. Dimensions, cross-sectional area SA) volume (Vol), number of fibers calculated (NFC) and number of fibers designed (NFD) of tendons and ligaments of the knee joint model.

Soft tissues	Length (mm)	Width (mm)	Height (mm)	SA (mm²)	Vol (mm³)	NFC (Fibers)	NFD (Fibers)
<u>ACL</u>	11.57	8.68	35.90	64.52	2319	228	50
<u>PCL</u>	9.11	6.96	33.30	56.38	1558.12	199	45
<u>MCL</u>	14.14	4.14	78.14	67.75	4361.82	240	60
<u>LCL</u>	13.14	7.60	46.06	71.17	2994.60	252	50
QT	28.93	8.54	37.61	207	10502.40	732	100
PT	25.20	8.38	66.70	63.87	16343.14	226	45
<u>MPL</u>	12.56	5.01	43.40	53.35	2877.39	189	30
<u>LPL</u>	12.46	3.78	40.63	53.62	2363.14	190	30
<u>MPR</u>	17.99	3.32	56.88	50.70	2810.48	179	25
<u>LPR</u>	12.2	3.25	57.06	35.47	2344.22	125	20

Sensor approach

The measurement of behavior and strain of ligaments in the body is still one of the most challenging endeavors in Biomechanics. Results of those measurements are essential to create accurate and valid biomechanical models thus allowing a better and thorough comprehension of mechanisms, related diseases, and the creation of new surgical techniques to restore a physiological functionality. Mechanical testing of tissue *in situ* is very complex and hence not commonly performed. Some of the techniques that have been utilized include (1) buckle transducers to monitor tendon and ligament forces, (2) telemetried pressure sensors to measure joint contact pressure, and (3) strain gauges to quantify bone and ligament strain. Some noninvasive approaches have also been employed. Ultrasound techniques have been used to detect changes in the speed of sound in different tissues, and these changes have been correlated with the tissue’s elastic properties. Various imaging techniques have also been used to quantify tissue geometry and deformation *Pal et al.2004*.

In the literature, traditional approaches using conventional *Strain gauges* are widely described. However the data recorded using this type of sensor is insufficient for this purpose. This is mainly because these are rigid sensors and their geometry does not allow integrating the ligament structures. The multi-material knee biomodel as an alternative to the cadaveric knee joint. Our goal is to include *The Summit sensoron: fiber optic sensors* inside the ligaments and measure its stretching during a kinematic task. Unlike *Strain gauges* that provide superficial sensing, *Summit sensoron system* provides fully distributed sensing.

Due to the impossibility of including the *fiber optic sensors* during the biomodel printing. To perform this approach, three collagen fibers of each ligament (two lateral ones, one medial) will be eliminated, leaving the paths by which the *fiber optic sensors* will be positioned. Figure 15 illustrates a sensor inside the LCL.



Figure 16. Fiber optic sensor positioned inside LCL. Fiber and multi-sensing platform are shown.

First approach print 3D model and tensile test

To printing the improved model of the knee joint, a key aspect was to determine the appropriate material to emulate the mechanical properties of real tissues. For this, a comparison was made between the shore hardness scales of the print materials available and real materials reported for the anatomical structures of the knee joint (Table 5).

The objective was to establish a comparison between the initial model and the improved model with the hierarchical structure composed of the fibers matrix. An initial model of ACL-R corresponded to previous study was printed based on the materials matching according to shore hardness scale. The commercial materials Digital ABS RGD5130 (Engineering plastics) and the *Tango FLX950-FLX973* (rubber-like materials family) were selected to print the bone components and soft tissues respectively. High Mix 27 μ m layer thickness mode was selected for the model

printing. However, the results were not satisfactory, the ligaments (structures that were subject to greater tension) collapsed easily after the manipulation Figure 15.

Table 5. Range of the elastic modulus (tension) and Durometers of the shore hardness scale reported for the anatomical structures and *Stratasys i750™* materials: Engineering plastics: *Digital ABS* Green (RGD5160-DM-RGD5161-DM-RGD515-RGD535), *Ivory* (RGD5130-DM-RGD5131-DM-RGD515-RGD531) and *High Temperature* (RGD525). Transparent standard plastics: (RGD720), *Veroclear* (RGD810). Rigid opaque: *VeroPurewhite* (RGD837), *Verogray* (RGD850), *Veroblackplus* (RGD875), *Verowhiteplus* (RGD835), *Veroyellow* (RGD836), *Verocyan* (RGD841), *Veromagenta* (RGD851) and *Veroblue* (RGD840). Simulated polypropylene: *Duruswhite* (RGD430), *Rigur* and (RGD450). Rubber-like: *Tango black plus* (FLX980), *Tango plus* (FLX930) *Tango black* (FLX973), *Tango gray* (FLX950), *Agilus30* (FLX935), *Agilus30 black* (FLX985) *Stratasys Ltd 2016.*

Tissue	Elastic modulus	Durometer	Material	Elastic modulus	Durometer
<u>Femur</u>	18-20 GPa	A 80	Digital ABS	2.6-3 GPa	D 85-87
<u>Tibia</u>	18-20 GPa	A 80	High Temp.	3.2-3.5 GPa	D 85-87
<u>Patella</u>	18-20 GPa	D 15-20	Transparent	2.3 GPa	D 83-86
<u>Fibula</u>	18-20 GPa	D 15-20	Vero	2.3 GPa	D 83-86
<u>Fibula lig.</u>	300-450 MPa	A 45-55	Rigid Vero	2.3 GPa	D 83-86
<u>ACL</u>	300-450 MPa	A 45-55	Durus	1-1.2 GPa	D 74-76
<u>PCL</u>	300-450 MPa	A 45-55	Veroblue	2.3 GPa	D 83-86
<u>MCL</u>	300-450 MPa	A 45-55	Rigur	1.7-2.1 GPa	D 80-84
<u>LCL</u>	300-450 MPa	A 45-55	Tangoplus	N/R	A 26-28
<u>QT</u>	580-600 MPa	A 65-75	Tangoblack	N/R	A 60-62
<u>PT</u>	580-600 MPa	A 65-75	Tangogrey	N/R	A 70-73
<u>MPL/LPL</u>	12-15 MPa	A 35-45	Agilus 30	N/R	A 30-35
<u>MPR/LPR</u>	12-15 MPa	A 35-45	-	-	-
<u>Menisci</u>	225-500KPa	A 35-45	-	-	-
<u>/Cartilage</u>					

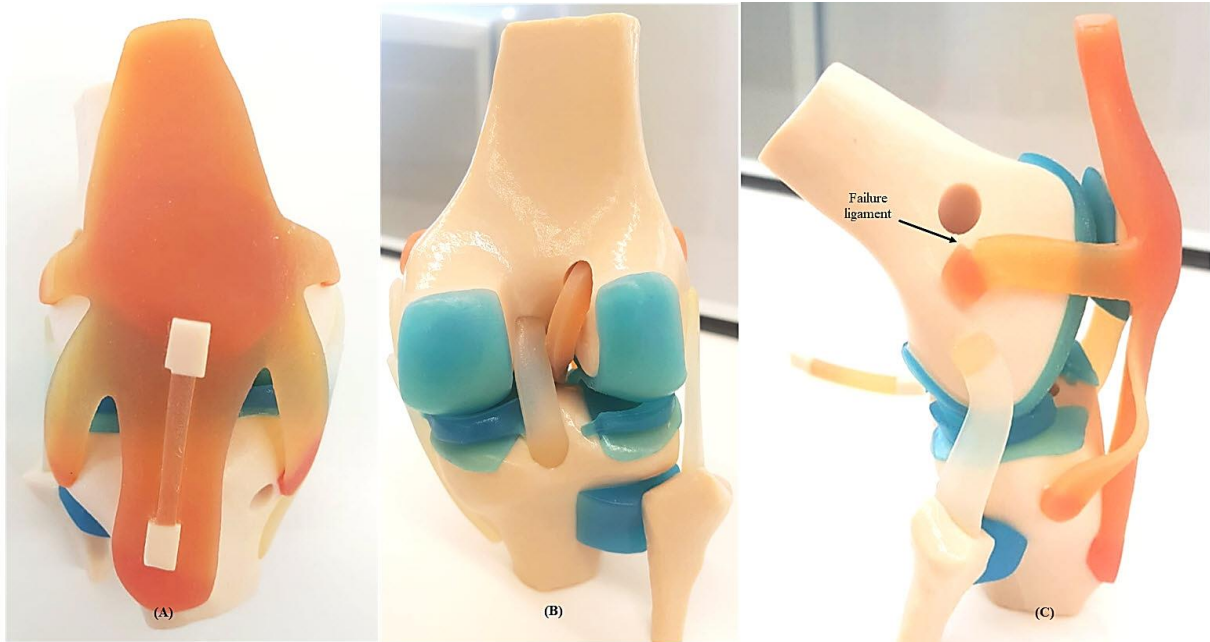


Figure 17. Illustration of the initial model of ACL-R without fibers: (A) Anterior view of the knee joint with BPTB graft,(B) Posterior view of the knee joint with BPTB graft inside, (C) Lateral view of the knee joint in flexion, rupture of the LPL.

For the selection of the materials of the improved model, different combinations between the hardness of the fibers and the structure were proposed. Agilus30 rubber-like materials family (Table 6) were selected to replace Tango FLX950-FLX973 materials.

Table 6. Fibers-specimen hardness combinations (Agilus30) for the tensile test.

Combinations	Fibers Durometer	Specimen Durometer
<u>No 1</u>	18-20 GPa	A 80
<u>No 2</u>	18-20 GPa	A 80
<u>No 3</u>	18-20 GPa	D 15-20
<u>No 4</u>	225-500KPa	A 35-45

Mechanical uni-axial tensile tests were conducted using an Instron S3300, Canton, MA uniaxial testing instrument, following the test designation D412-C for rubber and elastomers. To perform the test was necessary to design the bone specimens with the fibers inside, in the software SolidWorks software following the specifications of the standard (Figure 16). Three bone specimens (n = 3) were printed for each combination, the dimensions (thickness, length, width) of the each bone specimen were measured with the calibrator and the values were entered in the system software BlueHill, Instron SA France, Elancourt. A tensile test was performed using a 10

mm min. This sequence is a standard, validated test protocol *Pailhé et al. 2015*. Each bone specimen was attached between extensometer grips of the materials testing system to apply tensile loads. The test was performed until the bone specimen failed; the data was recorded and exported to *Microsoft Excel-2016*. This sequence was repeated with all the bone specimens. The strain-stress curves of each specimen were elaborated in *MathWorks - MATLAB R2018a*, from them average curves were elaborated for each combination, values of elastic modulus, Yield strength and proportional limit were reported in the section Results.

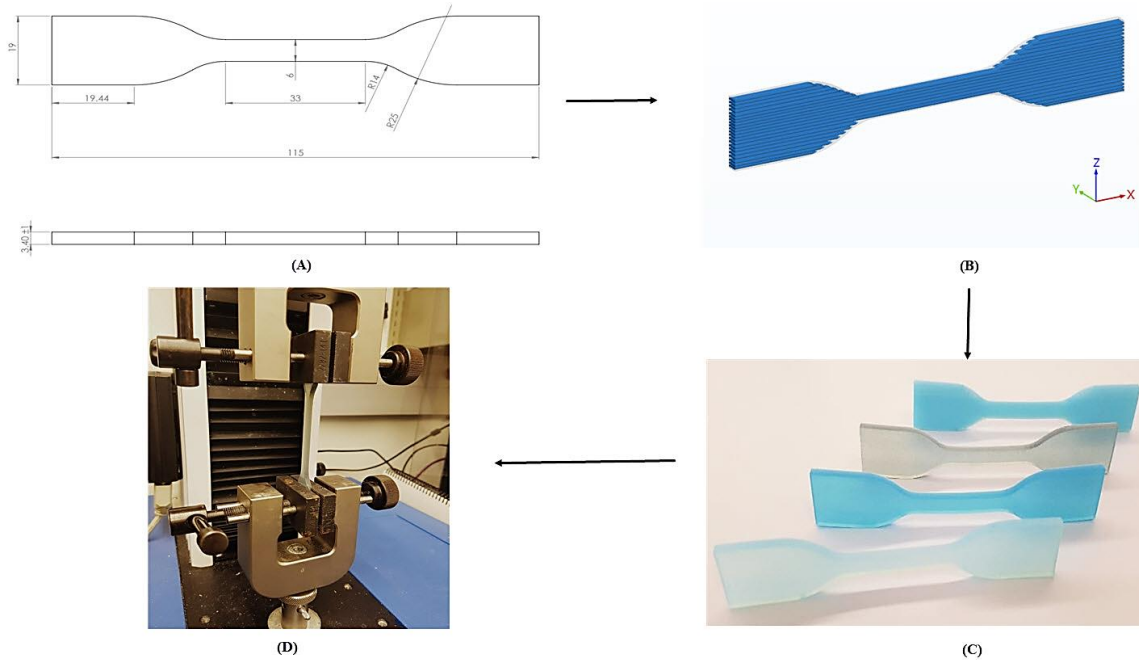


Figure 18. Schematic illustration of the application of the standard D412-C: (A) Dimensions bone specimen, (B) Render bone specimen in SolidWorks software, (C) Printed bone samples with different combinations, (D) Bone specimen attached to a materials testing system Instron S3300, Canton, MA uniaxial testing instrument, to apply tensile load.

4.1.4 Results

The tensile test were performed with the purpose of comparing the stiffness of the different combinations between the fibers matrix and the anatomic structure. Table 7. Includes values of: Average-standard deviation of proportional limit (AVG/STD-PL), Average-standard deviation Yield strength (AVG/STD-YS), Average-standard deviation of elastic modulus (AVG/STD-E) and linear adjustment coefficient or Pearson's correlation coefficient R^2 - range [0-1].

Table 7. Tensile test data. The average and standard deviations of the strain-stress curve properties of the different combinations of the print materials.

Combinations	AVG-PL (MPa)	STD-PL	AVG-YS (MPa)	STD-YS	AVG-E (MPa)	STD-E	R ²
No 1	1.533	0.030	1.560	0.008	0.769	0.011	0.980
No 2	1.436	0.035	1.516	0.034	0.751	0.009	0.975
No 3	1.486	0.012	1.580	0.008	0.660	0.005	0.970
No 4	2.336	0.016	2.426	0.002	1.822	0.003	0.991

The selection of materials for printing of the final models was performed based on the stiffness (α Elastic modulus) of the different combinations of materials and the anatomical structures. The approximate Young's modules and the linear tendencies were calculated in the range corresponding to elastic deformation (a linear approximation from end points of the toe-region to the linear region.) of the stress-strain curves (Figures 17-18) - Table 8.

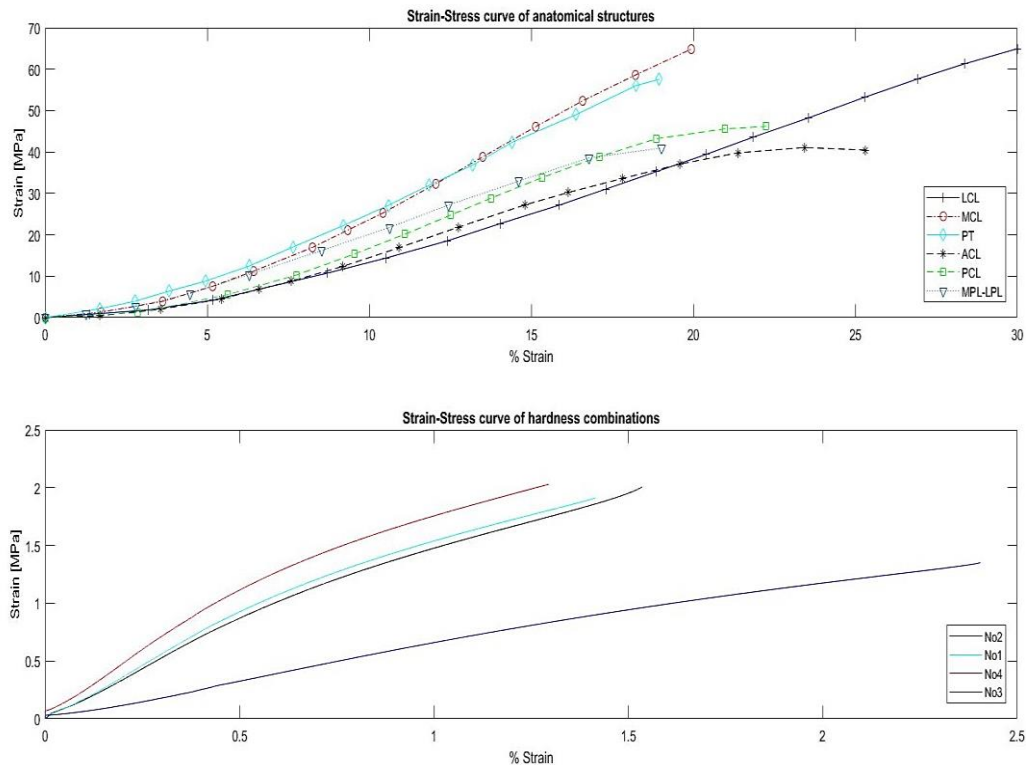


Figure 19. Average Stress-Strain curves for anatomical structures and hardness combinations.

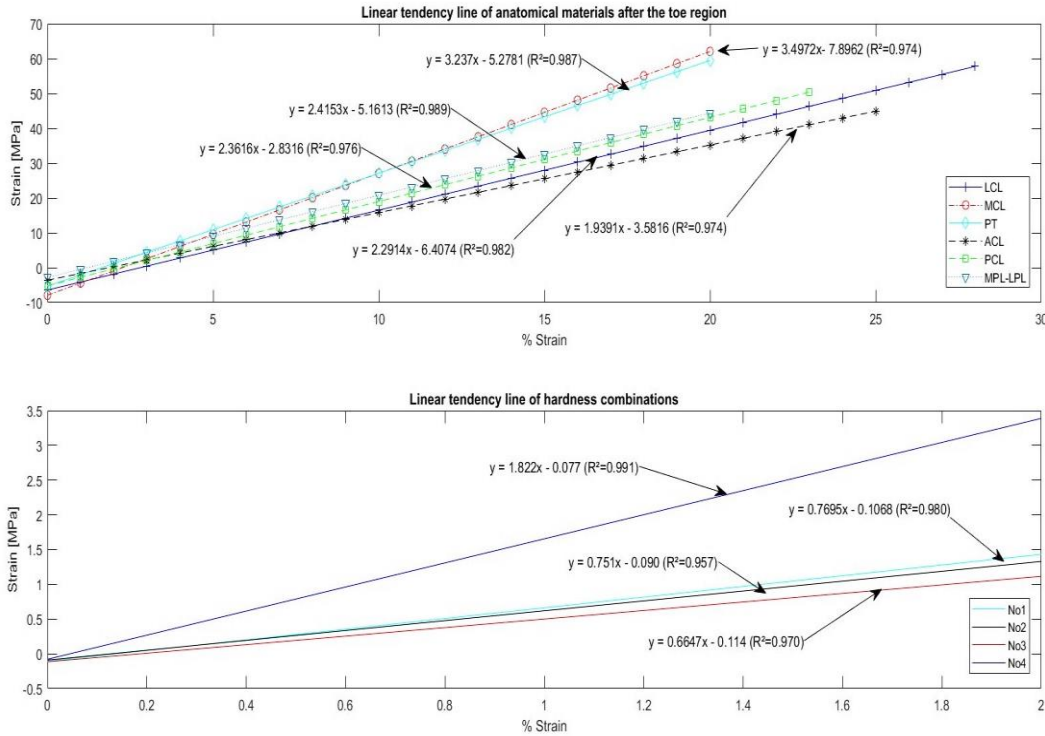


Figure 20. Average linear tendencies for anatomical structures. Hardness combinations, equations and correlation coefficients were reported.

Table 8. Match of the anatomical structures with the selected combinations for the printing of the model.

Soft Tissue	Elastic modulus (MPa)	Selected combination	Elastic modulus (MPa)
<u>MCL</u>	3.5	No 4	1.8
<u>PT-QT</u>	3.23	No 4	1.8
<u>MPL-LPL</u>	2.41	No 1	0.76
<u>PCL</u>	2.36	No 1	0.76
<u>LCL</u>	2.29	No 1	0.76
<u>ACL</u>	1.93	No 1	0.76

Agilus30 - A 50 was chosen for joint surfaces and menisci.

4.1.5 Discussion

The results of this chapter show that the approach of imitating the hierarchical structure of the connective tissues of the knee joint was successful. When we compare the real curves with the curves obtained with the composite material of different durometers, we can note that these have

the same mechanical pattern exhibiting approximately linear behavior (Figure 18.). From a functional point of view, facing the first knee joint printed model (without hierarchical structure) and the improved model. We can conclude that print material match and model manipulation fulfilled with the expected results, since the improved model did not present rupture of the structures (Figures 16-24).

Analyzing the results of the mechanical test. The matching of the printing materials with knee structures was based on the stiffness. It was possible thanks to the Pearson's correlation coefficient. All proposed combinations have a R^2 close to one (Table 7). Which means that data linear adjustment had an excellent approximation. When we compare the stiffness and elastic modulus of printed combinations/ real materials (Figure 19). We can conclude that combinations No1-4 were the most similar to real materials with elastic modulus of 1.8 and 0.7 respectively (Table 8).

The limitation of this chapter was the validation of the model proposed with optical fiber sensors. This because of its high price (summit platform ~ \$70k USD-RTS125 platform~\$125k). The validation through sensors is necessary for understanding of ligament strains and behavior and create biomechanical models.

4.2 Chapter 2: ACL-R biomodel manufacture and Pre-operative surgical planning to improve surgery outcomes

4.2.1 Introduction

Knee injuries are very common in United State (US), particularly, injuries to knee ligaments, which are related mostly to sports activities *Woo et al. 2006*. There are different types of knee injuries, nevertheless, the rupture of the anterior cruciate ligament (ACL) remains as one of the most frequently intra-articular injuries of the knee joint, with an estimated annual incidence ranging that varies from 30 to 78 per 100,000 person-years *Grawe et al.2014*. In addition, the rupture of ACL can result in chronic instability and secondary damage to other structures, such as the cartilage and menisci *Samuelsson et al. 2009*. Several treatments options are available for repair the ligament, but ACL reconstruction (ACL-R) remains as the operative treatment of choice, especially for active patients who frequently participate in sports activities *Frank et al. 2017*. After primary ACL reconstruction, a rerupture can be devastating. The reported rate of ACL reruptures range from 1% to 11%. Reruptures may be caused by traumatic reinjuries, graft failure, or technical surgical errors *Gans et al. 2018*.

It is of particular interest the problem associated with graft failure. Nowadays, different tendon autogenous and allograft options exist for the ACL-R. However, the patellar tendon (PT) and the hamstring tendon are the most commonly used as auto-graft alternatives. Each type of graft is associated with its own inherent risks and benefits *Grawe et al.2014*. Nevertheless, there is no "ideal" graft to use in surgery for ACL-R. The success or failure of the procedure depends on several surgical factors: Accurate dimensions and stiffness of the graft, architecture and orientation

of the tunnel, fixation sites within the tunnel, pre-tensioning of the graft, and surgical technique *Dhafer et al. 2014*. Moreover, after reconstruction could be possible problems such as donor site morbidity.

From a clinical point of view, the bone-patellar-tendon-bone (BPTB) auto-graft is used mostly due to its successful trajectory *Frank et al. 2017*. On the other hand, surgical reconstruction has not been shown to completely restore the knee stability. It has been reported a predominant long-term result of surgical ACL-R showing the development of degenerative joint diseases such as knee osteoarthritis (OA) *Muthuri et al. 2011*. Studies show non-anatomic transtibial techniques result in high percentage of OA *Simon et al. 2015*.

As mentioned, the success of the ACL-R depends on several surgical factors, in order to restore the knee kinematics, various specialists give strong importance to the surgical technique, which is associated with an adequate medical training and a correct preoperative planning. The use of 3D printing technology and the development of specialized software in the healthcare field has attracted considerable interest. High-fidelity anatomical biomodels play a significant role in clinical treatment, surgical analysis and pre-operative training *Wang et al. 2017*.

3D printing technology offers a great opportunity towards development of patient-specific anatomic models, for medical device testing and physiological condition evaluation. Personalized medical models with complex shapes can provide clinicians and engineers a means of diagnosis, and can assist in proper surgical planning particularly in complex procedures. Additionally, there is no requirement for biocompatibility of materials in some applications, which include anatomic models for medical training and in vitro equipment of pre-operative planning such as prosthesis and splints, testing devices (such as osteosynthesis material), and so on, because printed parts will not enter the body *Yan et al. 2018*. The manufacture of anatomical biomodels is based on 3D modeling solids through: computer-aided design (CAD), computed tomography (CT), magnetic resonance imaging (MRI) or 3D scanning of anatomical models. This Technology also provides an accurate manufacturing of patient-specific SG. These advantages reducing surgical time and the associated risks. In addition, 3D printing has the advantage of rapidly manufacturing biomodels at a lower cost *Berman et al. 2012*.

Increased accessibility of 3D printing in the medical field has led to significant growth in the clinical work and medical research. Data reported by *Vaishya et al. 2018* show an increasing tendency in research and publications involving applications of 3D printing in the healthcare field, especially, in virtual pre-operative planning and manufacture of 3D biomodels. Several authors consider 3D technology and its applications as a new era in manufacturing. A search on the web made through *Google trends* (<https://trends.google.com>) has shown the upward trend of the use of 3D printing in the last 15 years worldwide. The keywords used were 3D printing-3D printed Figure19.

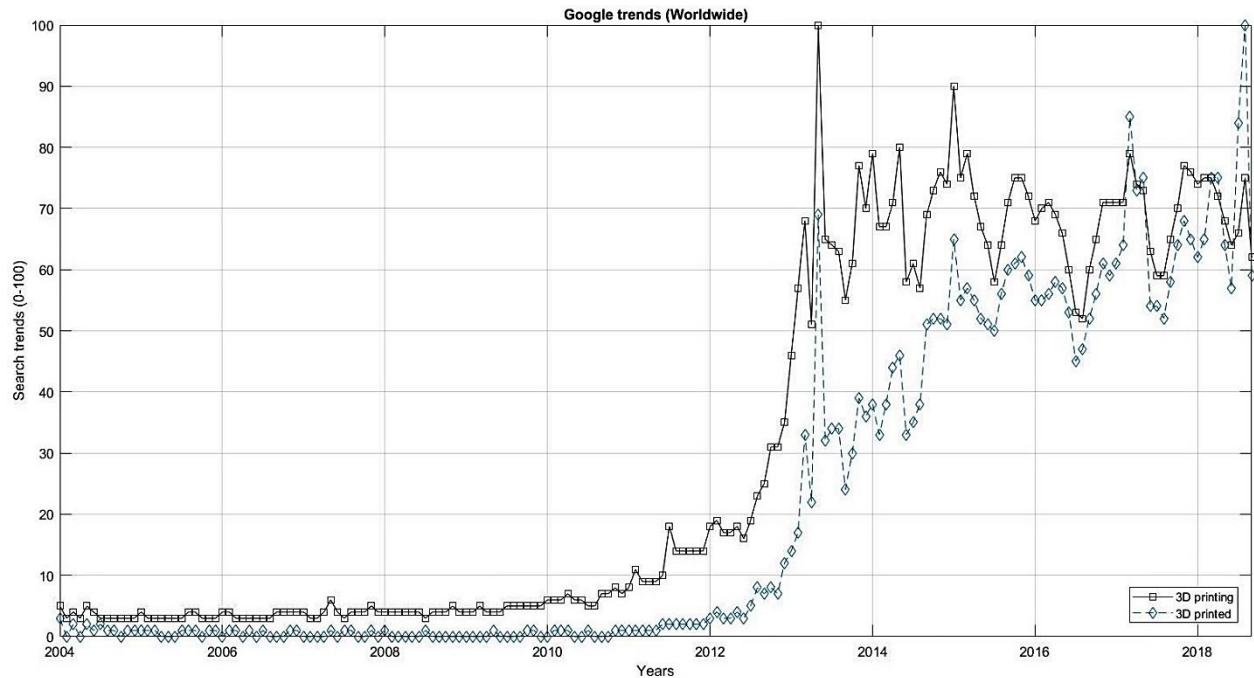


Figure 21. Search trends in the last fifteen years related to 3D printing and 3D printed. Ordinate axis represents search interest relative to the highest point on the graph. A value of 100 is the peak popularity for the term. A value of 50 means that the term is half as popular. A score of 0 means there was not enough data for this term. Abscissa axis represents the period of time in which the search was made.

The increase in the use of 3D technology and its application in the clinical field, especially taking advantage of the multi-material printing application are the focus of interest of this work. Therefore, it is proposed to complement the findings present in the research and to deal with relative problems, ACL-R procedure with BPTB auto-graft, improving the outcomes and providing a surgical training and feedback for the surgeons.

4.2.2 Problem specifications

The statistics of post-operative clinical outcomes represent the definitive proof of innovations in the treatment of ligament injuries. Rather, it is the theoretical basis for clinical innovations aimed at improving the results in the ACL-R procedure. In search of predictive solutions for the kinetic and kinematic post-operative behavior of the knee. 3D biomechanical models of finite elements (FE) are developed. These include several parameters (hard-soft material properties) and experimental data (quadriceps muscle force for instance). Digitized data of musculoskeletal morphologies lead from in vitro experiments using cadaveric specimens of knee joints. Biomechanical models of articular joints are highly useful for understanding joint functions in normal and pathological states *Cohen et al. 2003*.

Overall, an experimental study (cadaveric knee joint) is performed with kinematic parameters such as passive flexion, for example, under certain load conditions, generating a response that is used in the FE simulations. The predictive power of a model depends on its structure/formulation (number of degrees of freedom (DOF) and the uncertainties associated with its constituents (material properties). Previous studies have provided extensive experimental quantification of knee joint tissue properties for use in developing and validating numerical models. Wide range of resulting values has been reported, which may be explained in part by outcome differences due to in the donor's activity level, age, gender, and species. However, the main limitation of this approach is the availability of the knees cadaverous. Obtaining data derived from cadaveric specimens is not viable; therefore, others alternatives are being sought. This chapter sought the manufacture of an ACL-R biomodel that emulate the ACL-R procedure using a BPTB auto-graft and transtibial technique (TT). The approach incorporated an accurate pre-operative planning. The biomodel development is proposed as an alternative to the use of cadaveric specimens (Figure 20).

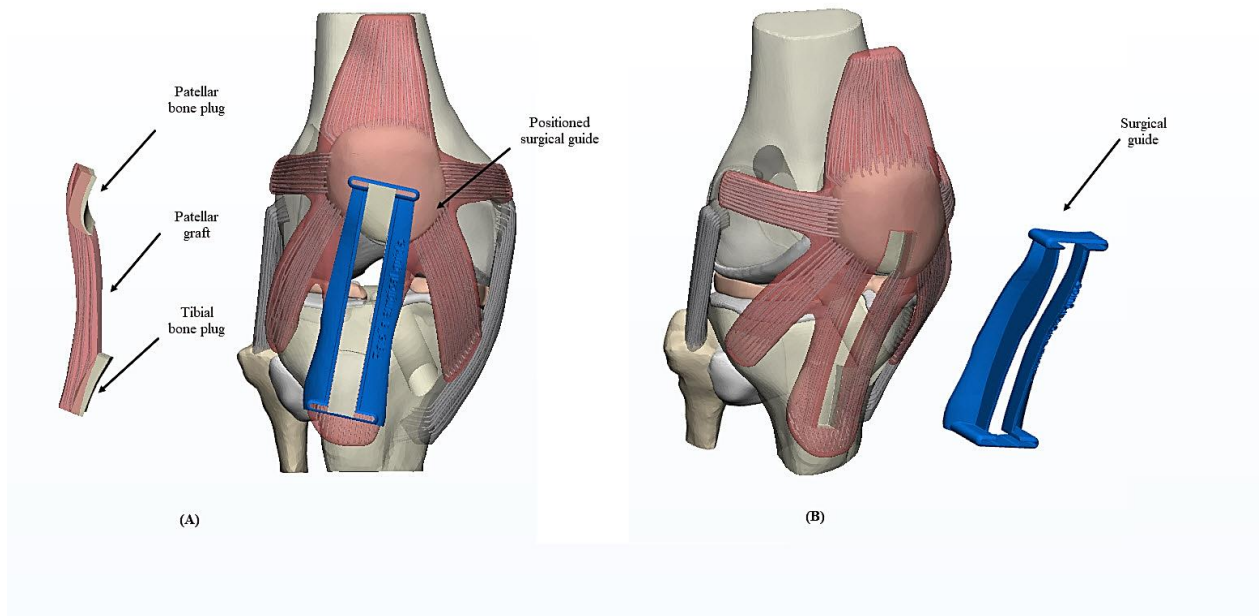


Figure 22. Schematic illustration central part of patellar tendon removed for ACL-R in the improved biomodel of the right knee joint: (A) Lateral view BPTB auto-graft. Anterior view SG positioned on the knee joint. (B) Isometric view knee joint - SG.

4.2.3 Materials and methods

The ACL-R biomodel manufacture and development of the pre-operative planning was based on the improved 3D biomodel of the right knee joint. As mentioned previously, the success of the ACL-R procedure using BPTB auto-graft depends on several factors. Our focus was mainly to improve the surgical technique with addition of the accurate surgical planning incorporating orientation-architecture of the femoral/Tibial tunnels and auto-graft dimensions (mismatch and

donor-site morbidity problems commonly occur in patients who have an excessively long patellar tendons) reported by *Dhafer et al 2014 – Grawe et al. 2014* and a personalized surgical guide (SG) based on the anatomy of the patella tendon (PT). The SG aimed to solve the problem associated with auto-graft and tunnel length mismatch. The computer-aided surgery used 3D imaging, design software, and multi-material 3D printing. The software system used for handle the whole project was *Materialize 3-matic Software*.

Pre-operative planning of ACL-R (Figures 21-22)

1. Pre-operative measurement of the length of the auto-graft, specifically, the distance, measured from the origin in the lower portion of the patella until its insertion in the tibial tubercle. If this length is greater than or equal to 40 mm, the technique can be used *Grawe et al. 2014*. Several authors suggest an average length of 40 mm for graft and 20 mm for each bone plug. The BPTB block must have a rectangular geometry, the width of the graft and of the bone plugs (tibial and patellar) can range between 9 and 11 mm, a width of 9 mm was chosen. The measurements and landmarks were made in the 3D model of the knee joint with the commands *Measure & Create point*.
2. Design of the SG based on the anatomy of the PT, considering an oscillating saw blade of 0.8 mm wide. *Cut-plans, Boolean tools, marking & extrude commands* were used.
3. The extraction of the BPTB block and resection of ACL was simulated with *Boolean tools & Trim commands* following the limits of the SG.
4. Femoral and tibial tunnels of the knee were drilled following the orientations and dimensions reported by *Dhafer et al. 2014* with 10 mm drills.

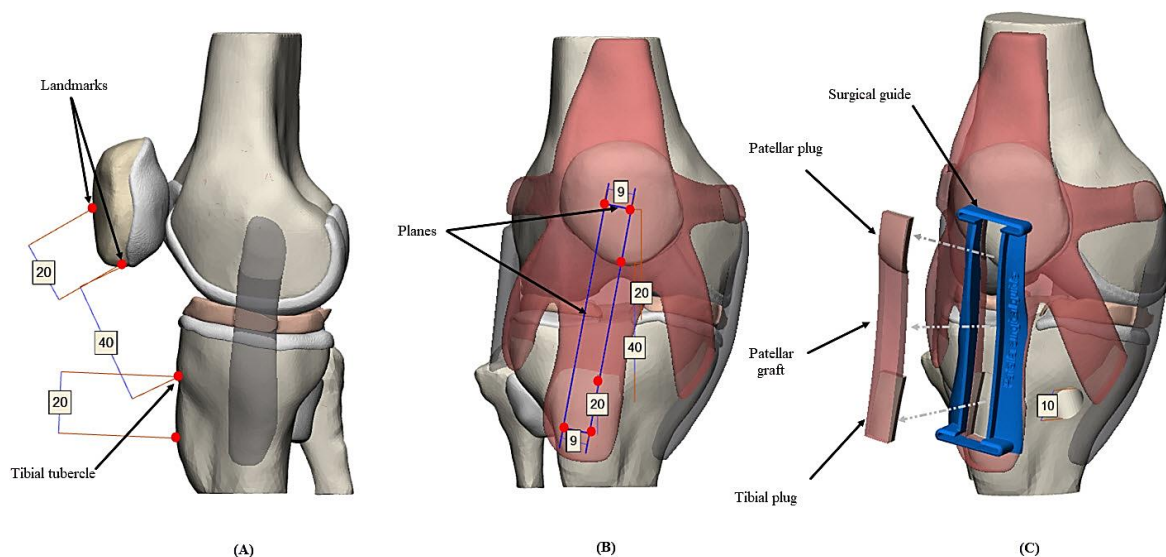


Figure 23. Schematic illustration of the pre-operative measurements of the virtual surgical planning. (A) Preliminary measures (mm) and landmarks of BPTB auto-graft, (B) Simulation of the cut-planes in the graft resection (harvest), (C) Positioned SG and graft resection according to the pre-operative guidelines.

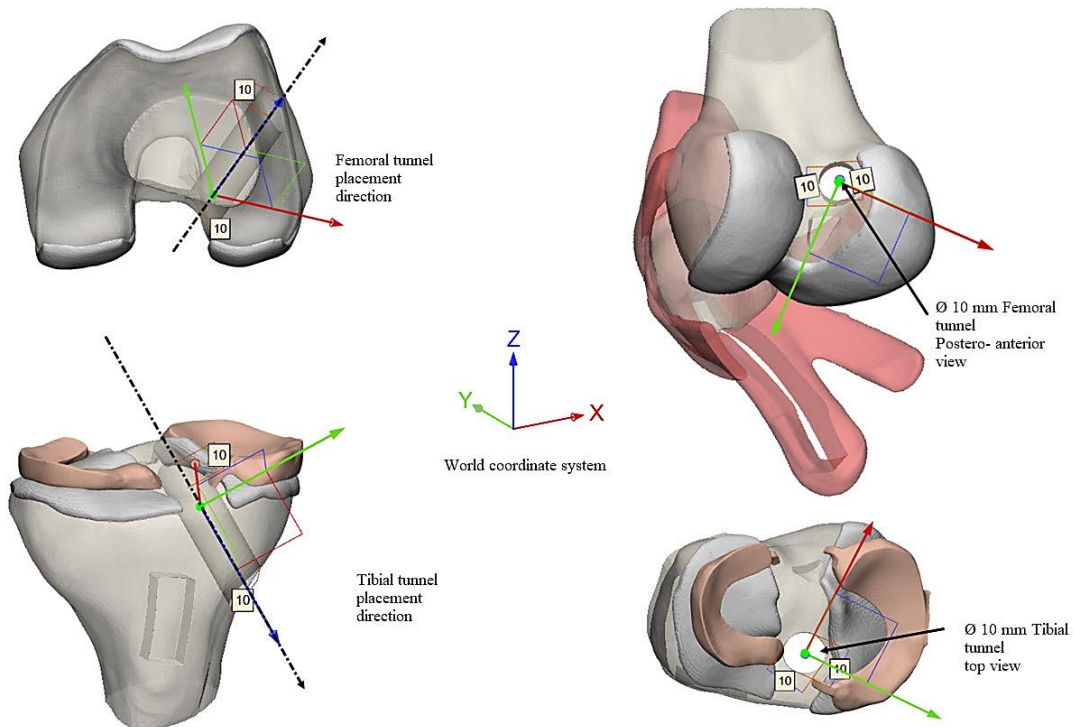


Figure 24. Schematic illustration of the tunnel directions and locations.

4.2.4 Results

The Figure 23. shows the printed functional models of ACL-R (last version) and ACL-R. In order to obtain them, first was necessary to perform a final passage corresponding to the removal of the support material. One of the advantages of the *Polyjet™* technology was the easy removal of the support material, the process took about a 15 mints. Other technologies use soluble plastics in chemical baths at high temperatures and take a day or more in removing the support material that extends the manufacturing process. In addition, the combination of the materials in the models was successful, resulting in a 3D printing of the high quality. The functional biomodel coincided completely with digital models replicating fibers and the features of the anatomy of the knee joint. In The ACL-R model, the SG matches perfectly with the anatomy of the PT in the same way that it was planned. From the mechanical point of view, the selection of the materials to different durometers (Agilus30) was key for the success of the printing described in this approach. The biomodel was manipulated easily, simulating the movement of the knee and did not present ruptures in its components. From the economic point of view, the orientation was closely related to the resolution, printing time and consequently the costs. The printing of the biomodels parallel to the extrusion tray determined an approximate printing time and cost ~14 hours and \$ 250 USD. The biomodels was printed perpendicular to the extrusion tray with the aim to get better resolution. High Mix 27 mm layer thickness mode was selected for its printing.

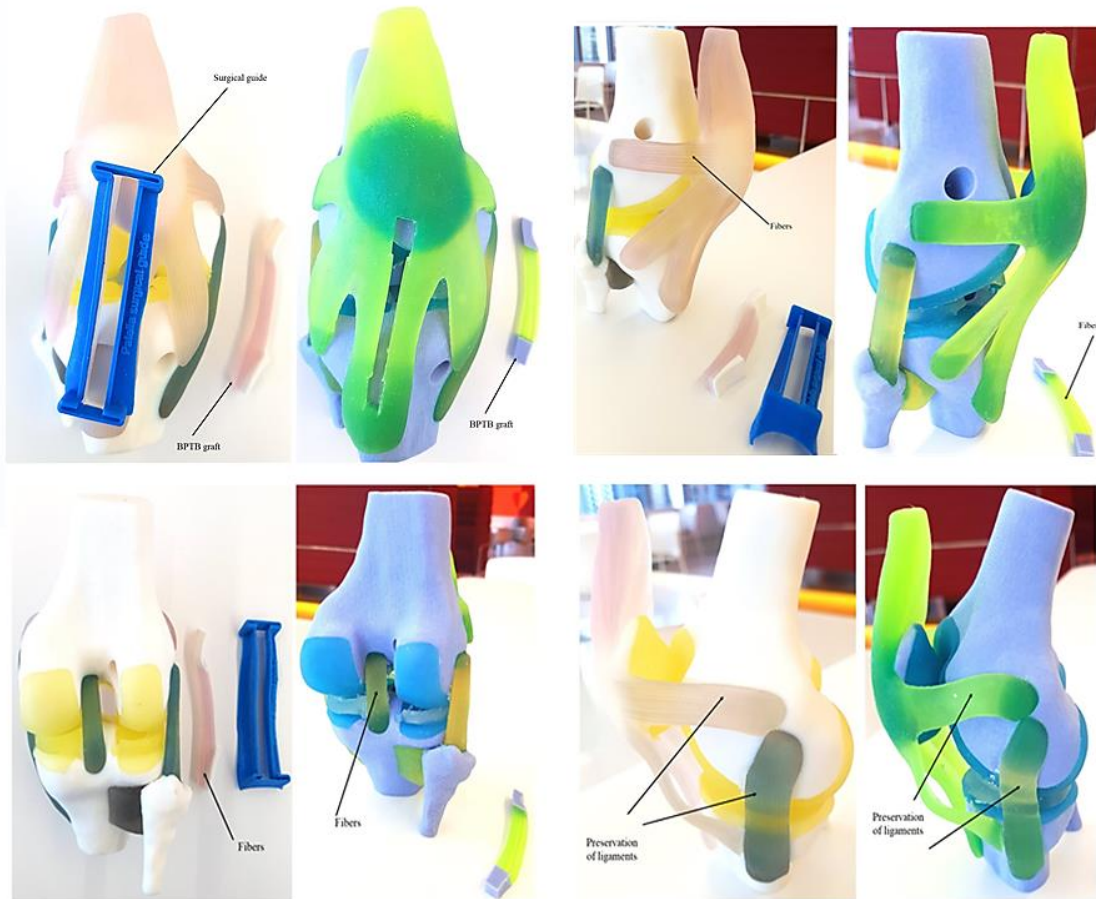


Figure 25. Illustration of 3D printed biomodels of the knee joint. Posterior-Anterior-Lateral-Isometric views ACL-R (last version) and ACL-R. They show the same details as the 3D digital models, the fibers are evident in the grafts and other anatomical structures. The surgical guide was adapted perfectly to the anatomy of the knee joint. Lateral views show conservation of the ligaments without rupture when the knee joint is flexed.

4.2.5 Discussion

The discussion of this chapter is based on the impression of the ACL-R models. The design/manufacture processes of a biomodel involves multiple factors including data acquisition, material requirement, resolution of the printing technique, cost-effectiveness of the printing process and end-use requirements.

The initial ACL-R model comes from a few data with a very low resolution. Additionally, the source files were meshes used in a simulation of finite elements. In the process of reconstruction of the 3D objects the ligaments, tendons and meniscus were integrated to the bone components of the model as well as gaps were filled in the geometries and a smooth finish of the parts was given.

When comparing the initial digital model and the final model, we can conclude that the changes made significantly improved the initial ACL-R model. Moreover, after the models printing the models were manipulated without showed failure (Figure 24)

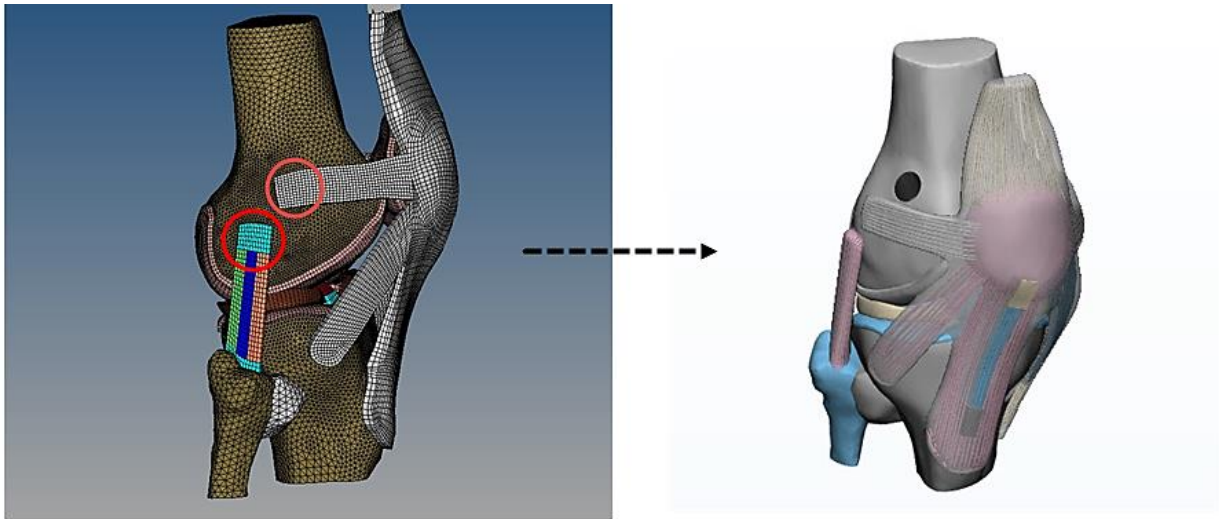


Figure 26. Comparison between the initial FE model and the improved ACL-R model

The design of the SG was based on the problematic related with graft tunnel length mismatch and the uncertainty in the patella graft harvest. It is expected that the guide design protocol can be used in the application of real cases of ACL-R. The Figure 26. Shows the traditional approach for separated and extracted the graft.

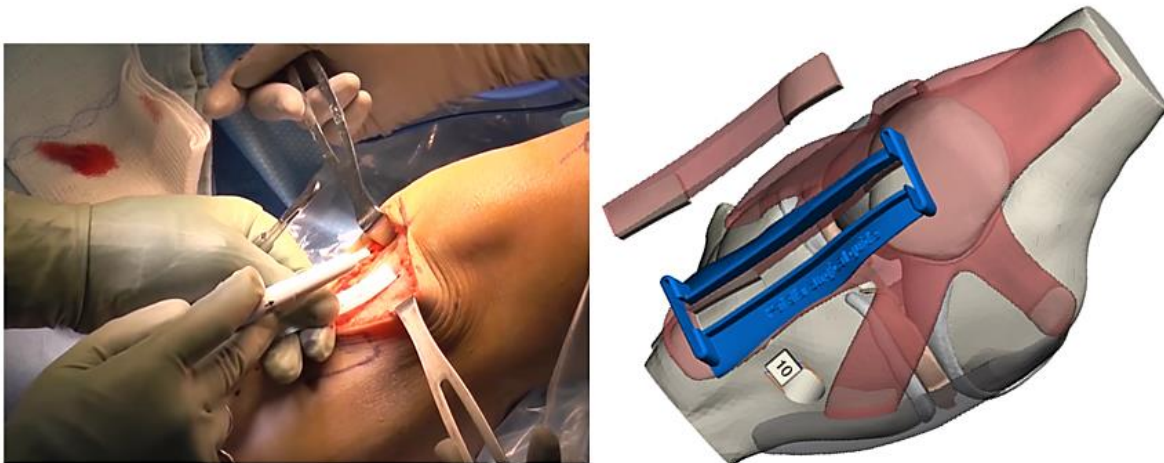


Figure 27. Traditional approach harvest BPTB autograft and use of the SG.

4.3 Chapter 3: TKR biomodel manufacture, custom design and adjustment of prosthetic components in the improved 3D knee joint model

4.3.1 Introduction

The main purpose of the ACL-R is to restore stability of rotation and translation between the femur and tibia as well as return to healthy functional activity levels of the knee joint *Edd et al. 2015*. However, the surgical procedure does not guarantee a complete restoration of the normal patterns of joint movement. In some cases, the risks of developing a degenerative disease increase considerably if the patient performs repetitive cycles during his daily activities *Stergiou et al. 2007*. Abnormal movement patterns are linked with an abnormal joint contact loading, altering mechanical environment and resulting in the development and progression of degenerative diseases such as osteoarthritis (OA) *Tashman et al. 2007*. It has been estimated that the 50% of patients who have undergone an ACL-R develop premature OA *Butler et al. 2008*.

The OA is one of the main health problems worldwide due to its high prevalence; it has been considered the most common cause of permanent disability. This degenerative arthropathy results from progressive structural and functional compromise to articular components in the knee joint, affecting the cartilage, adjoining bones, synovial lining, even the periarticular muscle *Gelber et al. 2011*. Total knee replacement (TKR), is recommended for those patients in an advanced stage of the disease, which present severe pain and total disability. Statistical data show that TKR procedure continues increasing at a rapid pace in the US. Roughly, 1 million primary knee replacements per year are made. It has been projected an increase to 3.5 million by 2030 *Liddle et al 2013*. Unfortunately, revision surgery to replace failed primary arthroplasties also continues to grow in number. Cumulative results from a large series of joint registries indicate that revision rates are 6% at 5 years and 12% after 10 years of in vivo service *Zimmerman et al. 2016*. The most common risks and complications associated with a revision of TKR are thrombosis, infection, stiffness, aseptic loosening, osteolysis and pain. The success of surgery depends on several factors such as knee condition, age, weight, activity level, design/manufacture of implanted prosthesis, materials used in the implants among others. Although all these reasons for revision might be related to implant, other factors contribute to risk of revision. These factors include the surgical technique, surgical experience, skill, and post-operative care *Carr et al. 2012*. Surgical outcomes can be improved with a proper pre-operative planning coordinated by an engineer and the clinician and a correct choice of prosthetic components. In addition, standard femoral/tibial knee components have generic shape while every patient has a unique shape of knee joint and this is causes some problems. Overall, conventional prosthetic components gives a satisfactory result in many cases that carry the patient back to active lifestyle especially for younger patients. Most patients' gaits are altered after TKR due to the change in surface geometry of prosthetics components, especially femoral implant. The main objective of this chapter is to design custom knee implants to improve surgical outcomes. Moreover, the manufacture of the TKR biomodel can be useful in the study and development of biomechanical models of finite element, as mentioned in the chapter 2.

4.3.2 Problem specifications

TKR involve three critic components: femoral, tibial, and patellar components. Femoral component is perhaps the most complex of the three. This has a convex shape which is a large plate bent to help the curvatures of the femoral condyles (located at distal femur). The common cause for premature failure of the TKR is aseptic Loosening of the femoral component. After then, all components fail. Many countries delay the surgical operation of knee joint replacement until the patient has reach 65 years; because younger patients have more active lifestyle which cause premature failure for knee prostheses *Krackow et al. 1990*.

The wrong relation between bone and implant usually causes aseptic loosening of the femoral implant. This causes an uneven stress distribution, which leads the component to the failure. To prevent any kind of complication, the first step is the correct pre-operative planning. This study addresses the virtual planning surgical and adjustment of prosthetic elements in the improved 3D model of the right knee joint following these functional requirements: (1) prosthetic components must have the ability to replicate joint motion as closely as possible. (2) The size of the implants must be as close as possible to the actual anatomy of the knee. The Figure 24 illustrates the prosthetic designed for TKR, these were adapted to the bone components according to anatomical planes and points (landmarks) established in the pre-operative planning.

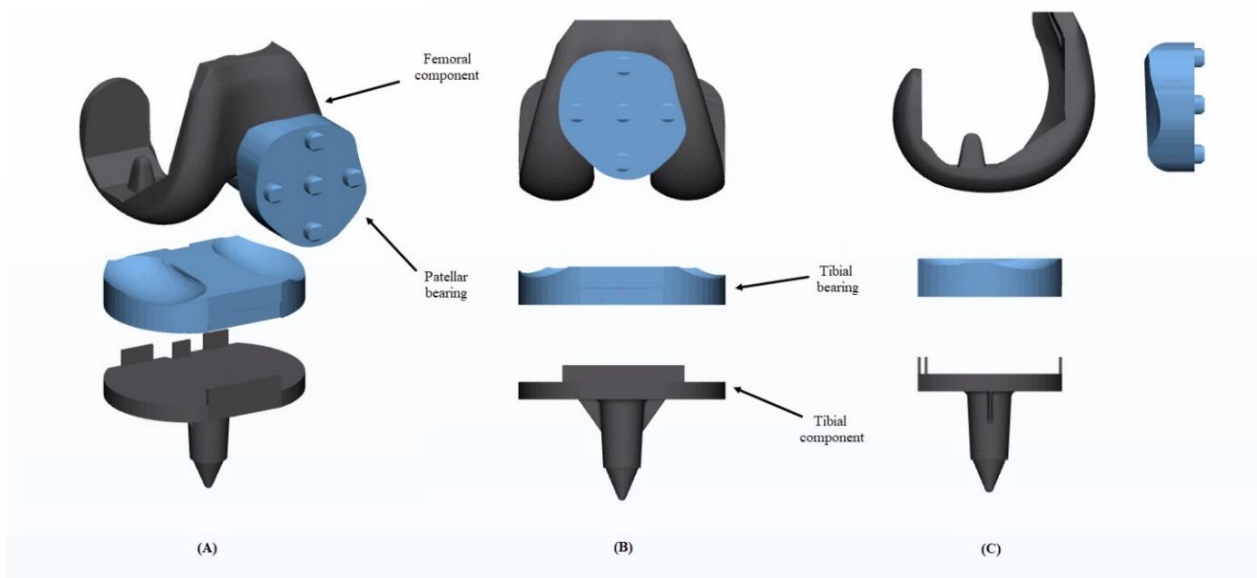


Figure 28. Prosthetic components designed for the TKR: (A) Isometric view (B) Posterior view (C) Lateral view

4.3.3 Material and methods

Pre-operative planning was designed considering a cruciate sacrificing implant (CS) with symmetric tibial bearing fixed. The personalized design of the femoral and tibial components was performed using the modeling software *Rhinoceros 3D v5.0* based on the anatomical characterization of the femur and the tibia. The prosthetic components were exported in *.STL format to the medical *Materialize 3-matic Software*, in which the femur and tibia osteotomies were performed. The patellar and tibial bearings were designed in this same application considering patellar and tibial geometries.

Pre-operative planning of TKR (Figures 25-26-27)

1. Measurement of bone components, identification of the anatomical and mechanical axes in the knee joint and measure of the anatomical angles: anatomic-mechanic femoral angle (FMAa) [5-7°], anatomic lateral distal femoral angle (FDLAa) [79-83°] and mechanical lateral distal femoral angle (FDLMA) [85-90 °] *Jingjit-et al. 2014*.
2. Simulation of the cuts in the tibia and femur following the indications reported by *Smith & Nephew et al. 2018* were resected: 11 mm of the proximal tibia (cross section), 8 mm of the distal femur (cross section), 7 mm in the posterior region of the femur (coronal section), 11 mm in the postero-inferior region of the femur (cross section) and 6 mm in the anterior region of the femur (coronal section), guaranteeing a space of 20 mm for the replacement of the joint component. The patella was resected 14 mm from the anterior region (coronal section).
3. The design of the symmetrical and conventional tibial and femoral components were based on the measurements of bone components. These were adapted to the bone component, the tibial and patellar bearings were designed from them using using *Boolean & marking tools*. These were adapted to the trajectory and geometry of the femoral and tibial components respectively. In the neutral position, the femoral component was aligned, so that the resection of the distal bone was perpendicular to the mechanical axis of the femur, and the anterior and posterior resections are parallel to each other.

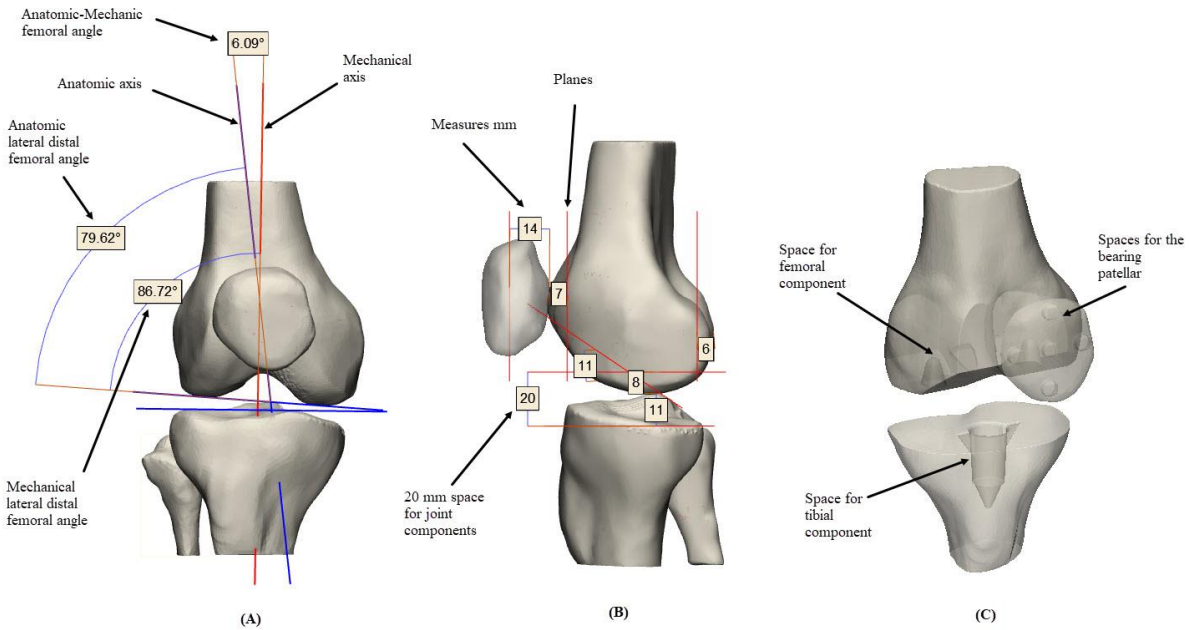


Figure 29. Schematic illustration of the pre-operative measurements and anatomical angles of the surgical planning: (A) Mechanical and anatomical axes, and anatomical angles, $FMAa = 6.09^\circ$ - $FDLAa = 79.62^\circ$ - $FDLMa = 86.72^\circ$, (B) Anatomical measurements and simulation of the cut planes in the bone components, (C) subtraction of the prosthetic components of the bone component.

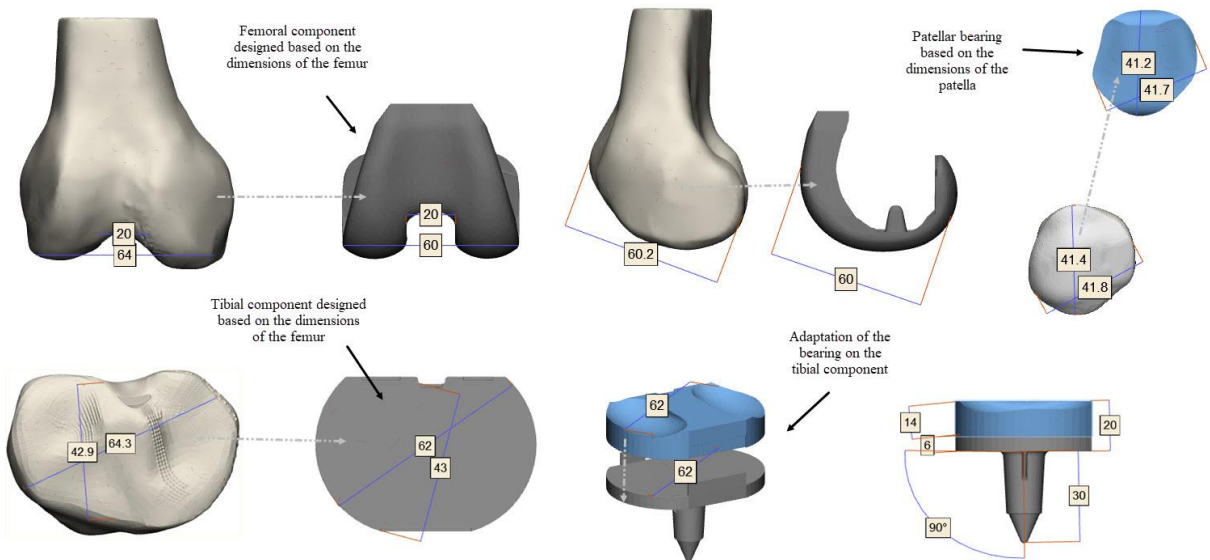


Figure 30. Schematic illustration of the design and adaptation of the prosthetic components designed based on the anatomy of the bone components. Patellar and tibial bearings were designed based on the real articular component.

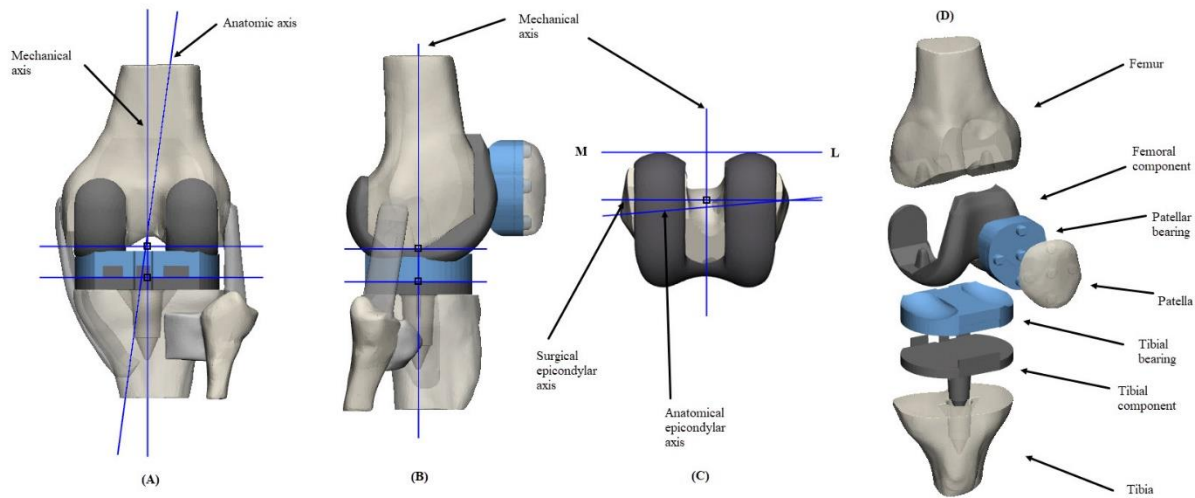


Figure 31. Schematic illustration of the developed TKR biomodels (A) Posterior view knee joint with prosthetic components, femoral and tibial component are aligned perpendicular to the mechanical axis. (B) Lateral view of the knee joint with prosthetic components, the alignment corresponded to 90° with respect to the mechanical axis. (C) Transverse view of the knee joint with the femoral component, anatomic axes-alignment surgical epicondylar axis and mechanical axis corresponded to 90° . (D) Isometric view assembly of all the components of the TKR.

4.3.4 Results

The results of this chapter are based on the results corresponding to the materials test presented in Chapter 1. The Figure 28. Shows the assemblies and the list of materials selected for the manufacture of the three biomodels. After manufacture, personalized implants showed to accomplish with its function according to the established pre-operative planning. TKR biomodel preserved connective structures during its manipulation. Figure 29.

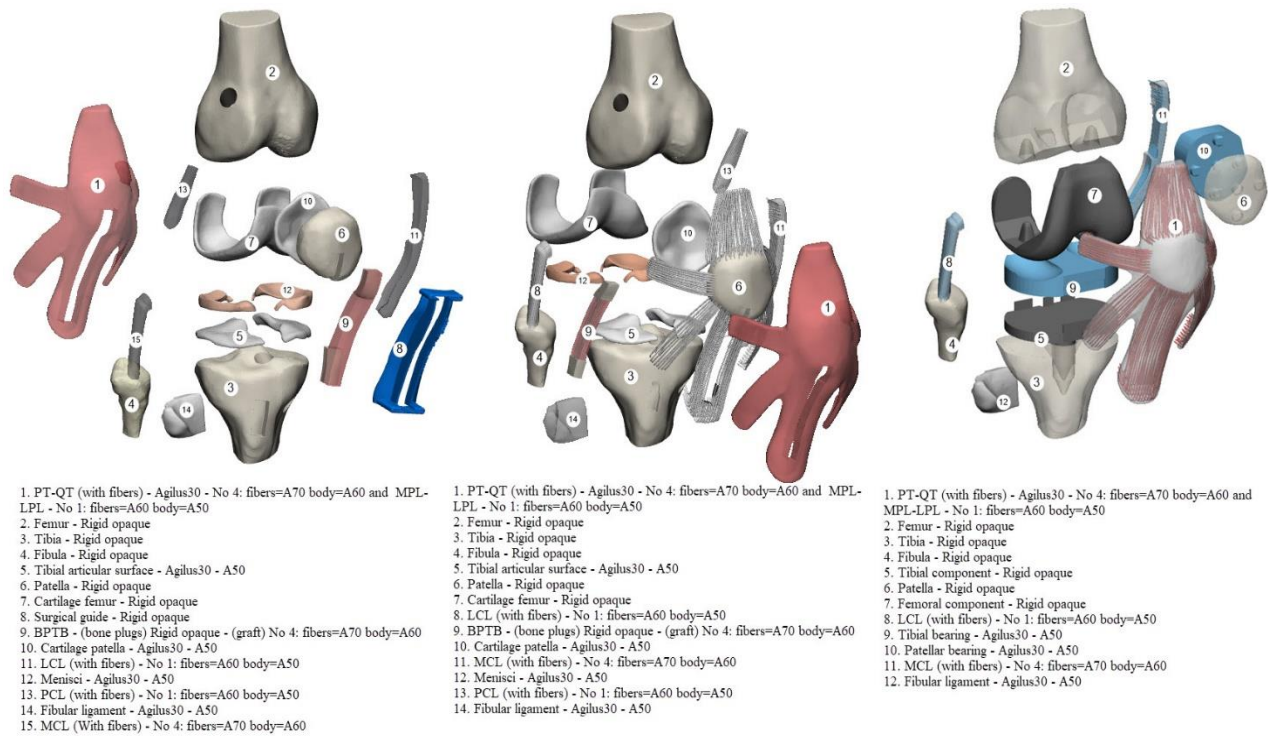


Figure 32. Schematic Illustration of assemblies and list of anatomical structures of the printed models of the knee joint with the selected materials.

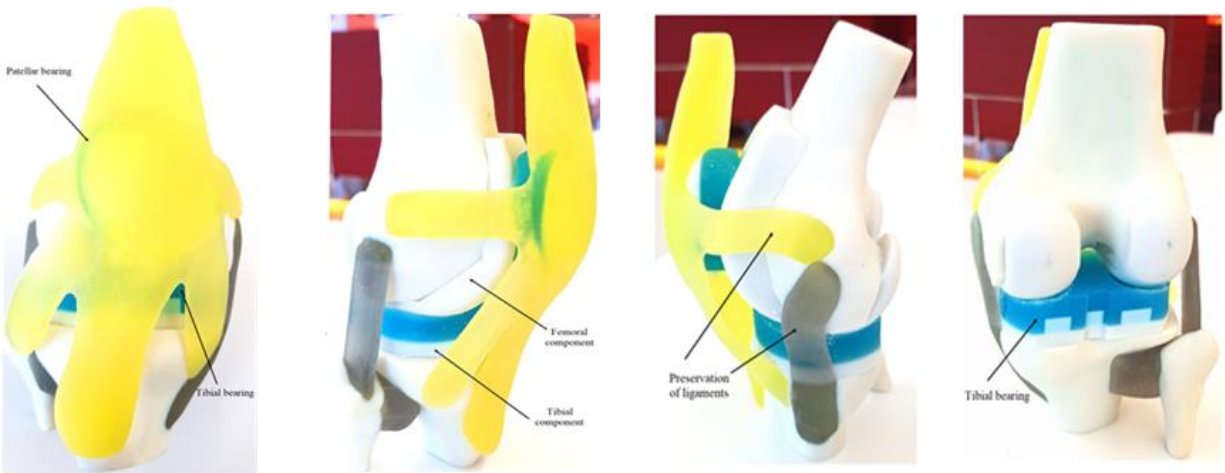


Figure 33. Illustration of TKR biomodel. Posterior-Anterior-Lateral-Isometric views show some details as the fibers and prosthetic components.

4.3.5 Discussion

The purpose of this chapter was emulate a TKR using cruciate sacrificing implant (CS) with symmetric tibial bearing fixed prosthetic. The results of the TKR model printing as in the previous

chapters achieved to replicate with accuracy the operating protocol designed (Figures 28-29-30-32). As future work a finite element analysis (FEA) is proposed to evaluate stress distribution on the implants. The specialized *Materialize 3-matic Software* proved to be quite useful, its measurement/simulation/positioning/design tools allowed the development of the model TKR.

5. Conclusion

Full color multi-material printing can produce functional anatomical models, which offer a diverse range of user interaction. The Stratasys J750™ printer was able to reproduce three functional biomodels with high fidelity. This technology combined with the medical software can radically change the way in which orthopedists plan and execute complex procedures. The combination of hard/stiff and soft/elastic materials allows a much greater diversity in the manufacture of customized models that can illustrate anatomy, biomechanics or function principles. The Personalized design, virtual pre-operative planning and the manufacture of implants/splints/surgical guides specific-patient can greatly help reduce the error rates in complex procedures such as ACL-R and TKR. In addition, proposed models are a close approximation to the real knee joint and can be considered as a real alternative to the use of cadaveric specimens for biomechanical simulation or medical training.

In this study, multi-material 3D printing enabled the combination of hard and deformable materials in a single project. Personalized designs of the knee joint models with realistic physiological and anatomical features were created simulating hierarchical structure and complex operative procedures. The main limitation of this approach was the validation with *Sensuron multiplatform system* (high cost~70000 USD) and the medical validation criteria of the ACL-R –TKR biomodels due to the printed models are derived from a healthy knee joint and not from pathological cases. Overall, printing price of the biomodels could be considered economical in relation to the costs associated with the use of cadaveric models and surgical failure. Their production using High Mix 27 mm layer thickness mode was \$ 570 USD with a production time of 28 hours. considering the application the costs can be reduced using other modes of printing with lower resolution.

As a future work, it is proposed not to abandon the validation approach with the *Sensuron multiplatform system* and to contrast the recorded data with recent experimental data present in literature. It is also suggested to apply the ACL-R pre-operative planning results in real cases.

6. Biography

Abdallah, N. H. (2007) *Prospective study in knee joint osteoarthritis*.

Acker, J. H., & Drez, D. (1989). Analysis of isometric placement of grafts in anterior cruciate ligament reconstruction procedures. *Am J Knee Surg*, 2, 65-70.

- Amiel, D., Kleiner, J. B., & Akeson, W. H. (1986). The natural history of the anterior cruciate ligament autograft of patellar tendon origin. *The American journal of sports medicine*, 14(6), 449-462.
- Anderson, D. R., Weiss, J. A., Takai, S., Ohland, K. J., & Woo, S. L. Y. (1992). Healing of the medial collateral ligament following a triad injury: a biomechanical and histological study of the knee in rabbits. *Journal of orthopaedic research*, 10(4), 485-495.
- ALM, A. (1974). Vascular anatomy of the patellar and cruciate ligaments: a microangiographic and histologic investigation in the dog. *Acta Chir Scand Suppl*, 445, 25-35.
- Arcas, M. A., Gálvez, D. M., León, J. C., Paniagua, S., & Pellicer, M. (2004). Manual de fisioterapia. *Modulo I. Generalidades. Sevilla: Ed. Mad.*
- Arnett, F. C., Edworthy, S. M., Bloch, D. A., Mcshane, D. J., Fries, J. F., Cooper, N. S & Medsger Jr, T. A. (1988). The American Rheumatism Association 1987 revised criteria for the classification of rheumatoid arthritis. *Arthritis & Rheumatism: Official Journal of the American College of Rheumatology*, 31(3), 315-324.
- Beck Jr, C. L., Paulos, L. E., & Rosenberg, T. D. (1992). Anterior cruciate ligament reconstruction with the endoscopic technique. *Operative Techniques in Orthopaedics*, 2(2), 86-98.
- Berman, B. (2012). 3-D printing: The new industrial revolution. *Business horizons*, 55(2), 155-162.
- Betts, J. G., DeSaix, P., Johnson, E., Johnson, J. E., Korol, O., Kruse, D. H., & Young, K. A. (2014). *Anatomy and physiology*.
- Biewener, A. A. (2008). Tendons and ligaments: structure, mechanical behavior and biological function. In *Collagen* (pp. 269-284). Springer, Boston, MA.
- Burgener, F. A., Meyers, S. P., Tan, R. K., & Zaunbauer, W. (2002). Differential diagnosis in magnetic resonance imaging.
- Butler, R. J., Minick, K. I., Ferber, R., & Underwood, F. (2009). Gait mechanics after ACL reconstruction: implications for the early onset of knee osteoarthritis. *British journal of sports medicine*, 43(5), 366-370.
- Britannica, E. (1965). *Encyclopedia Britannica. Inc., Chicago*, 111, 720.
- Carr, A. J., Robertsson, O., Graves, S., Price, A. J., Arden, N. K., Judge, A., & Beard, D. J. (2012). Knee replacement. *The Lancet*, 379(9823), 1331-1340.
- Cockshott, W. P., Racoveanu, N. T., Burrows, D. A., & Ferrier, M. (1985). Use of radiographic projections of knee. *Skeletal radiology*, 13(2), 131-133.
- Clark, J. M., & Sidles, J. A. (1990). The interrelation of fiber bundles in the anterior cruciate ligament. *Journal of orthopedic research*, 8(2), 180-188.

- Cohen, Z. A., Henry, J. H., McCarthy, D. M., Van Mow, C., & Ateshian, G. A. (2003). Computer simulations of patellofemoral joint surgery: patient-specific models for tuberosity transfer. *The American journal of sports medicine*, 31(1), 87-98.
- Dhaher. &, Salehghaffari, S. (2014). A model of anterior cruciate ligament reconstructive surgery: a validation construct and computational insights. *Journal of biomechanics*, 47(7), 1609-1617.
- Drake, R., Vogl, A. W., & Mitchell, A. W. (2009). *Gray's Anatomy for Students E-Book*. Elsevier Health Sciences.
- Driban, J. B., Eaton, C. B., Lo, G. H., Ward, R. J., Lu, B., & McAlindon, T. E. (2014). Association of knee injuries with accelerated knee osteoarthritis progression: data from the Osteoarthritis Initiative. *Arthritis care & research*, 66(11), 1673-1679.
- Daniel, D. M., Pedowitz, R. A., O'Connor, J. J., & Akeson, W. H. (2003). *Daniel's knee injuries: ligament and cartilage structure, function, injury, and repair*. Lippincott Williams and Wilkins.
- Diamant, J., Keller, A., Baer, E. L. H. M., Litt, M., & Arridge, R. G. C. (1972). Collagen; ultrastructure and its relation to mechanical properties as a function of ageing. *Proc. R. Soc. Lond. B*, 180(1060), 293-315.
- David, L., Grood, E. S., Noyes, F. R., & Zernicke, R. E. (1978). Biomechanics of ligaments and tendons. *Exercise and sport sciences reviews*, 6(1), 125-182.
- Danylchuk, K. D., Finlay, J. B., & Kreck, J. P. (1978). Microstructural organization of human and bovine cruciate ligaments. *Clinical orthopaedics and related research*, (131), 294-298.
- Ehrlich, M. G., Mankin, H. J., Jones, H. A. R. D. I. N., Wright, R. I. C. H. A. R. D., Crispin, C. H. A. R. L. E. S., & Vigliani, G. L. O. R. I. A. (1977). Collagenase and collagenase inhibitors in osteoarthritic and normal cartilage. *The Journal of clinical investigation*, 59(2), 226-233.
- Edd, S. N., Giori, N. J., & Andriacchi, T. P. (2015). The role of inflammation in the initiation of osteoarthritis after meniscal damage. *Journal of biomechanics*, 48(8), 1420-1426.
- Fanelli, G. C., Giannotti, B. F., & Edson, C. J. (1996). Arthroscopically assisted combined anterior and posterior cruciate ligament reconstruction. *Arthroscopy: The Journal of Arthroscopic & Related Surgery*, 12(1), 5-14.
- Frank, R. M., Higgins, J., Bernardoni, E., Cvetanovich, G., Bush-Joseph, C. A., Verma, N. N., & Bach Jr, B. R. (2017). Anterior Cruciate Ligament Reconstruction Basics: Bone–Patellar Tendon–Bone Autograft Harvest. *Arthroscopy techniques*, 6(4), e1189-e1194.
- Frank, C. B. (2004). Ligament structure, physiology and function. *Journal of Musculoskeletal and Neuronal Interactions*, 4(2), 199.

- Frank, C., Akeson, W. H., Woo, S. L., Amiel, D., & Coutts, R. D. (1984). Physiology and therapeutic value of passive joint motion. *Clinical orthopedics and related research*, (185), 113-125.
- Figueroa, R. M., Figueroa, C. M., Rodriguez, R. C., & Poblete, D. F. (2015). Osteoarthritis (artrosis) de rodilla. *Revista Chilena de Ortopedia y Traumatología*, 56(3), 45-51.
- Fetto, J. F., & Marshall, J. L. (1980). The natural history and diagnosis of anterior cruciate ligament insufficiency. *Clinical Orthopaedics and Related Research*, (147), 29-38.
- Gelber, A. C. (2011). Knee pain and osteoarthritis: lessons learned and lessons to be learned. *Annals of internal medicine*, 155(11), 786-787.
- Gans, I., Retzky, J. S., Jones, L. C., & Tanaka, M. J. (2018). Epidemiology of Recurrent Anterior Cruciate Ligament Injuries in National Collegiate Athletic Association Sports: The Injury Surveillance Program, 2004-2014. *Orthopaedic Journal of Sports Medicine*, 6(6), 2325967118777823.
- Grawe, B., Smerina, A., & Allen, A. (2014). Avoiding Graft-Tunnel Length Mismatch in Anterior Cruciate Ligament Reconstruction: The Single-Bone Plug Technique. *Arthroscopy techniques*, 3(3), e417-e420.
- Goh, K. L., Listrat, A., & Béchet, D. (2014). Hierarchical mechanics of connective tissues: Integrating insights from nano to macroscopic studies. *Journal of biomedical nanotechnology*, 10(10), 2464-2507.
- Grooff, P. N., Schils, J. P., & Resnick, D. L. (2003). Part B: Imaging. *Daniel's Knee Injuries: Ligament and Cartilage Structure, Function, Injury, and Repair*, 1, 356.
- Hoehn, K., & Marieb, E. N. (2007). *Human anatomy & physiology*. Benjamin Cummings.
- Hsieh, A. H., Tsai, C. M. H., Ma, Q. J., Lin, T., Banes, A. J., Villarreal, F. J., ... & Paul Sung, K. L. (2000). Time-dependent increases in type-III collagen gene expression in medial collateral ligament fibroblasts under cyclic strains. *Journal of Orthopaedic Research*, 18(2), 220-227.
- Hatze, H. (1974). The meaning of the term "biomechanics". *Journal of biomechanics*, 7(2), 189.
- Jingjit, W., Poomcharoen, P., Limmahakhun, S., Klunklin, K., Leerapun, T., & Rojanasthien, S. (2014). Femoral mechanical-anatomical angle of osteoarthritic knees. *J Med Assoc Thai*, 97(12), 1314-8.
- Krackow, K. A. (1990). *The technique of total knee arthroplasty*. Mosby Inc.
- Kahle, W., Leonhardt, H., Platzer, W., Palmer, E., & Werner, Platzer. (2004). *Color atlas and textbook of human anatomy. Vol. 1, locomotor system*. Thieme.
- Levangie, P. K., & Norkin, C. C. (2000). Joint Structure and function: a comprehensive analysis. 3rd. *Philadelphia: FA. Davis Company*.

- Lee, D. W., & Kim, J. G. (2017). Anatomic single-bundle anterior cruciate ligament reconstruction using the modified transtibial technique. *Arthroscopy techniques*, 6(1), e227-e232.
- Liddle, A. D., Pegg, E. C., & Pandit, H. (2013). Knee replacement for osteoarthritis. *Maturitas*, 75(2), 131-136.
- Liddle, A. D., Pegg, E. C., & Pandit, H. (2013). Knee replacement for osteoarthritis. *Maturitas*, 75(2), 131-136.
- Láctico, A. (2006). *Apoyo científico y tecnológico para el deporte*.
- Merican, A. M., & Amis, A. A. (2008). Anatomy of the lateral retinaculum of the knee. *The Journal of bone and joint surgery. British volume*, 90(4), 527-534.
- Muthuri, S. G., McWilliams, D. F., Doherty, M., & Zhang, W. (2011). History of knee injuries and knee osteoarthritis: a meta-analysis of observational studies. *Osteoarthritis and Cartilage*, 19(11), 1286-1293.
- Masouros, S. D., Bull, A. M. J., & Amis, A. A. (2010). (I) Biomechanics of the knee joint. *Orthopaedics and Trauma*, 24(2), 84-91.
- News-Medical, Y. Smith. (2018). Types of Osteoarthritis, available: www.news-medical.net/health/Osteoarthritis-Types.aspx
- Oosthuizen, C. R., Takahashi, T., Rogan, M., Snyckers, C. H., Vermaak, D. P., Jones, G. G., ... & Pandit, H. (2019). The Knee Osteoarthritis Grading System for Arthroplasty. *The Journal of arthroplasty*, 34(3), 450-455.
- Pal, S. (2014). Mechanical properties of biological materials. In *Design of Artificial Human Joints & Organs* (pp. 23-40). Springer, Boston, MA.
- Pal, S. (2014). *Design of artificial human joints & organs* (p. 23). Boston, MA: Springer US.
- Panesso, M. C., Trillos, M. C., & Tolosa Guzmán, I. (2009). *Biomecánica clínica de la rodilla*. Editorial Universidad del Rosario.
- Pailhé, R., Cavaignac, E., Murgier, J., Laffosse, J. M., & Swider, P. (2015). Biomechanical study of ACL reconstruction grafts. *Journal of Orthopaedic Research*, 33(8), 1188-1196.
- Rivard, C. H. (1989). Studies on the anterior cruciate ligaments: a 10-year experience review. *Nihon Seikeigeka Gakkai zasshi*, 63(5), 687-691.
- Simon, D., Mascarenhas, R., Saltzman, B. M., Rollins, M., Bach, B. R., & MacDonald, P. (2015). The relationship between anterior cruciate ligament injury and osteoarthritis of the knee. *Advances in orthopedics*, 2015.
- Smith & Nephew Inc. (2018) key products: *Orthopaedic reconstruction* available: www.smith-nephew.com/

Stratasys Ltd. (2016). FDM and Polyjet 3D printing. *Popular Plastics & Packaging* available: www.stratasys.com.

Steiner, M. E., Murray, M. M., & Rodeo, S. A. (2008). Strategies to improve anterior cruciate ligament healing and graft placement. *The American journal of sports medicine*, 36(1), 176-189.

Scheffler, S. (2012). The cruciate ligaments: Anatomy, biology, and biomechanics. In *The Knee Joint* (pp. 11-21). Springer, Paris.

Samuelsson, K., Andersson, D., & Karlsson, J. (2009). Treatment of anterior cruciate ligament injuries with special reference to graft type and surgical technique: an assessment of randomized controlled trials. *Arthroscopy: The Journal of Arthroscopic & Related Surgery*, 25(10), 1139-1174.

Stergiou, N., Ristanis, S., Moraiti, C., & Georgoulis, A. D. (2007). Tibial rotation in anterior cruciate ligament (ACL)-deficient and ACL-reconstructed knees. *Sports medicine*, 37(7), 601-613.

Sophia Fox, A. J., Bedi, A., & Rodeo, S. A. (2009). The basic science of articular cartilage: structure, composition, and function. *Sports health*, 1(6), 461-468.

Scott, N. (1992). Lesiones de los ligamentos y del aparato extensor de la rodilla. *Diagnóstico y tratamiento*. Nueva York: Mosby.

Shrive, N. G., Thornton, G. M., Hart, D. A., & Frank, C. B. (2003). Ligament mechanics. *Daniel's knee injuries, 2nd edn*. Lippincott Williams & Wilkins, Philadelphia, PA, 97-112.

Smith, J. (2002, March). Techniques in Musculoskeletal Rehabilitation. In *Mayo Clinic Proceedings* (Vol. 77, No. 3, p. 299). Mayo Foundation for Medical Education and Research.

Tashman, S., Kolowich, P., Collon, D., Anderson, K., & Anderst, W. (2007). Dynamic function of the ACL-reconstructed knee during running. *Clinical Orthopaedics and Related Research®*, 454, 66-73.

Todd Pietila, Global Business Development, Materialise (2018)

Thorpe, C. T., Birch, H. L., Clegg, P. D., & Screen, H. R. (2013). The role of the non-collagenous matrix in tendon function. *International journal of experimental pathology*, 94(4), 248-259.

Vaishya, R., Patralekh, M. K., Vaish, A., Agarwal, A. K., & Vijay, V. (2018). Publication trends and knowledge mapping in 3D printing in orthopaedics. *Journal of clinical orthopaedics and trauma*.

Viidik, A. (1973). Functional properties of collagenous tissues. In *International review of connective tissue research* (Vol. 6, pp. 127-215). Elsevier.

Vrancken, A. C. T., Buma, P., & van Tienen, T. G. (2013). Synthetic meniscus replacement: a review. *International orthopaedics*, 37(2), 291-299.

Woo, S. L. Y., Abramowitch, S. D., Kilger, R., & Liang, R. (2006). Biomechanics of knee ligaments: injury, healing, and repair. *Journal of biomechanics*, 39(1), 1-20.

Wang, K., Ho, C. C., Zhang, C., & Wang, B. (2017). A review on the 3D printing of functional structures for medical phantoms and regenerated tissue and organ applications. *Engineering*, 3(5), 653-662.

Yan, Q., Dong, H., Su, J., Han, J., Song, B., Wei, Q., & Shi, Y. (2018). A Review of 3D Printing Technology for Medical Applications. *Engineering*.

Zimmerman, W. F., Miller, M. A., Cleary, R. J., Izant, T. H., & Mann, K. A. (2016). Damage in total knee replacements from mechanical overload. *Journal of biomechanics*, 49(10), 2068-2075.